Role of Protein phosphatase V in Cell Cycle Control

Dissertation

for the award of the degree

"Doctor rerum naturalium (Dr.rer.nat.)"

of the Georg-August-Universität Göttingen

within the doctoral program Biology

of the Georg-August University School of Science (GAUSS)

submitted by

Boyang Liu

刘博洋

from Hohhot, China

GÖTTINGEN 2016

THESIS COMMITTEE

Prof. Dr. Jörg Großhans (Supervisor)

Institute for Developmental Biochemistry, Universitätsmedizin Göttingen

Prof. Dr. Gregor Bucher

Department of Evolutionary Developmental Genetics, University of Göttingen

Prof. Dr. Stefan Luschnig

Institute of Neuro- and Behavioral Biology, University of Münster

MEMBERS Of The EXAMINATION BOARD

Prof. Dr. Jörg Großhans (Reviewer)

Institute for Developmental Biochemistry, Universitätsmedizin Göttingen

Prof. Dr. Gregor Bucher (Second Reviewer)

Department of Evolutionary Developmental Genetics, University of Göttingen

Prof. Dr. Stefan Luschnig

Institute of Neuro- and Behavioral Biology, University of Münster

Prof. Dr. Holger Bastians

Institute of Molecular Oncology, Universitätsmedizin Göttingen

Prof. Dr. Reinhard Schuh

Research Group Molecular Organogenesis, Max Planck Institute for Biophysical Chemistry

PD Dr. Halyna Shcherbata

Research Group Gene Expression and Signaling, Max Planck Institute for Biophysical Chemistry

Date of the oral examination: 30. Sept. 2016

Date of online submission: Aug. 2017

AFFIDAVIT

I hereby declare that I prepared the doctoral thesis "Role of Protein phosphatase V in Cell Cycle Control" on my own with no other sources and aids than quoted.

EMS mutagenesis was carried out collaborated within the research group of Prof. Dr. S. Luschnig, University of Zurich, Switzerland. Live-imaging and mapping was in part conducted by my colleague Dr. L. Henn and master student L. Chandran.

The introduction "Link of zygotic genome activation and cell cycle control" was submitted for publication within the series "Methods in Molecular Biology". The manuscript was written by myself and revised by Prof. Dr. J. Großhans. Mapping of the X9 mutant was carried out by Prof. Dr. J. Großhans and Dr. H. Sung. The mathematical calculation of the fluctuation analysis was carried out by Dr. I. Gregor, Third Institute of Physics, University of Göttingen. Mass spectrometry of the phosphopeptide analysis was carried out by Prof. Dr. H.-A. Müller and the staff in Proteomics Facility, University of Dundee, UK.

_____

Boyang Liu

Göttingen, 15.08.2016

Contents

Part II: Role of Protein phosphatase V in Cell Cycle Control in *Drosophila* Blastoderm

Abbreviations

aa	amino acid(s)
ATR	ataxia telangiectasia and Rad3-related
bp	base pair(s)
BSA	bovine serum albumin
Cdc	cell division cycle protein
Cdk	Cyclin dependent kinase
cDNA	complementary DNA
Chk	Checkpoint kinase
CyO	*Curly of Oster* balancer chromosome
C. elegans	*Caenorhabditis elegans*
d	day(s)
DAPI	4',6-diamidino-2-phenylindole
ddH$_2$O	double distilled water
Dia	Diaphanous
DIC	differential interference contrast
DNA	deoxyribonucleic acid
Dr	*Drop* eyes
dsRNA	double-stranded RNA
DTT	dithiothreitol
EDTA	ethylenediaminetetraacetic acid
EMS	ethyl methanesulfonate
ens	*ensconsin*
Eve	Even skipped
E. coli	*Escherichia coli*
FCS	fluorescence correlation spectroscopy
Fig.	Figure
Flp	Flipase
Frt	Flipase recognition target
g	gram(s)

GFP	Green fluorescent protein
G2 phase	gap 2 phase
h	hour(s)
His/H	Histone
hs-hid	heat shock-head involution defective
ICM	inner cell mass
int	interphase
kb	kilo bases
kDa	kilo Dalton
l	liter(s)
LSM	confocal laser scanning microscopy
m	mitosis; meter(s)
M	Marker
MBT	mid-blastula transition
min	minute(s)
mRNA	messenger RNA
MW	molecular weight
MZT	maternal-zygotic transition
m-	milli-
N/Nr	number
NC	nuclear cycle
ND	not detected
nls	nuclear localization signal
N:C ratio	nucleocytiplasmic ratio
ORF	open reading frame
PAGE	polyacrylamide gel electrophoresis
PBS	phosphate-buffered saline
PCR	polymerase chain reaction
Pol II	RNA polymerase II
PpV	Protein phosphatase V

qPCR	quantitative real-time PCR
RNA	ribonucleic acid
RNAi	RNA interference
RPA70	Human replication protein A
RFP	Red fluorescent protein
rpm	revolutions per minute
RT	room temperature
SDS	sodium dodecyl sulfate
sec	second(s)
Slam	Slow as molasses
Sp	*Sternopleural* bristles
S phase	synthesis phase
S2 cells	Schneider 2 cells
Tab.	Table
Tap42	Two A-associated protein of 42kDa
TBS	Tris-buffered saline
TM3/6	third multiple 3/6 balancer chromosome
Tris	tris(hydroxymethyl)aminomethane
TSS	transcription start site
Tub	Tubulin
UAS	upstream activation sequence
UTR	untranslated region
Vfl/Zld	Vielfältig/Zelda
w	*white* eyes
WT	wild type
y	*yellow* body
ZGA	zygotic genome activation
µ-	micro-
°C	degree Celsius

Summary

The cell cycle mode is variant among different cell and tissue types and is remodeled during development. This change between modes is referred as cell cycle switch or remodeling. In *Drosophila melanogaster*, the canonical cell cycle contains G1, S, G2 and M phases. During early embryogenesis, the cell cycle mode changes from fast syncytial cycle with only S-M phases to an embryonic mode with introduction of a G2 phase. This mode switch is a prominent feature of the mid-blastula transition (MBT). However, it is unclear how the cell cycle remodeling is linked to the developmental program.

In the first part "Isolation of new germline clone mutations with blastoderm defects", I conducted an EMS-induced mutagenesis screen to identify novel genes, which are maternally required for *Drosophila* blastoderm formation. 26 candidate mutants with defects in preblastoderm, blastoderm, cellularization, gastrulation as well as cell cycle were successfully isolated on the third chromosome. By means of mapping and sequencing, novel genes and new function of known genes involved in blastoderm formation have been identified.

In the second part "Role of Protein phosphatase V in Cell Cycle Control in *Drosophila* Blastoderm", I characterized a novel mutation in *Protein phosphatase V* (*PpV*), the homologue of human *Protein phosphatase 6* (*PP6*), from a genetic screen and analyzed its cell cycle function during the MBT. A G2 phase is introduced by the Tribbles and other zygotic factors induced degradation of phosphatase Cdc25/Twine in interphase 14, but the mechanisms how Cdc25/Twine protein levels are controlled and how the striking robustness of the cell cycle switch are ensured are not fully understood. I show that maternal PpV is critical in timing the cell cycle remodeling by maintaining the low Cdc25/Twine level in pre-MBT. Complementary to PpV, zygotic Tribbles is involved in the induced degradation of Cdc25/Twine during MBT by enhancing the decay rate. PpV may directly act on Cdc25/Twine, as we identified three additional phosphorylation sites of Twine in *PpV* mutants. Mutation of these PpV-dependent phosphorylation sites led to high proportion of extra embryonic nuclear cycle, similar to *PpV* mutants.

Part I

Isolation of new germline clone mutations with blastoderm defects

1 Introduction

1.1 Mutagenesis screen

To define genes controlling developmental processes, forward genetic screens have been used to isolate corresponding mutants. Since natural allelic mutations are rare, mutagens are applied to populations of individuals. Large-scale genetic screens need efficient mutagens, including chemical mutagens, for instance ethyl methanesulfonate (EMS), methyl methanesulfonate (MMS), nitrogen mustard (HN2), *N*-ethyl-*N*-nitrosourea (ENU), triethylenemelamine (TEM) and formaldehyde; ionizing radiations, for instance X-rays and γ-rays; and insertional mutagens, for instance transposable elements and viruses (Grigliatti 1998; Laurencon et al. 2004). Besides the above, new biological methods including RNA interference (RNAi), genome-wide deletions and CRISPR/Cas9-System can induce site-directed mutagenesis in defined target loci (Parks et al. 2004; Jia et al. 2015; Schmitt-Engel et al. 2015; Port and Bullock 2016; Tanaka et al. 2016). The function and identity of thousands of genes in eukaryotic organisms have been successfully uncovered with the help of genetic screens.

EMS as an efficient mutagen induces usually single-base changes (point mutations) randomly along the whole genome, and disrupts gene functions by leading missense or nonsense mutations (St Johnston 2002). With a low probability, small deletions and other arrangements are occasionally induced (Greenspan 2004). This mutagen was first described in *Drosophila* in 1968 (Lewis and Bacher 1968), and later employed in the classical large-scale "Heidelberg Screen" (Nüsslein-Volhard and Wieschaus 1980; Jürgens et al. 1984; Nüsslein-Volhard et al. 1984; Wieschaus et al. 1984; Wieschaus and Nüsslein-Volhard 2016) (Fig. 1A). In this milestone work, the genetic control of *Drosophila* early embryonic development was revealed by scoring the phenotypes of cuticles of dead unhatched larvae. After that, saturation mutagenesis screens were carried out and around 30 genes functional in embryonic pattern formation were identified from recessive female-sterile mutations (Perrimon et al. 1986; Schupbach and Wieschaus 1986; Nüsslein-Volhard et al. 1987; Schupbach and Wieschaus 1989; Schupbach and Wieschaus 1991).
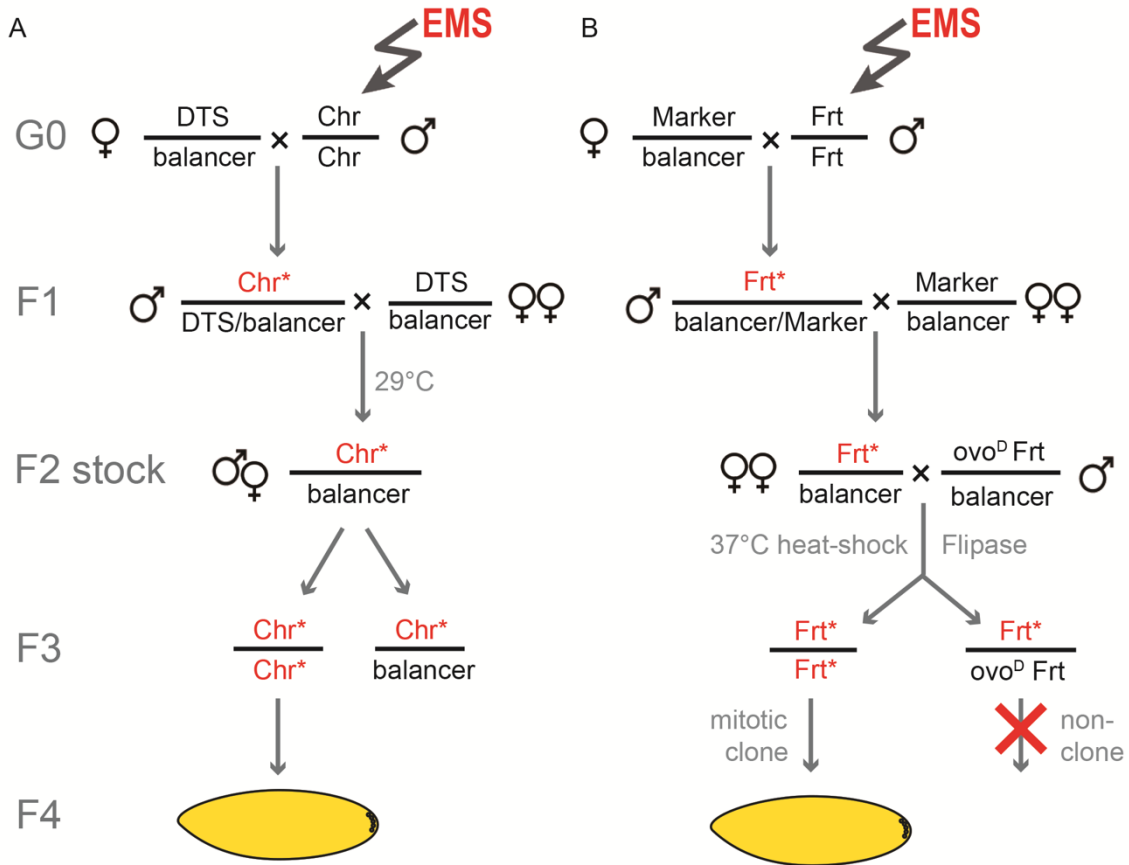
Figure 1: Comparison of autosomal maternal screen and germline clone screen. (A) Crossing scheme of the maternal "Heidelberg Screen". (B) Crossing scheme of germline clone screen which was utilized in this study. F2 flies with mutagenic and balancer chromosomes are keeping as stocks. ovo^D is the dominant female-sterile mutant which causes female germ cells death during early oogenesis. After heat-shock, recombination was induced between two Frt sites which are very close to centromere by Flipase. F3 females carrying recombinant Frt/ovo^D Frt are fertile as their ovaries are homozygous. Therefore nurse cells are not possible to deposit maternal components of mutations to the oocytes, so the eggs show maternal-effect phenotypes. Non-recombinant Frt/ovo^D Frt females are sterile. Chr: autosomal chromosome. DTS: dominant temperature sensitive. Frt: Flipase recognition target. The asterisk indicates an EMS-induced mutation.

Drosophila blastoderm formation is controlled mainly by maternally supplied products (Rice and Garen 1975). These maternal-effect genes are essential and corresponding mutations often cause zygotic lethality in embryonic, larval or pupal stages. Therefore it is not possible to obtain females homozygous for essential gene

mutations and to analyze their offspring. With the development of an ingenious technique dominant female-sterile (DFS), germline clone screen can be implemented to make it easy (Perrimon and Gans 1983; Chou et al. 1993; Chou and Perrimon 1996). By using this approach mosaic females containing heterozygous somatic and homozygous germline cells can be generated, thereafter lethal embryos lacking of certain maternal materials can be analysed (St Johnston 2002; Greenspan 2004) (Fig. 1B).

Germline clone screens of maternal genes which are required essentially in development were carried out on all five major *Drosophila* chromosomal arms (Perrimon et al. 1996; Luschnig PhD dissertation 2000; Schnorrer et al. 2002; Yohn et al. 2003; Luschnig et al. 2004; Vogt et al. 2006). In these studies, mutated embryos stopped development mostly with late embryonic defects, which were scored by cuticle phenotypes.

Although with many advantages, the main difficulty of mutagenesis screen is to identify the molecular lesions. Typically, identification of mutations is carried out by complementation analysis, mapping and sequencing, and the procedure is time-consuming because of the duration of generation cycles. Dominant-marker recombination mapping and whole-genome sequencing (WGS) were developed to reduce this workload (Blumenstiel et al. 2009; Sapiro et al. 2013). However, several studies applying different approaches were performed but they did not provide universal and direct solution to practically optimise the strategy.

1.2 Aims of this project

Genes controlling *Drosophila* blastoderm formation may be screened according to embryonic lethality and cuticle morphological defects. However, mutations of maternal genes with essential functions during blastoderm stage often fail to form basic larval tissue structure, leading to undifferentiated, unstructured or lack of cuticles. Distinct from genes with oogenesis and egg activation functions, the fertilization and pronuclear fusion of these mutations appear normal, but the phenotypes were found in preblastoderm and syncytial blastoderm stages, therefore

development is interrupted. When the phenotype initially occurs, it could be defined under live-imaging microscopy.

Drosophila genome encodes approximately 13,600 genes (Adams et al. 2000), one third of which are assumed to have essential functions (De Renzis et al. 2007; Thomsen et al. 2010). Very few zygotic but many maternal genes affect blastoderm formation. Previous screens gave crucial insights into the essential function of genes in early *Drosophila* development, in particular axis-forming and embryonic segmentation, but so far limited number of the maternal genes were identified, for example *diaphanous* (*Dia*), *Actin-related protein 2/3* (*Arp2/3*), *Kinesin 1* and *SCAR*, et al (Richardson et al. 2007; Yan et al. 2013; Winkler et al. 2015). It can be expected that the genes involved in early blastoderm formation has not been saturated discovered yet. Screens for cuticle-less mutants were performed for X, second and third chromosomes but not saturated (Schnorrer et al. 2002; Yohn et al. 2003; Vogt et al. 2006). Chromosome 3 right and left arms contain approximately 5,000 genes, so we estimate roughly 2,000 genes among them may act as essential and maternal genes. Nevertheless, no extensive screen on chromosome 3 was carried out for early blastoderm defects.

In this study, we applied EMS-induced mutagenesis and germline clone screen, attempted to identify new maternal and essential genes involved in blastoderm formation on chromosome 3. We also aimed to find new function in known genes and novel loci in regulatory sequences.

2 Results

2.1 Summary of the mutagenesis screen

2.1.1 Overview of the screen

Eight rounds of mutagenesis for the third chromosome were carried out in this screen (Crossing scheme see Fig. 2 and Materials and methods). 739 stocks were established and 1,311 germline clone crosses were set up on 3L and 3R arms (Tab. 1). For the primary screen, the egg laying rates, embryonic lethality (hatching rate) and cuticle phenotypes were scored and 92 lines (7% of germline clone lines) were selected as interesting candidates based on the criteria (Section 4.2.3). 21.9% of germline clone lines laid no eggs indicating a defect in oogenesis. For the retest, time-lapses of early embryonic development were recorded and analysed.

The lines were classified according to variance and penetrance of the phenotype with one to three stars. Mutants were classified based on their developmental phenotypes into the following categories: egg defect, preblastoderm defect, syncytial blastoderm defect, cellularization defect, gastrulation/germ-band extension defect, extra/fewer mitotic division and other phenotypes.

The 3-star group defined by high penetrance and an invariant phenotype comprised 14 lines. 12 lines, which showed variant phenotypes were defined as 2-star, and 17 lines which showed egg defect or very low development rate were defined as 1-star (Tab. 1). Some of 3- and 2-star mutation lines have been further characterized, so far by immunostainings with specific antibodies depending on phenotypes.

Initial mapping has been performed, so far, for some selected 3-star and 2-star mutations by meiotic recombination with visible markers. The lethality was mapped by backcross of the recombinant chromosomes to the original line. Embryonic phenotypes were mapped by inducing germline clones of the recombinant chromosomes. If lethality and embryonic phenotypes were associated, the Bloomington deficiency kits for 3L and 3R were employed for fine mapping (Mapping scheme see Fig. 12 and Materials and methods). The screen was conducted as a collaboration in the laboratory of Prof. Dr. S. Luschnig at the University of Zurich,

Switzerland. My colleague Dr. L. Henn was partially involved in the mapping of the mutations. Master student L. Chandran was partially involved in recording the developmental movies.
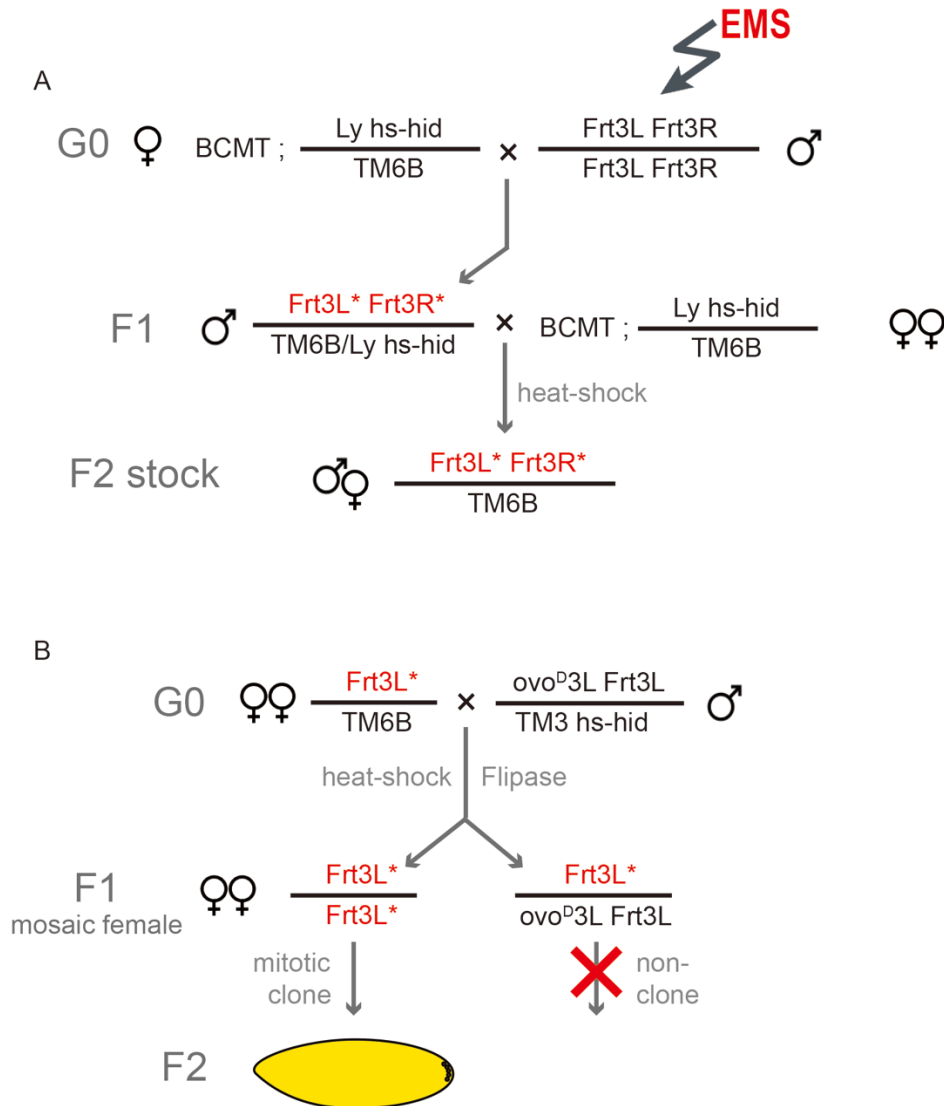

Figure 2: Crossing scheme of mutagenesis and germline clone screen in this study. (A) Crossing scheme of EMS-induced mutagenesis. BCMT: btl-Gal4 UAS-Serp-CBD-GFP UAS-myr-tdTomato. *Ly*: *Lyra* dominant marker. hs-hid: heat shock-head involution defective. (B) Germline clone crossing scheme exemplified for left arm of chromosome 3. The asterisk indicates an EMS-induced mutation.

Table 1: Overview of the screen

Chromosome arm	3L	3R	Sum
Crosses started	739	739	1478
Germ-line clone	654	657	1311
Cuticle preparation	267 (41%)	283 (43%)	550 (42%)
Interesting line (% of germ-line clone)	38 (6%)	54 (8%)	92 (7.0%)
3-star line	5	9	14
2-star line	5	8	13
1-star line	6	11	17

Table 2: List of 3- and 2-star mutation lines

Line Nr.	Stars	Hatching rate (%)	Phenotypes	Mapping position
3R-13	2	50	Gastrulation defect	
3R-15	3	0	Extra division and gastrulation defect	
3L-55	3	0	Extra division and germ-band extension defect	70C9
3R-3C86	3	0	Gastrulation defect	
3R-3D70	3	0	Gastrulation defect	*eclair*/p24
3R-3D71	3	0	Gastrulation defect and nuclear fallout	
3R-3D104	2	40	Nuclear fallout, cellularization defect	
3R-3D117	3	0	Cellularization and gastrulation defect	91F4
3R-3D124	3	0	Syncytial blastoderm defect	
3L-3D172	2	0	Cellularization and gastrulation defect	
3R-3F24	3	0	Nuclear fallout during elongation, extra division	
3R-3F26	2	40	Improper nuclei division	
3R-3G37	2	50	Different variations of phenotypes	

3R3G79	2	0	Germ-band extension defect and extra division	
3L-3G83	3	10	Cellularization defect, extra division	
3R-3G89	2	0	Cellularization and gastrulation defect	98E1/99A1
3L-3G97	3	0	Cellularization defect, no furrow invagination, nuclear fallout	*ensconsin*
3R-3H38	2	0	Germ-band extension defect	
3L-3H53	3	0	Syncytial blastoderm defect	
3L-3H58	2	0	Gastrulation defect	
3R-3H80	2	0	Syncytial blastoderm defect	
3R-3H93	3	0	Extra division and gastrulation defect, nuclear fallout	84E13
3L-3I23	2	0	Preblastoderm defect	
3R-3I26	3	10	Syncytial blastoderm defect	
3L-3I26	2	0	incomplete cellularization, nuclear fallout	
3L-3I34	2	0	Syncytial blastoderm defect	
3L-3I51	3	0	Germ-band extension defect	

2.1.2 Mutagenesis efficiency

I first measured the rate of mutagenesis. As EMS induces mutations that are randomly distributed on the chromosome, the number of lethal hits per each chromosome is according to a Poisson process. To determine the Poisson distribution I measured the number of chromosomes without a lethal mutation, $P(0)$ (zero class). Assuming a Poisson distribution the number of chromosomes with one or more lethal mutations, $P(n)$, $n>0$ and the Sum of $P(0)+P(1)+…+P(n) =1$, can be calculated. Viable homozygous Frt3L Frt3R in one stock were counted as no lethal hit. Otherwise there could be greater than or equal to one lethal hits. The average rate of lethal mutations was estimated according to Poisson distribution. In 259 stocks with mutagenized Frt3L3R chromosomes, which were treated by 35mM EMS, 61 stocks were homozygous viable and referred as $P(0)$ class. The estimated frequency of lethal mutations was 1.45 on average (Fig. 3).
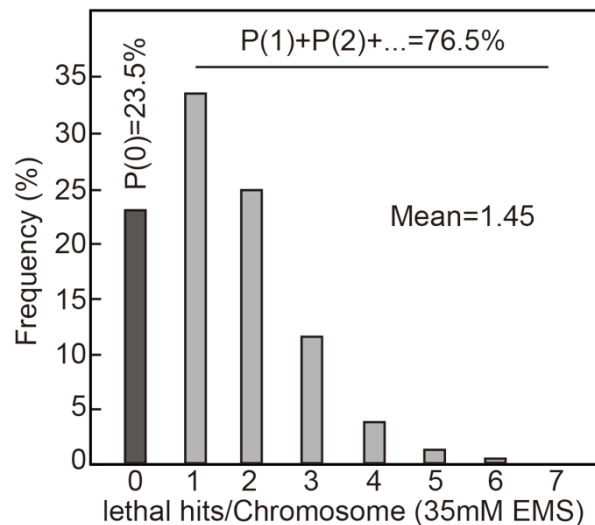
Figure 3: Estimate of mutagenesis frequency. In the graph, the mutagenesis frequency under 35 mM EMS treatment is estimated according to Poisson distribution. The fraction of lethal-free lines on the third chromosome was tested and 61 out of 259 stocks appeared homozygous viability. These 23.5% lethal-free lines are referred as P(0) class, meaning 0 lethal hit on the whole chromosome. Therefore 76.5% lines contain at least one lethal hit. The mean lethal hits per chromosome are 1.45.

2.2 Description of selected mutations: phenotype and mapping

2.2.1 3L-55: Extra division and gastrulation defect

3L-55 germline clone embryos was fully embryonic lethal (0% hatching rate) and did not develop any cuticle material. Time-lapse imaging of embryos from 3L-55 germline clones revealed frequently an extra, 14th, nuclear division cycle in syncytial blastoderm. In contrast to WT, the plasma membrane invagination in 3L-55 germline clone embryos occurred twice, and the first furrow in cycle 14 was aborted after about 30 min. Following mitosis 14, cellularization was reinitiated (Fig. 4A). The invagination in cycle 15 appeared approximately 45 min later than the first one. In

interphase 14, WT embryos process gastrulation that the ventral epidermis extends along the anterior-posterior axis and the pole cells move towards dorsal side. The cephalic furrow forms at the meantime. In 3L-55 germline clone embryos, germ-band extension did not occur and cephalic furrow was not detectable (Fig. 4A). The failure of gastrulation may be a consequence of the extra mitosis and delayed cellularization or due to an independent function of the 3L-55 gene. More detailed time-lapse movies are required to distinguish these options. Cases of 3L-55 with a normal number of mitotic divisions would be informative, as they would reveal if there is a link of extra mitosis and gastrulation defect.

Immunostaining of 3L-55 with cellularization marker Discs large 1 (Dlg, marks lateral domain), pattern formation marker Even skipped (Eve) and DAPI revealed apparent normal until early interphase 14/15. Nonetheless, gastrulation did not initiate in 3L-55 embryos and lateral membrane formation was observed occasionally abolished at anterior-posterior side of the embryo in late interphase 14/15 (Fig. 4B). Staining with Eve antibody revealed seven elevated stripes but the boundaries were not as sharp as WT. This indicates that onset of zygotic gene expression is functional and the pair-rule gene pattern is established in 3L-55.

In order to identify the mutation that causes these abnormal phenotypes, 3L-55 was mapped and the mutation was narrowed down to 58,326 bp in 70C9 cytogenetic region. There are four genes and five unannotated codon in this region (Fig. 5). Among them, *Meiotic central spindle* (*Meics*) and *short spindle 2* (*ssp2*) appear high possibility because of the expression profile of *Meics* is moderate in both early embryo and female ovary, while *Ssp2* expresses moderately high in female ovary (High-throughput expression data from http://flybase.org/, the same below).

2.2.2 3R-3D70: Gastrulation defect

Embryos from 3R-3D70 germline clones developed normally until mid-cellularization but failed to gastrulate. Following a normal cellularization, attempt for gastrulation did not initiate. No germ-band extension, cephalic furrow or stomodeal invagination was observed in this mutant (Fig. 6). Embryonic development was completely lethal (Hatching rate was 0%) and partial cuticles formed denticle belts.
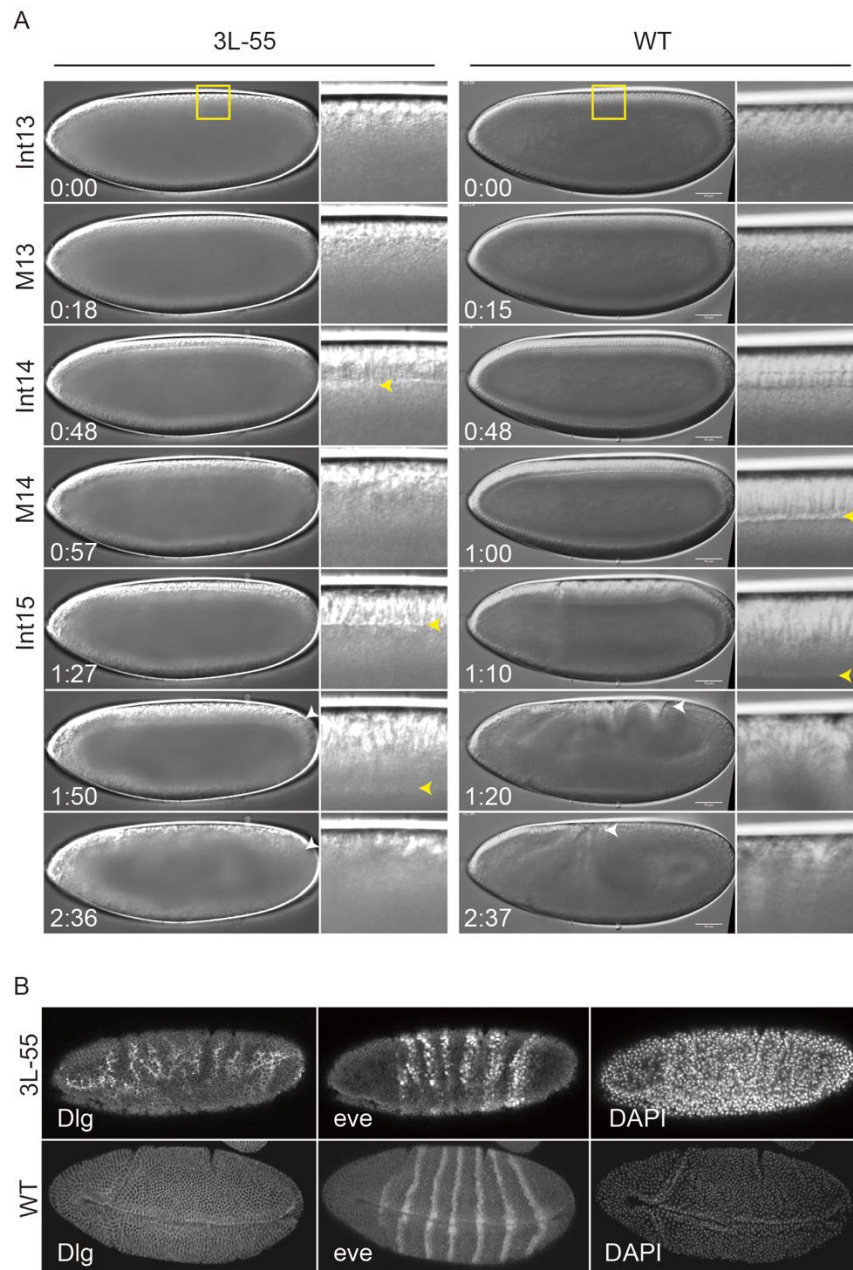
Figure 4: Phenotype of 3L-55 germline clone embryos. (A) Development of WT and 3L-55 embryos were imaged by DIC microscopy. Imaging of the whole embryos show 3L-55 undergoes additional syncytial nuclear division, and furrow invagination initiates twice. Compared with WT, germ-band extension and cephalic furrow do not occur. M: mitosis. Int: interphase. Magnified region is depicted in yellow box. Yellow arrow heads point to the invaginating membrane front. White arrow heads point to pole cells. Scale bar represents 50 μm. (B) Immunostaining of fixed 3L55 embryos with Dlg, Eve and DAPI. Cellularization appeared normally in early interphase 14/15, whereas in late interphase 14/15, Dlg staining occasionally abolished at anterior-posterior sides. Eve is located within seven stripe-like patterns, but the boundaries were not as sharp as WT.

The lethality and embryonic phenotype were mapped to 85E4 region (Fig. 7). The mapped region comprises 16 genes including *eclair* and *p24-2*, which may be candidate mutations. The phenotype of *p24/eclair* germline clones is very reminiscent of the 3R-3D70 (Bartoszewski et al. 2004). *Eclair* has moderate expression level in early embryo and moderately high in female ovary, whereas very low expression level of *p24-2* in both early embryo and adult ovary. Further complementary confirmation is needed.
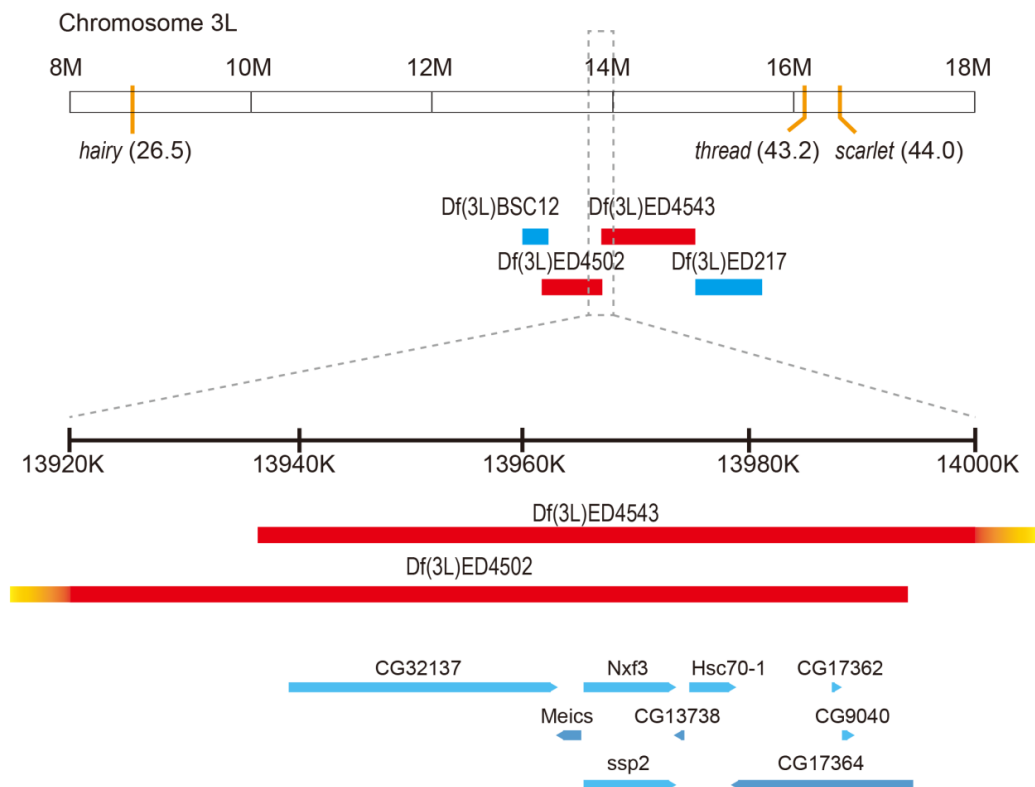
Figure 5: Mapping of 3L-55. The 3L-55 line was mapped by meiotic recombination and deficiencies on the left arm of chromosome 3. Cytological positions, gene names and deficiency fly lines are indicated. From lethality of recombinant flies with different recessive visible markers, the position of 3L-55 was restricted between *hairy* and *thread*. Deficiency lines Df(3L)ED4543 and Df(3L)ED4502 did not complement the lethality of 3L-55. Overlapping region is 58,326 bp and contains 9 genes. The deficiencies which successfully complemented are depicted in blue, which failed to complement are depicted in red. Deficiencies end out of the frame are depicted in smeared red.
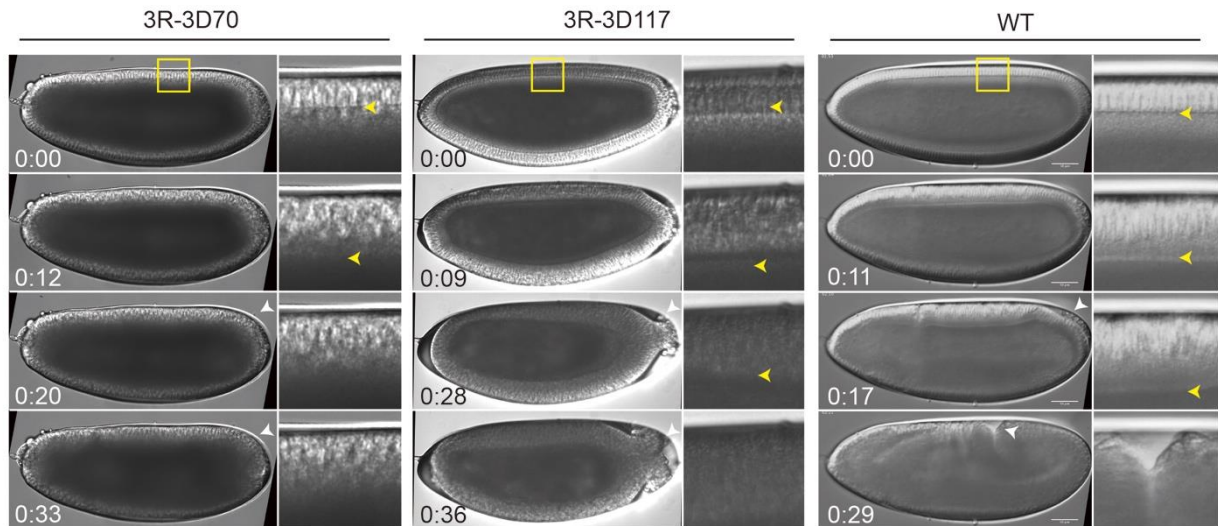
Figure 6: Phenotypes of 3R-3D70 and 3R-3D117 germline clone embryos. 3R-3D70 embryos complete cellularization apparent normally but fail to initiate gastrulation. Embryos from 3R-3D117 germline clone show premature stopped cellularization and absence of gastrulation. The phenotype is reminiscent to terminal mutants. Magnified view on the cortical part of the embryo is depicted in yellow box. Yellow arrow heads point to the invaginating membrane tips. White arrow heads point to pole cells. Scale bar represents 50 µm.

2 Results
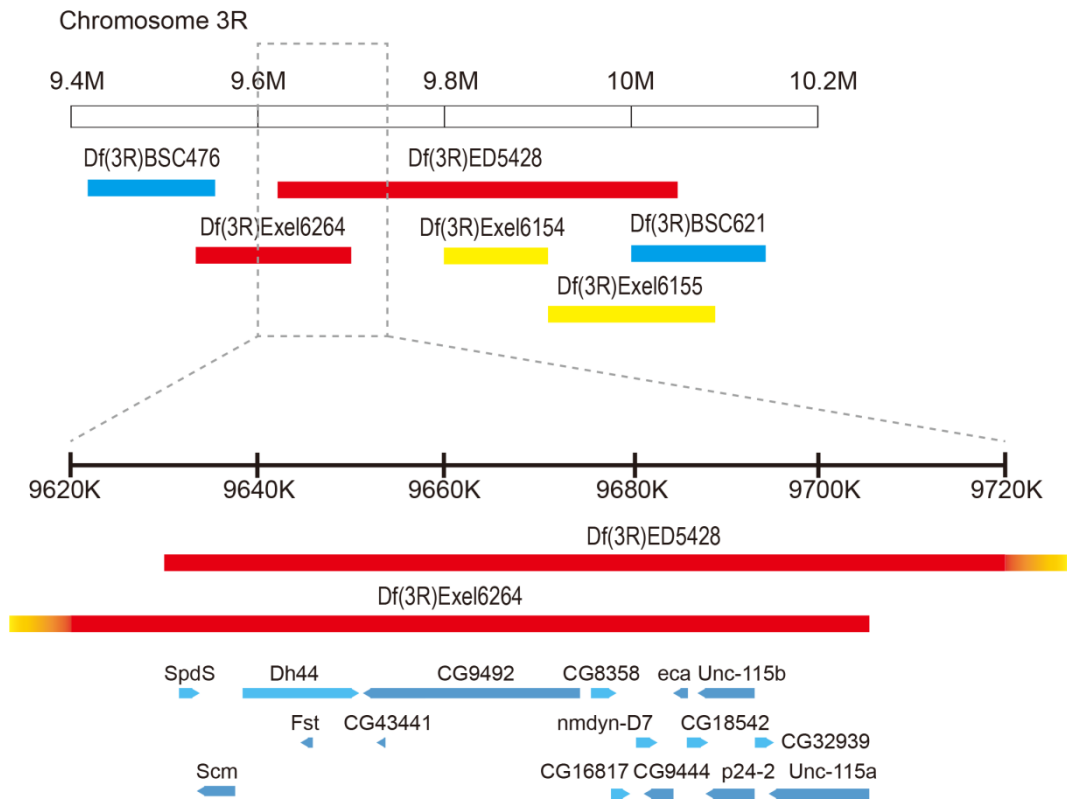
Figure 7: Mapping of 3R-3D70. Meiotic recombination with different recessive visible markers revealed the position of 3R-3D70 was between centromere and *curled*. Deficiency lines on the right arm of chromosome 3 Df(3R)Exel6264 and Df(3R)ED5428 failed to complement the sterility. When crossing 3R-3D70 with Df(3R)Exel6154 and Df(3R)Exel6155 the progenies were also sterile and laid defective eggs, but the breakpoints of Df(3R)Exel6154 and Df(3R)Exel6155 chromosomes do not overlap. Overlapping of Df(3R)Exel6264 and Df(3R)ED5428 comprises 16 genes. The deficiencies which successfully complemented are depicted in blue, which failed to complement are depicted in red. Df(3R)Exel6154 and Df(3R)Exel6155 are depicted in yellow.

2.2.3 3R-3D117: Gastrulation defect

Embryos of 3R-3D117 showed a gastrulation phenotype with 0% hatching rate similar to 3R-3D70. Cellularization initiated normally and nuclei elongated properly. However furrow invagination seems to stop premature so that nuclei might not be enclosed completely. Gastrulation did not occur and pole cells failed to shift their positions in well-organized group, eventually messed up the developmental process (Fig. 6). The phenotype is reminiscent to terminal mutants, such as *torso*.

- 16 -

The mutation was located in a ~40,000 bp region containing *squeeze* (*sqz*), CG14282, CG5555 and CG31475 (Fig. 8). *Squeeze* is most likely the candidate, since the expression profile is either high or moderate in early embryo and ovary. Previous studies showed Squeeze is a zinc-finger transcription factor which has function in wing development and leucokinergic neurons specification (Herrero et al. 2007; Terriente Felix et al. 2007). So far, however, no report concerns function of *squeeze* in blastoderm formation.
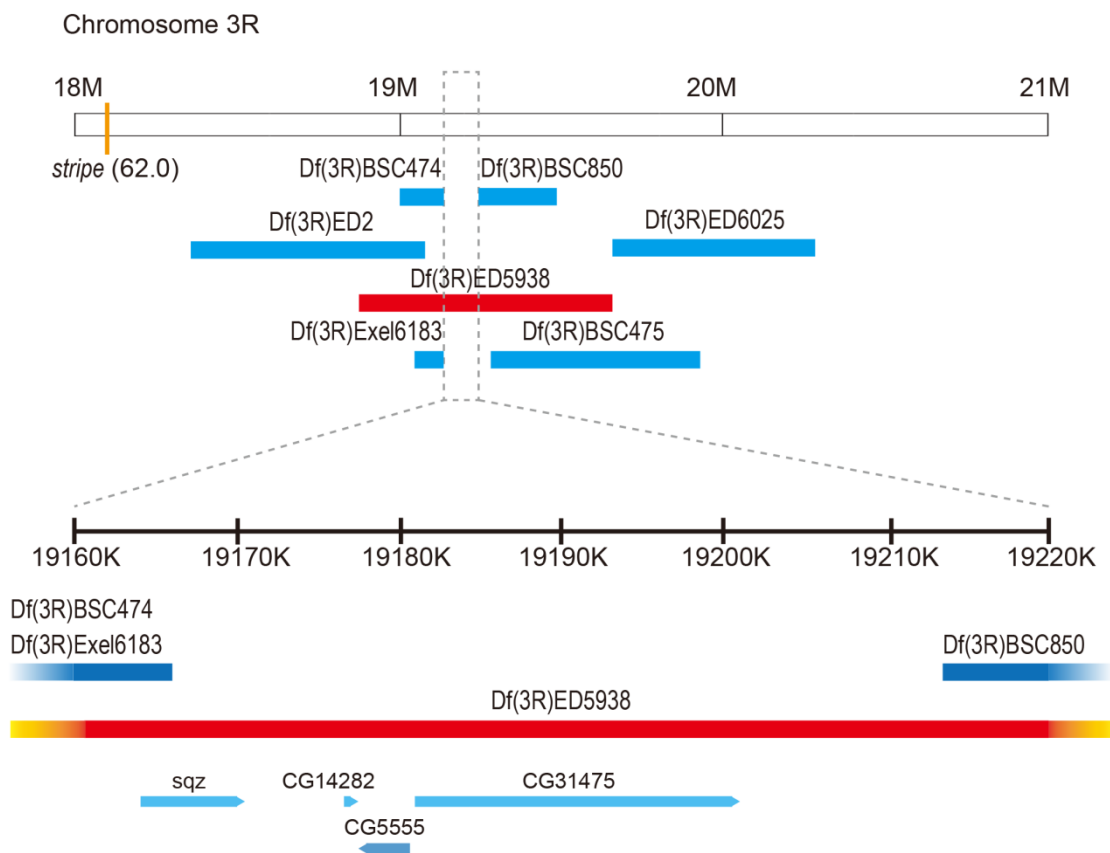
Figure 8: Mapping of 3R-3D117. Recombinant test narrowed the position of 3R-3D117 to *stripe* and *ebony*. Deficiencies covering this region were used and Df(3R)ED5938 was not able to complement the lethality. The 3R-3D117 mutation was further restricted by subset of deficiencies which have breakpoints covered by the Df(3R)ED5938. The region 3R:19,165,783–3R:19,212,136 which are not covered by these deletions may comprise the gene. *squeeze* is considered to be the candidate mutation. The deficiencies which successfully complemented are depicted in blue, which failed to complement are depicted in red.

2.2.4 3L-3G97: Cellularization defect, no furrow invagination

Embryos from 3L-3G97 germline clones showed a cellularization defect. Following normal development until early interphase 14, when the nuclei elongated comparably to WT, the ingression of the furrow failed so that single blastoderm nuclei were not able to be separated. With absence of cytokinesis, nuclei morphology started to be misshaped and group nuclei were disorganized at 30–40 min of interphase 14. Individual nucleus appeared to fall into the yolk which is referred as "nuclear fallout", and then the whole dorsal epidermis eventually lost their arrangement (Fig. 9). The phenotype is very reminiscent to *Slam* and *Kinesin1* (Acharya et al. 2014; Winkler et al. 2015). 3L-3G97 did not complement an *ensconsin* mutant *ens* [Δ3277] (Sung et al. 2008). Therefore, 3L-3G97 represents a new allele of *ensconsin*.
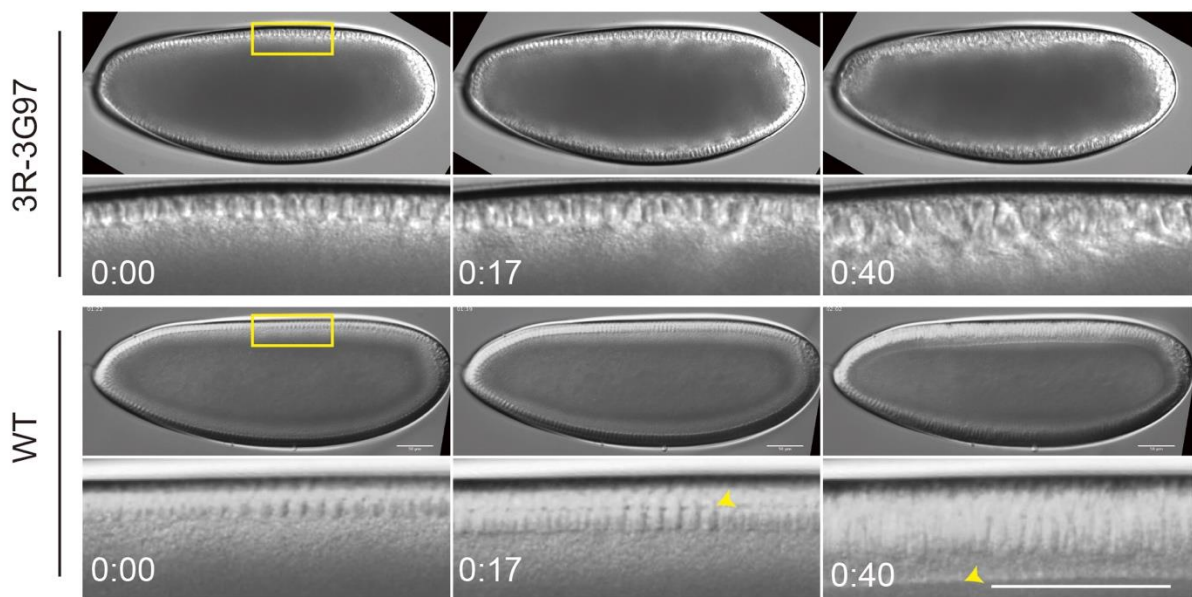
Figure 9: Phenotype of 3R-3G97 germline clone embryos. At the onset of interphase 14, the ingression of the membrane furrow fails so that the cellularization does not occur. Nuclear fallout appears corresponding with nuclei morphology misshapes. Embryos stop development 30–40 min after interphase 14. Magnified view on the cortical part of the embryo is depicted in yellow box. Yellow arrow heads point to the invaginating membrane front. Scale bar represents 50 μm.

2.2.5 3R-3H93: Extra division and gastrulation defect

3R-3H93 was classified in the same group as 3L-55, but the phenotype was not all identical (Fig. 10). The hatching rate of 3R-3H93 was 0% and loss of cuticle material. Embryos from 3R-3H93 germline clones exhibited abnormalities already prior mitosis 13 that nuclear fallout was observed occasionally. Later on, 40% embryos (N=11) underwent partially additional mitosis 14. Following cellularization, cephalic furrow was formed but pole cells did not move dorsalwards. Therefore gastrulation failed to complete and the embryos stopped developmental processes.

Mapping defined the region 84E13 with 11 genes (Fig. 11), among them 5 may be potential candidates: *puckered*, CG9667 and *GTPase indispensable for equal segregation of chromosomes* (*Gie*) express moderate in both early embryo and ovary; CG7878 and *transcriptional Adaptor 2b* (*Ada2b*) show very high expression level in early embryo and moderate expression in female ovary.
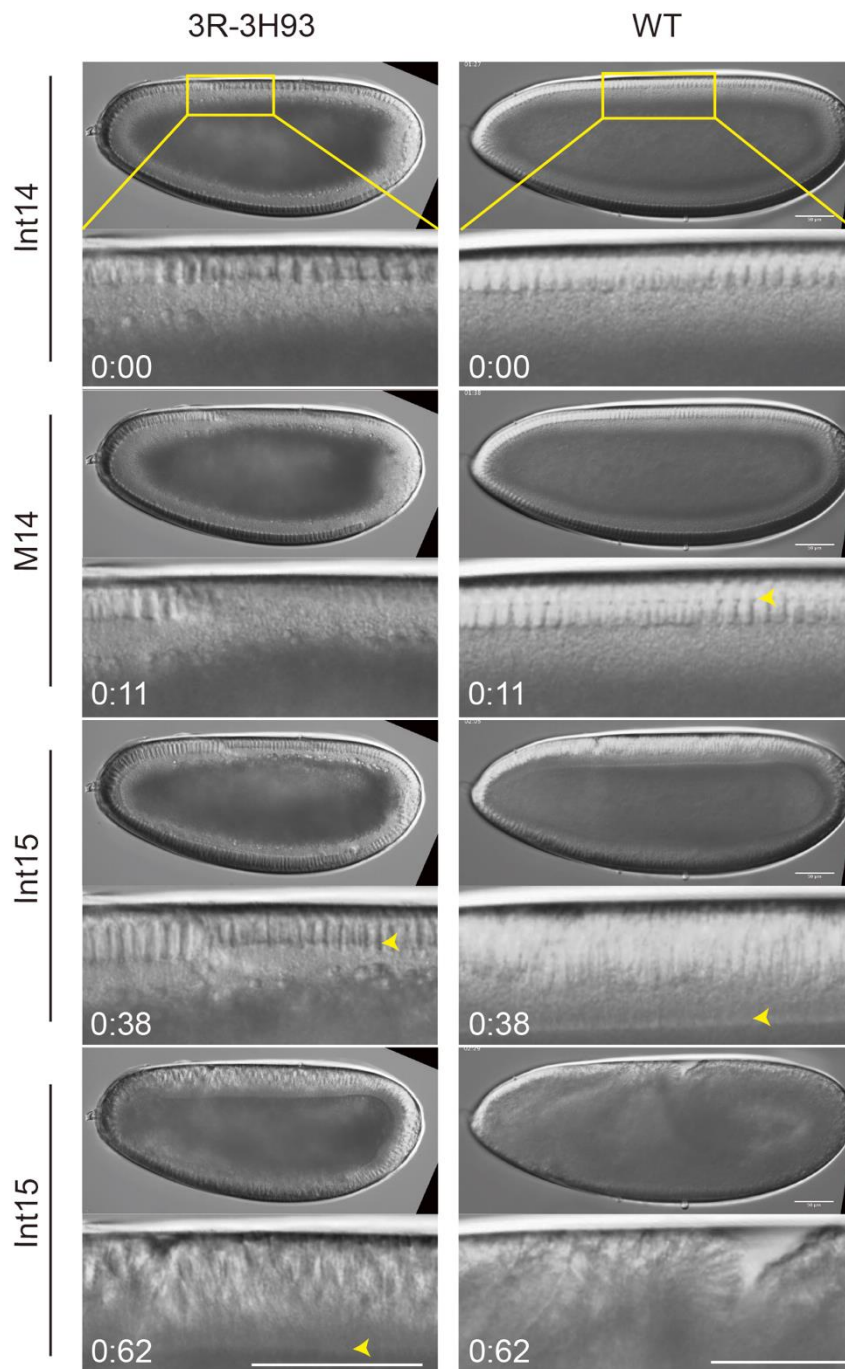
Figure 10: Phenotype of 3R-3H93 germline clone embryos. Partial extra mitosis is shown in this embryo. Obvious nuclear fallout is observed occasionally before mitosis 13, and approximately 40% embryos undergo additional mitosis division cycle. Cephalic furrow is formed but germ-band extension does not occur. M: mitosis. Int: interphase. Magnified region is depicted in yellow box. Yellow arrow heads point to the invaginating membrane front. Scale bar represents 50 μm.
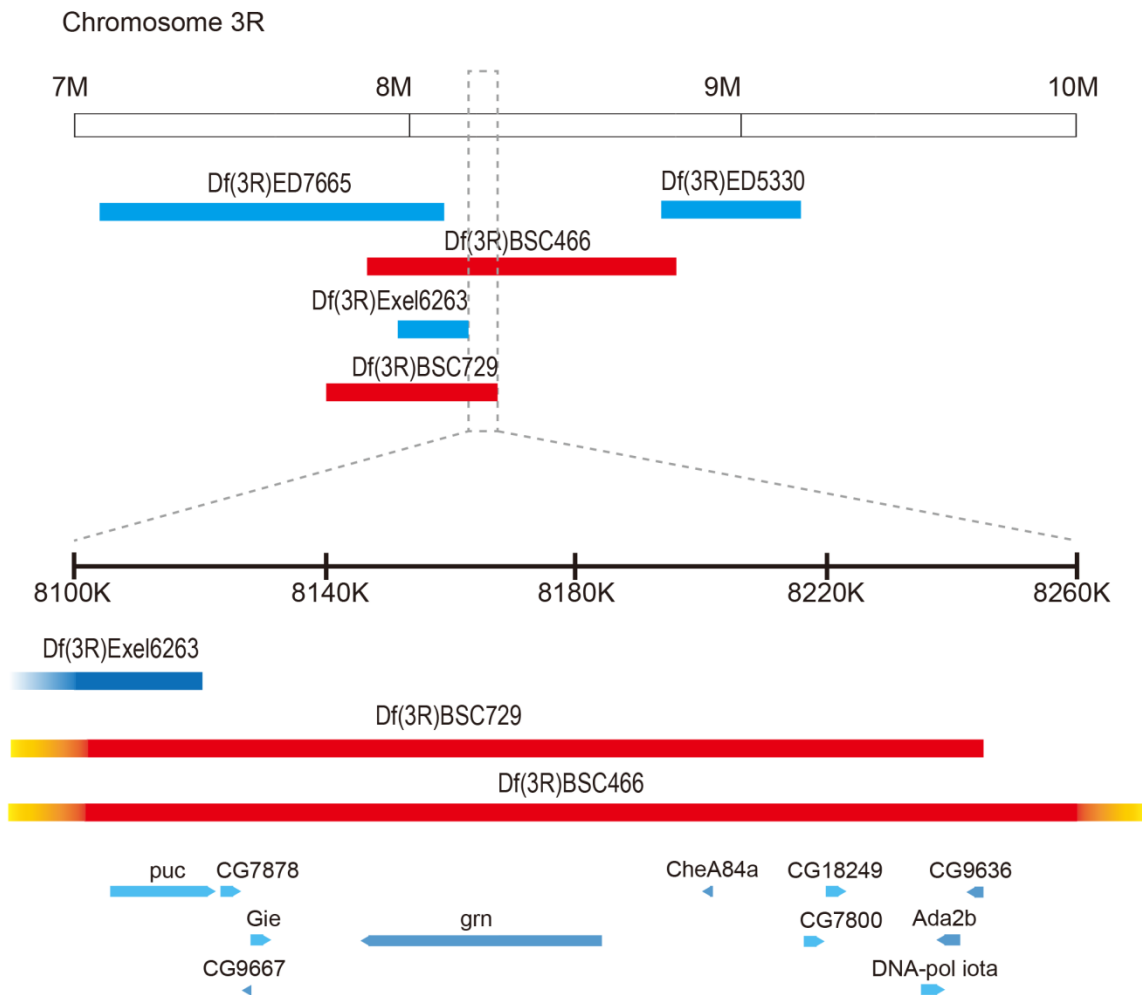
Figure 11: Mapping of 3R-3H93. The mutation responsible for maternal lethal phenotype is mapped between centromere and *curled*. The lethality of 3R-3H93 did not complement by Df(3R)BSC466. Smaller deficiencies were used and Df(3R)BSC729 also failed to complement the lethality. Overlapping of Df(3R)BSC466 and Df(3R)BSC729 contain 11 genes. The deficiencies which successfully complemented are depicted in blue, which failed to complement are depicted in red.

3 Discussion

Mutagenesis screen is a powerful tool to identify new genes and novel function of known genes. It is utilized widespread among model organisms as a genetic approach to identify critical, and often unexpected, regulators of biological processes. Furthermore, phenotypic information of *Drosophila* mutations from EMS-induced germline clone screen was even able to help for studying human genetic disease mechanisms (Haelterman et al. 2014; Yamamoto et al. 2014).

Roughly 4,000–5,000 genes in *Drosophila* are expected to have functions in early blastoderm formation (De Renzis et al. 2007; Thomsen et al. 2010). These gene products are mainly maternally supplied and fundamentally required during early embryogenesis. Absence of these maternal products lead to very early embryonic aberrance: eggs can be laid normally with proper size and shape, majority of which are possible to fertilize and initiate development, but ultimately have problems and stop developing. Traditional screens identified genes involved in pattern formation and segmentation by detecting denticle belts of cuticles, but those approaches missed early essential genes which cause lethality before segmentation occurs, leading cuticle-less phenotypes.

Germline clone screens for cuticle-less mutants have been performed for X, second and third chromosomes previously, and many maternal and essential genes involved blastoderm formation of *Drosophila* embryogenesis have been identified (Schnorrer et al. 2002; Yohn et al. 2003; Vogt et al. 2006). To this end, however, there is still a lack of saturated screen on chromosome 3 so far, which contains approximately 40% of the whole genome. In this study, we conducted EMS-induced mutagenesis and germline clone screen, and aimed to identify novel maternal and essential genes on chromosome 3.

We achieved 739 mutagenesis stocks and set up 1,311 germline clones on both left and right arms of chromosome 3. Approximately 23.5% of stocks with 35mM EMS were lethal-free on both of the third chromosomal arms. Based on Poisson distribution, 60% of the stocks contain one or two lethal hits and the mean frequency was 1.45, meaning most of the mutation stocks have at least one lethal mutation on either left or right arm of the chromosome 3. The mutation caused phenotype was

recorded by means of time-lapse imaging, and 14 lines were defined as 3-star with high penetrance and invariant phenotype; 13 lines which were defined as 2-star with high penetrance but variant phenotypes.

Analyse of the imaging movies revealed highly interesting lines which were classified into different groups including preblastoderm defect, syncytial blastoderm defect, cellularization defect, gastrulation/germ-band extension defect and extra/fewer mitotic division. Most of the 3- and 2- star lines (77%) do not hatch to larval stage, yet few of them still showed 10–50% hatching rate. These hatched cases may be due to zygotic rescue that mutation genes were expressed from fathers' WT compensatory chromosomes. We did not trace the lifespan of hatched larvae as we only focused on early embryogenesis. Our screen was not possible to detect mutations with early developmental defect but do not emerge immediate effect. For instance *maternal haploid* (*mh*) has hypomorphic allele that is viable. We would miss such cases due to the lethality criteria.

The mapping procedure of 3- and 2- star lines has not been completed yet. So far, two genes *eclair* (*eca*) and *ensconsin* (*ens*) were identified by complementation test. Both of these genes have been studied in early embryonic development previously (Bartoszewski et al. 2004; Winkler et al. 2015), and our screen provides new alleles whatsoever. By means of this study, genes with essential function in blastoderm formation were detected according to their phenotypes, and we expect more novel loci or novel function of known genes will be identified through subsequent mapping and sequencing.

4 Materials and methods

4.1 Materials

4.1.1 Fly stocks

Table 3: Fly stocks used in this study

Name	Genotype	Source
Frt3L Frt3R	Frt3L[2A,79D]{w+} Frt3R[82B]{neoR}	Luschnig lab
BCMT	btl-Gal4 UAS-Serp-CBD-GFP UAS-myr-tdTomato; *Ly* hs-hid/TM6B Dfd-YFP	Luschnig lab
ovo3L	*w*; ovoD3L{w+} Frt3L[2A, 79D]{w+] / *ru st* betaTub85D[D] *ss e[s]* / TM3, *Sb* hs-hid	Grosshans lab
ovo3R	*w*; Frt3R[82B]{neoR} P{ovoD1-18}3R / *st* betaTub85D[D] *ss e[s]* / TM3, *Sb* hs-hid	Grosshans lab
Dr/TM3 hs-hid	*y w*; *Pr Dr* /TM3, *Sb* hs-hid{w+}	Grosshans lab
TM3 TM6B	*w*; TM3, *Sb Ser* / TM6B, *Tb Hu*	Grosshans lab
Frt3L	*w*; *ru h th st* Frt3L[2A,79D] (w-)	generated in this study
Frt3R	*y w* Flp122{ry+} ; Frt3R[82B]{neoR} *cu sr e[s] ca*	Bloomington Drosophila Stock Center
ruPrica	*ru h th st cu sr e[s] Pr ca* / TM2	Tübingen collection
ubi-RFP, *ens*	P{Ubi-RFP}/*CyO*; *ens*[swo]/TM6 *Tb*	Rørth lab
Deficiencies on 3rd chromosome	-	Bloomington Drosophila Stock Center

4.1.2 Reagents

Table 4: Solutions used in this study

Name	Composition
EMS-sucrose solution	25–35 mM Ethyl methanesulfonate (Sigma-Aldrich) 1% sucrose
EMS inactivating solution	0.1 M NaOH 0.5% Thioglycolic acid
Hoyer's mountant	30 g gum arabic 200 g chloral hydrate 20 g glycerol 50 ml ddH$_2$O in working solution add lactic acid as 1:1

4.1.3 Antibodies

Table 5: Primary antibodies used in this study

Antibody	Raised in	Dilution / working concentration	Source
Discs large 1 (Dlg)	Mouse	1:100 (~0.4 µg/ml)	Hybridoma Bank 4F3
Even skipped (Eve)*	Guinea pig	1:1,000	Grosshans lab

* Serum

Alexa-conjugated secondary antibodies for immunostaining were purchased from Life Technologies /Invitrogen and used at a dilution of 1:500 (4 µg/ml). DAPI (4',6-Diamidino-2-phenylindole dihydrochloride) was obtained from Sigma-Aldrich and used as DNA staining dye at a working concentration (0.2 µg/ml).

4.2 Methods

4.2.1 Mutagenesis

100–150 male adult flies with an isogenized Frt3L Frt3R homozygous chromosome were collected into empty bottle and hungered for 6 h, and then feed with 25–35mM

EMS-sucrose solution for 14 h (Armbruster PhD dissertation 2011). The EMS-sucrose solution was prepared by mixing EMS liquid into 1% sucrose, and pumping by syringe for ten times until the dense oily EMS liquid had dissolved. After feeding, all EMS solutions and contaminated pipets and tubes were soaked with equal volume of EMS inactivating solution for 24 hours prior to disposal. Males were transferred into new bottle with wet filter paper for cleaning. After 5–6 h males were transferred into fresh food bottle and crossed to virgin females carrying BCMT; Lyra heat shock-head involution defective (Ly hs-hid)/TM6B at 25°C. Approximately 100 mutagenized males were mated to 200–300 virgin females. Males were removed after four days because mutagenized germline stem cells can appear as clonal mutations in spermatocyte (Greenspan 2004). Females were transferred to fresh bottle every two days. Progenies were heat-shocked in first instar larval stage to eliminate Ly hs-hid genotype and to allow only mutated Frt3L Frt3R/TM6B genotype to survive, which were then used for following crossing scheme (Fig. 2A).

4.2.2 Crossing scheme

Single F1 male was crossed with 4–6 BCMT; Ly hs-hid/TM6B virgin females (Fig. 2A). Adults were removed after four days and crosses were heat-shocked three times of 150 min each on three consecutive days, to eliminate all non-balanced progeny carrying the Ly hs-hid chromosome. F2 progeny were transferred to new vials to establish stocks. Stocks were labelled and kept for further analysis.

To set up germline clones, females from established stocks carrying balanced mutation points Frt3L Frt3R/TM6B were crossed with corresponding males containing ovo^D3L Frt3L/TM3 hs-hid or ovo^D3R Frt3R/TM3 hs-hid chromosomes (G0) (Fig. 2B). F1 progenies in first instar larval stage were heat-shocked twice of 30–40 min each in two days and cultured at 25°C. After heat-shock-induced recombination occurred between two Frt sites, mosaic offspring were generated with heterozygous Frt3L Frt3R/ovo^D soma and homozygous Frt3L Frt3R germline from germline clone (St Johnston 2002). F1 mosaic females can be mated with any genotype of males as it is assumed zygotic genome does not have extensive effect during syncytial blastoderm stage. F2 embryos from these mosaic females were collected and analysed (Fig. 2B). For one stock, germline clones were induced on both chromosome 3L and 3R arms.

4.2.3 Screening procedure

Primary screen was carried out by using the block-agar method (Wieschaus and Nüsslein-Volhard 1998). In G0, 2–3 females were crossed with 2 males in small food vials, and heat-shocked twice to induce germline clone (Fig. 2B). 5 females from F1 were crossed with 2 males in each blocks and cultured at 25°C. Egg laying and hatching rate were scored under stereomicroscope. If hatching rate is under 50%, unhatched embryos were collected and dechorionated in 50% Klorix bleach for 90 s, and then washed with distilled water and dried properly. Dechorionated embryos were transferred on glass slides and covered by Hoyer's mountant. The slides were incubated in 60°C oven for 6–8 h and ready to score. Cuticles were viewed by stereomicroscope under dark field to score overall cuticle pattern, under phase contrast to observe subtle details. The primary screen for each germline clone was repeated to confirm the phenotypes. Some germline clones with weak or inconsistent phenotypes were repeated twice.

The criteria of primary screen in this study were egg laying ≥3 per 5 females per 12 h; hatching rate ≤ 50%; cuticle showed empty, unstructured or early embryonic defect phenotypes, with low variance. Stocks over primary screen criteria were kept for the retest screen. In retest crosses were amplified with 3 males and 5–10 females, transferred four times and heat-shocked twice for each vial. F1 females were crossed with males into small cage with medium plate. F2 eggs were collected from the plates for the analysis.

4.2.4 Phenotypic detection

Spinning Disk microscope was used to record time-lapse imaging of embryonic development in retest. Live-imaging with differential interference contrast (DIC) optics and 25× water immersion objectives were utilized with a light intensity of 2.5–3.0 V, an exposure time of 80–100 ms and a frame interval of 1 min.

Interested candidate lines from the primary and retest screens were implemented immunostaining by specific antibodies depending on defined phenotypes, and observed under confocal microscope LSM780.

4.2.5 Complementation test and mapping

Mutants were classified according to their phenotypes. Mutations on respective chromosome arm within the same classification and showed a similar phenotype were crossed to each other or to suspected known alleles. Trans-heterozygous F1 generation of these crosses were tested for lethal complementation.

Non-complementation lines were subsequently mapped by meiotic recombination with Frt3L or Frt3R mapping lines (Fig. 12). The mapping lines carry multiple recessive marker mutations (*roughoid*, *hairy*, *thread*, *scarlet* and *white-* on the left arm; *curled*, *stripe*, *ebony*, and *claret* on the right arm) with visible phenotypes on chromosome 3. After crossing females from mutation stocks with males from mapping lines, F1 females with mutated Frt3L/ *ru h th st* Frt *w-* or Frt3R/ *cu sr e[s] ca* were mated with "ruPrica" (*ru h th st cu sr e[s] Pr ca*) males, which carries a dominant marker *Prickly* along with all recessive markers (Fig. 12A). Meiotic recombination occurs randomly during F1 females' first meiotic division between recessive markers, and the frequency of recombination is dependent on chromosomal distance of each locus (Orr-Weaver 1995) (Fig. 12B and 12C). Single recombinant F2 males recombination/ruPrica were crossed back to G0 females, and then viability and female sterility can be detected in F3 generations (Fig. 12A). If flies with recombination/Frt3L Frt3R genotype are lethal, mutation points may present within the region where recessive marker is missing. Therefore, mutation point can be narrowed down into smaller distance between two markers.

Phenotypes were confirmed by inducing germline clone of recombinant stock. For cytological mapping recombinant stocks showed the same phenotypes as screen were crossed to the third chromosome deficiency kits. Deficiencies which failed to complement recombinant stocks were replaced by overlapping smaller deficiencies. After 2–3 rounds the candidate genes were narrowed down among defined region, and then were sequenced for identification.
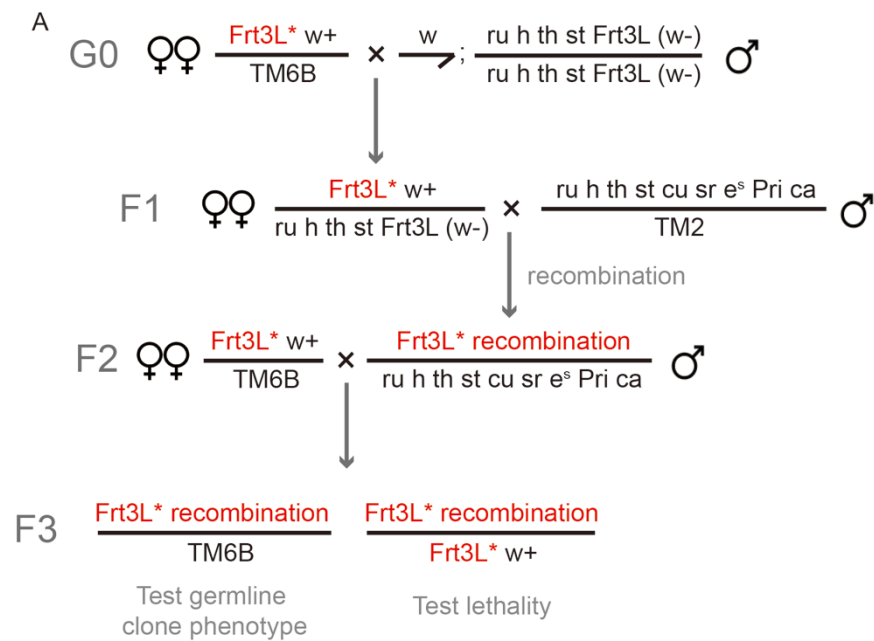
Figure 12: Mapping scheme of chromosome 3. (A) Crossing scheme exemplified for left arm of chromosome 3. The 3L mapping line carries 5 recessive markers including *roughoid* (*ru*), *hairy* (*h*), *thread* (*th*), *scarlet* (*st*) and *white-* (*w-*). Recombination occurs randomly during F1 female's first meiotic division between recessive markers, so the F2 single males carry different recombinant chromosomes with corresponding visible phenotypes. Single recombinant F2 males were crossed back to G0 females, and then lethality and germline clone phenotype can be detected in F3 embryos.
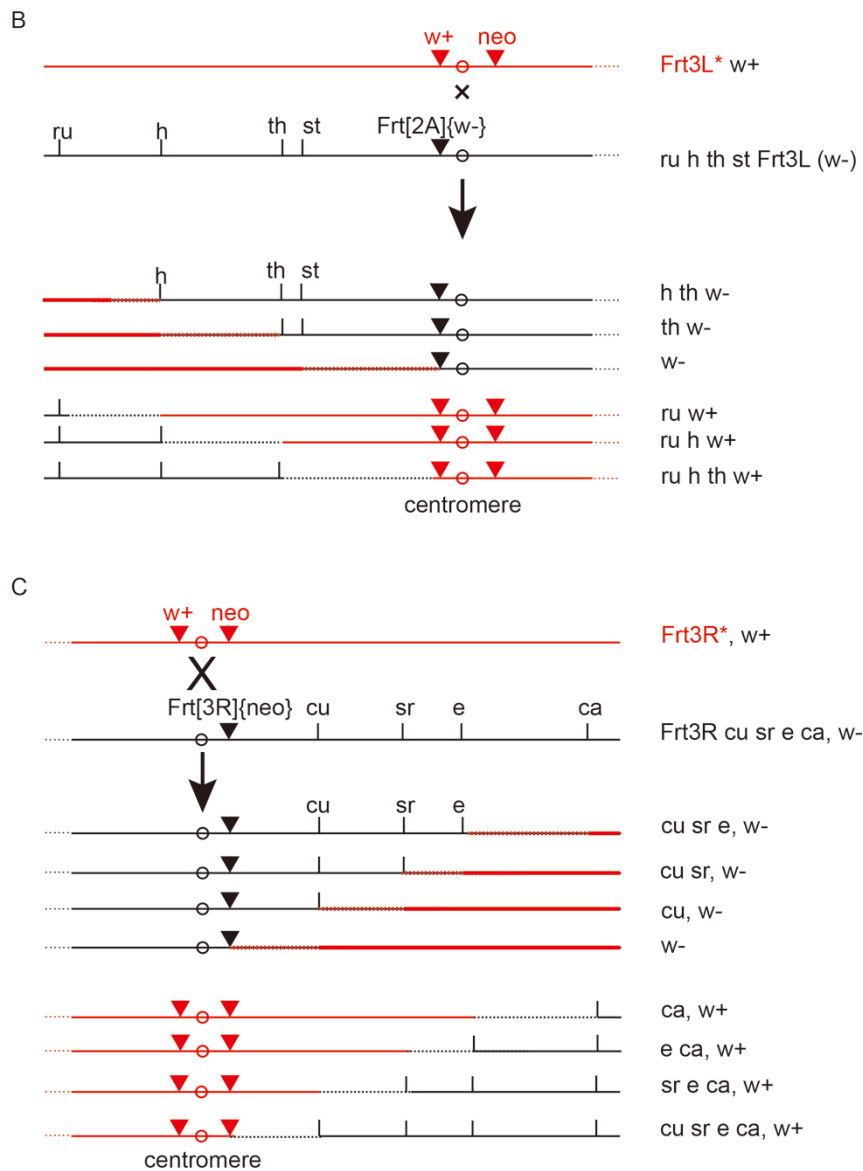
Figure 12-continuation: Mapping scheme of chromosome 3. (B and C) Schematic diagram of meiotic recombination. (B) Meiotic recombination on left arm of chromosome 3. After the recombination, F2 males may have six different genotypes according to recombinant positions. By analyzing the phenotypes, mutations are narrowed down into smaller distance between two markers. (C) Meiotic recombination on right arm of chromosome 3, where mapping line carries *curled* (*cu*), *stripe* (*sr*), *ebony* (*e*) *and claret* (*ca*). In both B and C we show the possibility that only one recombination happens. Practically chromosomes can recombine multiple times.

Bibliography

Acharya S, Laupsien P, Wenzl C, Yan S, Grosshans J. 2014. Function and dynamics of slam in furrow formation in early Drosophila embryo. *Dev Biol* **386**: 371-384.

Adams MD Celniker SE Holt RA Evans CA Gocayne JD Amanatides PG Scherer SE Li PW Hoskins RA Galle RF et al. 2000. The genome sequence of Drosophila melanogaster. *Science* **287**: 2185-2195.

Armbruster K. 2011. Genetic Control of Epithelial Tube Expansion in Drosophila melanogaster. PhD Dissertation, p. 125. Universität Zürich.

Bartoszewski S, Luschnig S, Desjeux I, Grosshans J, Nusslein-Volhard C. 2004. Drosophila p24 homologues eclair and baiser are necessary for the activity of the maternally expressed Tkv receptor during early embryogenesis. *Mech Dev* **121**: 1259-1273.

Blumenstiel JP, Noll AC, Griffiths JA, Perera AG, Walton KN, Gilliland WD, Hawley RS, Staehling-Hampton K. 2009. Identification of EMS-induced mutations in Drosophila melanogaster by whole-genome sequencing. *Genetics* **182**: 25-32.

Chou TB, Noll E, Perrimon N. 1993. Autosomal P[ovoD1] dominant female-sterile insertions in Drosophila and their use in generating germ-line chimeras. *Development* **119**: 1359-1369.

Chou TB, Perrimon N. 1996. The autosomal FLP-DFS technique for generating germline mosaics in Drosophila melanogaster. *Genetics* **144**: 1673-1679.

De Renzis S, Elemento O, Tavazoie S, Wieschaus EF. 2007. Unmasking activation of the zygotic genome using chromosomal deletions in the Drosophila embryo. *PLoS Biol* **5**: e117.

Greenspan RJ. 2004. *Fly Pushing: The Theory and Practice of Drosophila Genetics*. Cold Spring Harbor Laboratory Press, New York.

Grigliatti T. 1998. Mutagenesis. In *Drosophila: A Practical Approach*, (ed. DB Roberts), pp. 55-83. IRL Press, Oxford University Press.

Haelterman NA, Jiang L, Li Y, Bayat V, Sandoval H, Ugur B, Tan KL, Zhang K, Bei D, Xiong B et al. 2014. Large-scale identification of chemically induced mutations in Drosophila melanogaster. *Genome Res* **24**: 1707-1718.

Herrero P, Magarinos M, Molina I, Benito J, Dorado B, Turiegano E, Canal I, Torroja L. 2007. Squeeze involvement in the specification of Drosophila leucokinergic neurons: Different regulatory mechanisms endow the same neuropeptide selection. *Mech Dev* **124**: 427-440.

Jia D, Soylemez M, Calvin G, Bornmann R, Bryant J, Hanna C, Huang YC, Deng WM. 2015. A large-scale in vivo RNAi screen to identify genes involved in Notch-mediated follicle cell differentiation and cell cycle switches. *Sci Rep* **5**: 12328.

Jürgens G, Wieschaus E, Nüsslein-Volhard C, Kluding H. 1984. Mutations affecting the pattern of the larval cuticle in Drosophila melanogaster II. Zygotic loci on the third chromosome. *Wilhelm Roux's Archives of Developmental Biology* **193**: 283-295.

Bibliography

Laurencon A, Orme CM, Peters HK, Boulton CL, Vladar EK, Langley SA, Bakis EP, Harris DT, Harris NJ, Wayson SM et al. 2004. A large-scale screen for mutagen-sensitive loci in Drosophila. *Genetics* **167**: 217-231.

Lewis E, Bacher F. 1968. Method of feeding ethyl methanesulfonate (EMS) to Drosophila males. *Drosophila Information Service* **43**: 193.

Luschnig S. 2000. Genetische Suche nach neuen Komponenten der achsenbildenden Systeme im Embryo von Drosophila melanogaster. In *VVB Laufersweiler Verlag*, PhD Dissertation, p. 77. Eberhard-Karls-Universität Tübingen.

Luschnig S, Moussian B, Krauss J, Desjeux I, Perkovic J, Nusslein-Volhard C. 2004. An F1 genetic screen for maternal-effect mutations affecting embryonic pattern formation in Drosophila melanogaster. *Genetics* **167**: 325-342.

Nüsslein-Volhard C, Frohnhofer HG, Lehmann R. 1987. Determination of anteroposterior polarity in Drosophila. *Science* **238**: 1675-1681.

Nüsslein-Volhard C, Wieschaus E. 1980. Mutations affecting segment number and polarity in Drosophila. *Nature* **287**: 795-801.

Nüsslein-Volhard C, Wieschaus E, Kluding H. 1984. Mutations affecting the pattern of the larval cuticle in Drosophila melanogaster I. Zygotic loci on the second chromosome. *Wilhelm Roux's Archives of Developmental Biology* **193**: 267-282.

Orr-Weaver TL. 1995. Meiosis in Drosophila: seeing is believing. *Proc Natl Acad Sci U S A* **92**: 10443-10449.

Parks AL, Cook KR, Belvin M, Dompe NA, Fawcett R, Huppert K, Tan LR, Winter CG, Bogart KP, Deal JE et al. 2004. Systematic generation of high-resolution deletion coverage of the Drosophila melanogaster genome. *Nat Genet* **36**: 288-292.

Perrimon N, Gans M. 1983. Clonal analysis of the tissue specificity of recessive female-sterile mutations of Drosophila melanogaster using a dominant female-sterile mutation Fs(1)K1237. *Dev Biol* **100**: 365-373.

Perrimon N, Lanjuin A, Arnold C, Noll E. 1996. Zygotic lethal mutations with maternal effect phenotypes in Drosophila melanogaster. II. Loci on the second and third chromosomes identified by P-element-induced mutations. *Genetics* **144**: 1681-1692.

Perrimon N, Mohler D, Engstrom L, Mahowald AP. 1986. X-linked female-sterile loci in Drosophila melanogaster. *Genetics* **113**: 695-712.

Port F, Bullock SL. 2016. Creating Heritable Mutations in Drosophila with CRISPR-Cas9. *Methods Mol Biol* **1478:** 145-160.

Rice TB, Garen A. 1975. Localized defects of blastoderm formation in maternal effect mutants of Drosophila. *Dev Biol* **43**: 277-286.

Richardson BE, Beckett K, Nowak SJ, Baylies MK. 2007. SCAR/WAVE and Arp2/3 are crucial for cytoskeletal remodeling at the site of myoblast fusion. *Development* **134**: 4357-4367.

Sapiro AL, Ihry RJ, Buhr DL, Konieczko KM, Ives SM, Engstrom AK, Wleklinski NP, Kopish KJ, Bashirullah A. 2013. Rapid recombination mapping for high-throughput genetic screens in Drosophila. *G3 (Bethesda)* **3**: 2313-2319.

Schmitt-Engel C, Schultheis D, Schwirz J, Strohlein N, Troelenberg N, Majumdar U, Dao VA, Grossmann D, Richter T, Tech M et al. 2015. The iBeetle large-scale RNAi screen reveals gene functions for insect development and physiology. *Nat Commun* **6**: 7822.

Schnorrer F, Luschnig S, Koch I, Nusslein-Volhard C. 2002. Gamma-tubulin37C and gamma-tubulin ring complex protein 75 are essential for bicoid RNA localization during drosophila oogenesis. *Dev Cell* **3**: 685-696.

Schupbach T, Wieschaus E. 1986. Maternal-effect mutations altering the anterior-posterior pattern of the Drosophila embryo. *Roux's Archives of Developmental Biology* **195**: 302-317.

Schupbach T, Wieschaus E. 1989. Female sterile mutations on the second chromosome of Drosophila melanogaster. I. Maternal effect mutations. *Genetics* **121**: 101-117.

Schupbach T, Wieschaus E. 1991. Female sterile mutations on the second chromosome of Drosophila melanogaster. II. Mutations blocking oogenesis or altering egg morphology. *Genetics* **129**: 1119-1136.

St Johnston D. 2002. The art and design of genetic screens: Drosophila melanogaster. *Nat Rev Genet* **3**: 176-188.

Sung HH, Telley IA, Papadaki P, Ephrussi A, Surrey T, Rorth P. 2008. Drosophila ensconsin promotes productive recruitment of Kinesin-1 to microtubules. *Dev Cell* **15**: 866-876.

Tanaka R, Murakami H, Ote M, Yamamoto D. 2016. Clustered regulatory interspaced short palindromic repeats (CRISPR)-mediated mutagenesis and phenotype rescue by piggyBac transgenesis in a nonmodel Drosophila species. *Insect Mol Biol* doi:10.1111/imb.12232.

Terriente Felix J, Magarinos M, Diaz-Benjumea FJ. 2007. Nab controls the activity of the zinc-finger transcription factors Squeeze and Rotund in Drosophila development. *Development* **134**: 1845-1852.

Thomsen S, Anders S, Janga SC, Huber W, Alonso CR. 2010. Genome-wide analysis of mRNA decay patterns during early Drosophila development. *Genome Biol* **11**: R93.

Vogt N, Koch I, Schwarz H, Schnorrer F, Nusslein-Volhard C. 2006. The gammaTuRC components Grip75 and Grip128 have an essential microtubule-anchoring function in the Drosophila germline. *Development* **133**: 3963-3972.

Wieschaus E, Nüsslein-Volhard C. 1998. Looking at embryos. In *Drosophila: A Practical Approach*, (ed. DB Roberts), pp. 179-214. IRL Press, Oxford University Press.

Wieschaus E, Nüsslein-Volhard C. 2016. The Heidelberg Screen for Pattern Mutants of Drosophila: A Personal Account. *Annu Rev Cell Dev Biol* doi:10.1146/annurev-cellbio-113015-023138.

Wieschaus E, Nüsslein-Volhard C, Jürgens G. 1984. Mutations affecting the pattern of the larval cuticle in Drosophila melanogaster III. Zygotic loci on the X-chromosome and fourth chromosome. *Wilhelm Roux's Archives of Developmental Biology* **193**: 296-307.

Winkler F, Gummalla M, Kunneke L, Lv Z, Zippelius A, Aspelmeier T, Grosshans J. 2015. Fluctuation Analysis of Centrosomes Reveals a Cortical Function of Kinesin-1. *Biophys J* **109**: 856-868.

Yamamoto S, Jaiswal M, Charng WL, Gambin T, Karaca E, Mirzaa G, Wiszniewski W, Sandoval H, Haelterman NA, Xiong B et al. 2014. A drosophila genetic resource of mutants to study mechanisms underlying human genetic diseases. *Cell* **159**: 200-214.

Yan S, Lv Z, Winterhoff M, Wenzl C, Zobel T, Faix J, Bogdan S, Grosshans J. 2013. The F-BAR protein Cip4/Toca-1 antagonizes the formin Diaphanous in membrane stabilization and compartmentalization. *J Cell Sci* **126**: 1796-1805.

Yohn CB, Pusateri L, Barbosa V, Lehmann R. 2003. l(3)malignant brain tumor and three novel genes are required for Drosophila germ-cell formation. *Genetics* **165:** 1889-1900.

Part II

Role of Protein phosphatase V in Cell Cycle Control in *Drosophila* Blastoderm

1 Introduction

1.1 Link of zygotic genome activation and cell cycle control

In most animals, from nematodes to chordates, embryogenesis starts with a series of rapid cleavage cell cycles after fertilization. These fast divisions lead to an exponentially increasing number of cells without an accompanied growth of the embryo. After a species-specific number of divisions, the cell cycle slows down and finally enters a pause. Subsequently, the embryo enters gastrulation with its characteristic morphogenetic movements, loss of symmetry, and cell type-specific differentiation. Mammalian embryogenesis is special in that it begins with differentiation of inner cell mass (ICM) and trophoblast, and the fast embryonic cleavage cycles eventually arise at late blastocyst stage (Hiiragi and Solter 2004; O'Farrell et al. 2004; O'Farrell 2015). Maternally supplied materials, including proteins, RNAs, and conceivably also metabolites contribute to the initial developmental processes. Maternal products exclusively control development during this first period, as the zygotic genome starts expression only with a delay after fertilization. Following zygotic genome activation (ZGA), both maternal and zygotic factors contribute to developmental control. The switch from maternal to zygotic control is especially prominent in species with large, externally deposited eggs. ZGA coincides with striking changes in cell behavior and molecular processes, including cell cycle, DNA replication, maternal RNAs degradation, chromatin structure, metabolite composition, and status of DNA checkpoint. This morphologically visible switch in early development during the blastula stage was first described 120 years ago in sea urchin *Echinus microtuberculat* and *Sphaerechinus granularis*, and later has been referred to as mid-blastula transition (MBT) (Boveri 1893; Gerhart 1980).

MBT in model organisms

Many model organisms are well studied in terms of MBT. Amphibian *Xenopus laevis*, for instance, undergoes 12 short and synchronized cleavage cycles with a lack of gap phases, 35 min each and proceeds with a series of progressively longer and less synchronized divisions from cycle 13 to 15. The transition period is defined as

the MBT (Gerhart 1980; Newport and Kirschner 1982a; Newport and Kirschner 1982b; Newport and Kirschner 1984). S phase progressively lengthens, and the cell cycle pauses in G1 or G2 phases during the MBT (Farrell and O'Farrell 2014). Concomitantly, maternal transcripts are deadenylated and degraded. The first zygotic transcripts are detected at cycle 7 and the transcription rate increased up to and beyond MBT (Collart et al. 2014). During the MBT, developmental control is handed over from maternal genes to zygotic factors (maternal-zygotic transition, MZT).

In zebrafish *Danio rerio* embryo, 9 rapid cycles with approximately 15 min each are followed by gradually longer cell cycles (Kane and Kimmel 1993). MBT begins at cycle 10, and the cell cycle losses synchrony with acquisition of a G1 phase in cycle 11 (Zamir et al. 1997). Similar to *Xenopus*, ZGA is regulated by the nuclear-cytoplasmic ratio, but DNA damage checkpoint acquisition is independent of zygotic transcription (Zhang et al. 2014a). Maternal factors Nanog, Pou5f1, and SoxB1 are required for de novo zygotic transcription as well as inducing maternal clearance by activating the microRNA *miR-430* expression (Lee et al. 2013).

In the nematode *Caenorhabditis elegans* (*C. elegans*), zygotic transcription is already activated in the 4-cell stage. Multiple mechanisms and maternal factors, including OMA-1 and OMA-2, are involved and regulated by phosphorylation, nuclear shuttling and protein destabilization (Guven-Ozkan et al. 2008; Robertson and Lin 2015). In contrast to the other species discussed above, cells divide asynchronously and asymmetrically following fertilization in *C. elegans* embryos (Sulston et al. 1983; Rose and Gonczy 2014).

MBT in *Drosophila*

MBT is observed in embryos of the fruit fly *Drosophila melanogaster* at about 2 h post fertilization. Embryonic development starts with 13 rapid and meta-synchronized nuclear divisions, with extraordinary short S phases and no gap phases (Foe and Alberts 1983). The extraordinary speed of about 10 min per pre-blastoderm cell cycle is achieved by fast replication of DNA and the absence of cytokinesis (McCleland and O'Farrell 2008; Shermoen et al. 2010; Farrell et al. 2012). The syncytial mode of early development is a special feature of insect embryogenesis (Rabinowitz 1941).

Due to the absence of cytokinesis, the early cell cycles are often referred to as nuclear cycles (NC). The onset of the embryonic cell cycle is regulated by *pan gu*, *plutonium* and *giant nuclei* (Axton et al. 1994; Fenger et al. 2000; Lee et al. 2003; Laver et al. 2015b). From NC8 to 9, the nuclei move from the interior of the egg toward the periphery, forming the syncytial blastoderm. From NC10 to 13, nuclei undergo four more divisions at the egg cell cortex, until the nuclei number reaches approximately 6000. Some nuclei remain in the interior egg to differentiate into polyploid yolk nuclei. After mitosis 13, the cell cycle mode changes with the introduction of a long G2 phase, and the embryo enters into cellularization stage (Foe and Alberts 1983). Following NC11, the cell cycle gradually slows down from 10 min in NC11 to 21 min in NC13 and an hour-long G2 pause in interphase 14 (25°C) (Foe and Alberts 1983). The S phase lengthens and by cycle 14 a difference between early and late replicating euchromatin and the satellite DNA becomes obvious. In addition, the usage of replication origins changes (Schubeler et al. 2002).

Interphase 14 corresponds to the MBT in *Drosophila*. Interphase 14 is the stage when the cell cycle pauses in a G2 phase, zygotic transcription strongly increases, and DNA replication switches to a slow replication mode. During interphase 14, visible morphology changes from the syncytial to cellular blastoderm, in a process called cellularization. Cellularization is the first morphological process that depends on zygotic gene products (Edgar and Schubiger 1986; Merrill et al. 1988).

However, the first signs of MBT are already visible earlier, however. As mentioned above, the extending interphases in NC11-14 depend on zygotic transcription. The first transcripts and activated RNA polymerase II (Pol II) can be already detected in pre-blastoderm stages. Transcription slowly increases until cycle 12. In cycle 13 many zygotic genes are clearly expressed (Ali-Murthy et al. 2013). Genome-wide analysis showed that gene expression is initiated at different time points throughout early development (Graveley et al. 2011; Lott et al. 2011), suggesting that rather than a sharp switch, MZT is likely regulated by multiple and diverse mechanisms (Farrell and O'Farrell 2014; Lee et al. 2014; Harrison and Eisen 2015). The timing of these multiple and diverse mechanisms depends, to a certain degree, on the ratio of nuclear and cytoplasmic content (N:C ratio). This is further discussed in the Section "*What is the timer for MBT?*".

Approximately, two-thirds of all genes are contained in Drosophila eggs as maternal mRNAs (De Renzis et al. 2007; Harrison and Eisen 2015). A third of all maternal transcripts are eliminated in stages leading to MBT in three ways (De Renzis et al. 2007): First, maternally encoded factors activate mRNA degradation of over 20% of maternal transcripts after egg activation in a ZGA-independent manner (Tadros et al. 2003; Tadros et al. 2007; Tadros and Lipshitz 2009; Harrison and Eisen 2015). The RNA-binding protein Smaug is such a factor, acting together with the CCR4/POP2/NOT deadenylase complex (Semotok et al. 2005; Tadros et al. 2007; Chen et al. 2014). Another RNA-binding protein, Brain Tumor, functions in a similar way (Laver et al. 2015a). Second, 15% of maternal mRNAs are eliminated depending on zygotic transcription during MBT (Bashirullah et al. 1999; Walser and Lipshitz 2011). Third, microRNAs induce maternal RNA degradation. More than 100 maternal transcripts are degraded depending on zygotically expressed microRNAs from the *miR-309* cluster, which is activated by the early zygotic transcription factor Vielfältig/Zelda (Bushati et al. 2008; Huntzinger and Izaurralde 2011; Fu et al. 2014).

Mechanism of zygotic genome activation

Transcription of the zygotic genome only begins shortly after fertilization (Li et al. 2014). The highly dynamic transcription profile was characterized by number of methods, including high-throughput strategies, global run-on sequencing (GRO-seq), and fluorescent labelling of nascent RNA (Lecuyer et al. 2007; Harrison et al. 2011; Lee et al. 2013; Saunders et al. 2013; Ferraro et al. 2016). In general, the initiation of low-level zygotic transcription, mostly of signaling and patterning genes, already appears before NC10 ahead of large-scale ZGA (Pritchard and Schubiger 1996; Ali-Murthy et al. 2013). These include small and intron-less genes, as well as genes with TAGteam DNA motif in the control region (De Renzis et al. 2007). A comparable profile is also observed in that of the zebrafish (Heyn et al. 2014). Full activation of zygotic transcription is observed during MBT, when thousands of genes are transcriptionally activated and transcribed in high levels. Taken together, the activation of the zygotic genome is a gradual process rather than a single sharp switch. This suggests that ZGA is triggered by multiple and diverse events (Farrell and O'Farrell 2014; Lee et al. 2014; Harrison and Eisen 2015).

A contribution to ZGA is intrinsically provided by the division of nuclei and doubling of DNA with every nuclear cycle. Even with a constant activity of the individual zygotic transcription units, the total number of transcripts would exponentially increase. In general, zygotic transcription is quantified in relation to the number of embryos, total mass of embryos (protein or total RNA content), or in comparison to an abundant RNA, such as ribosomal RNA. Most of the older data are based on samples prepared from mixed stages comprising several nuclear division cycles. Alternatively, zygotic transcription may be normalized to the number of nuclei in an embryo. Given recent technological advances, transcription profiling can be conducted with few or even single *Drosophila* embryos, allowing highly accurate staging according to the nuclear division cycle (Lott et al. 2011; Chen et al. 2013). Such normalization is important to reveal the actual transcriptional activity of a locus.

This hypothesis was tested with normalized transcriptional profiles of selected early zygotic genes (Fig. 13) based on a data set from manually staged embryos (Sung et al. 2013). Normalization to number of nuclei was performed with the assumption of a doubling with every cell cycle. In case of a doubling transcript number from one cycle to the next, this results in a zero value. An increase in transcript number higher than a factor two results in a positive number, whereas an increase less than a factor two, in a negative number (Fig. 13). This simple and exemplary calculation indicates that both the increasing number of nuclei and an increased activity of the transcription units contribute to the overall increase in zygotic transcripts per embryo. There is, however, also transcript-dependent variation. A similar finding was reported recently for dorsoventrally patterning genes (Sandler and Stathopoulos 2016). This indicates that depending on the zygotic gene, both an increased activity of individual transcription units and an increased number of transcription units/nuclei contribute to ZGA.

Vielfältig/Zelda functions in ZGA regulation

The zinc-finger protein Vielfältig/Zelda (Vfl/Zld) plays a major role in ZGA. Vfl/Zld specifically binds to TAGteam elements in the early *Drosophila* embryo. The TAGteam CAGGTAG sequence was identified by genome-wide studies as a general *cis*-regulatory element and as the most highly enriched regulatory motif in genes involved in anterior-posterior patterning (ten Bosch et al. 2006; De Renzis et al. 2007;

Li et al. 2008). Vfl/Zld is an essential transcriptional activator during early zygotic gene expression, as demonstrated by the strongly reduced (but not absent) expression of many early zygotic genes in embryos from females with *Vfl/Zld* mutant germline (Liang et al. 2008). *Vfl/Zld* is maternally deposited and uniformly distributed throughout the egg and early embryo. The Vfl/Zld protein levels increase coincidently with the activation of zygotic genome during pre-blastoderm stage, prior to large-scale transcription (Staudt et al. 2006; Harrison et al. 2011).
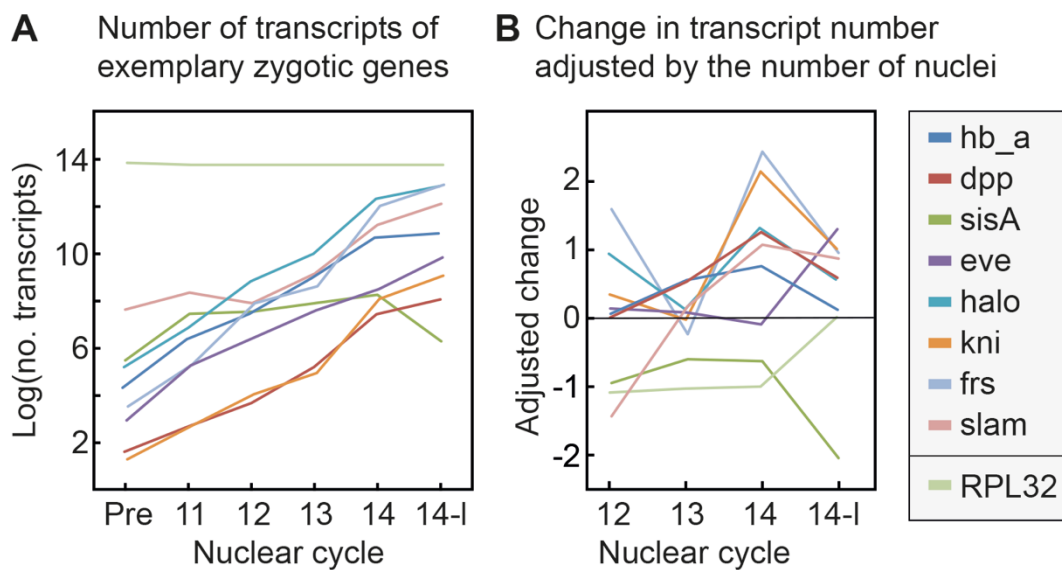

Figure 13: Zygotic transcription and number of nuclei. (A) Number of selected zygotic transcripts based on NanoString analysis with extracts from manually staged embryos plotted on a logarithmic scale. (B) The number of transcripts was normalized to the number of nuclei that double with every cycle. Plotted is the difference of $\log_2$ of the number of transcripts from one cycle to the previous cycle minus 1. The number of transcripts in pre-blastoderm stages is not included. Transcripts for the ribosomal protein L32 serve as a reference. Staging by the nuclear cycle, pre-blastoderm stage (Pre) and late cellularization (14-l). Data are from Sung et al. 2013.

Vfl/Zld consists of a cluster of four zinc fingers and a low-complexity activation domain, both of which are required for promoting DNA binding and mediating transcriptional activation (Hamm et al. 2015). Vfl/Zld binding to promoters is detected

already in NC8 for particular genes and roughly a thousand genes during NC10 (Foo et al. 2014; Schulz et al. 2015). The DNA binding is maintained at least until NC14 (Harrison et al. 2011). During ZGA, Vfl/Zld-binding sites are highly enriched specifically in regions of accessible chromatin, allowing transcription factors to subsequently bind and drive zygotic transcription (Foo et al. 2014; Schulz et al. 2015). Thus, Vfl/Zld acts as a co-activator during MZT. Vfl/Zld also controls the accurate temporal and spatial expression of microRNAs (Fu et al. 2014).

RNA polymerase II pausing

The binding of Pol II to promotor sequences is the key to transcriptional activation and elongation. Pol II regulates ZGA by three distinct binding statuses: active, no binding and stalled/paused (Zeitlinger et al. 2007). Among them, paused Pol II is critical in *Drosophila* ZGA, because approximately 100 genes are bound by active Pol II from NC8 to 12, yet in NC14, over 4000 promotors are occupied by Pol II at the transcription start site (TSS) (Boettiger and Levine 2009; Chen et al. 2013). Furthermore, compared with NC12, loci with paused Pol II near the TSS show a significant increase in NC13 (Blythe and Wieschaus 2015b).

Epigenetics and ZGA

Epigenetic marks, including histone modifications and chromatin remodeling, dramatically change in early embryogenesis and MBT. Formation of heterochromatin correlates with the emergence of late replication. Heterochromatin Protein 1 (HP1) together with histone modification of H3K9 and H3K4 is involved in this establishment of tightly packed chromatin structure (Rudolph et al. 2007; Yuan and O'Farrell 2016). Modifications of lysine acetylation and methylation in histones H3 and H4 appear during MZT. In zebrafish, a striking change in histone modification correlates with ZGA (Lindeman et al. 2011). An increase in histone methylation during MZT matches high level of zygotic transcription (Vastenhouw et al. 2010; Lindeman et al. 2011). In *Xenopus* embryo, maternally provided histones H3/H4 and their modification states control the regulation of transcriptional activation and cell cycle lengthening (Amodeo et al. 2015; Hontelez et al. 2015). Similarly, during *Drosophila* early development, genome-wide studies showed that domains of histone methylation H3K4me1, H3K4me3, H3K27me3, and H3K36me3 increased from

undetectable to widespread level at NC14 (Chen et al. 2013; Li et al. 2014; Boettiger et al. 2016). Levels of acetylation on H3K9 appear correspondingly to methylation marks, whereas H3K18ac, H3K27ac, and H4K8ac levels are evidently precocious at NC12 (Li et al. 2014). These early appearing acetylation marks are strongly correlated with maternal DNA-binding protein Vfl/Zld, demonstrating that Vfl/Zld may regulate transcriptional activation by recruiting histone acetylation, thus allowing opening of genome state (Li et al. 2014; Harrison and Eisen 2015). In contrast, the mark H4K5ac, whose level was previously shown to bookmark active transcription in mammalian cells, decreases from NC8 with slowing of the cleavage cycles (Zhao et al. 2011; Li et al. 2014). In addition to histone modifications, remodeling of nucleosomes and linker histones with histone variants may contribute to ZGA. *Drosophila* maternal-specific linker histone H1 dBigH1 is replaced by somatic H1 in early development (Perez-Montero et al. 2013). dBigH1 seems to suppress ZGA, since increase levels of activated Pol II and expression of zygotic genes are observed in embryos with reduced dBigH1 levels (Perez-Montero et al. 2013).

Both histone modification and Vfl/Zld DNA binding ultimately affect transcriptional activation by altering chromatin accessibility. Highly accessible chromatin regions are locally and globally marked by H3/H4 acetylation and Vfl/Zld enrichment from NC8 to 12 in *Drosophila* (Li et al. 2011). In NC13, however, thousands of enhancers and promotors with nucleosome-free regions accumulate additional transcription factors in a cascade way (Thomas et al. 2011; Li et al. 2014). This phenomenon has also been observed in zebrafish (Zhang et al. 2014b).

Other regulators

Drosophila zygotic transcription is modulated by multiple factors including *cis*-regulatory elements. For instance, TATA-dependent promoters, as well as enhancers, are central in transcriptional regulation (Juven-Gershon and Kadonaga 2010; Zabidi et al. 2015). Distinct enhancer-core-promoter specificities ensure that developmental and housekeeping genes are activated precisely across the entire genome (Zabidi et al. 2015). Likewise, the post-transcriptional regulation of TATA-binding protein (TBP) affects transcription pattern together with the earliest transcribed genes during the MZT (Chen et al. 2013). Smaug may involve ZGA regulation through maternal clearance of transcription factor *tramtrack* mRNA, which

is involved in triggering transcription of transcripts depending on the N:C ratio (Pritchard and Schubiger 1996; Tadros et al. 2007).

Switch in cell cycle mode during the MBT

The cell cycle switch from a fast syncytial mode to a mode with slow replication and extended G2 phase is a central and the most obvious aspect of MBT in morphological terms. A long-standing question is the functional relationship of the cell cycle switch with ZGA. According to one model, the cell cycle switch allows for the strong increase in zygotic transcription (Fig. 14)(Collart et al. 2013). In the opposing model, zygotic transcription triggers the remodeling of the cell cycle (Sung et al. 2013; Blythe and Wieschaus 2015b). Depending on the experimental system, strong experimental evidence speaks in favor of the first or the second model. A synthesis has not been achieved, yet.

Cell cycle regulation in *Drosophila* early embryogenesis

Cyclin and its partner cyclin-dependent kinase (Cdk) are essential for cell cycle control. In *Drosophila*, cyclin A/B/B3:Cdk1 complex regulates entry into M phase (Lehner and O'Farrell 1990; McCleland and O'Farrell 2008). The rapid S phases in pre-MBT cycles are maternally controlled, and the catalytic activity level of cyclin:Cdk1 complexes determines the timing for mitotic entry (Edgar and O'Farrell 1990; Shermoen et al. 2010). Distinct mechanisms regulate cyclin:Cdk1 complexes in pre-MBT: First, during each nuclear division, Cyclin A, B and B3 proteins are synthesized in S phase by maternally supplied mRNA (Edgar et al. 1994; Yuan and O'Farrell 2015), and degraded in mitosis by the ubiquitin pathway (Glotzer et al. 1991; Sigrist et al. 1995). Cyclin A, B, and B3 fulfill a redundant but essential function, as RNAi-mediated depletion stops the syncytial cycles (McCleland and O'Farrell 2008; Yuan et al. 2012). Cyclin B levels also contribute to the cell cycle switch as changes in *cyclin B* gene dose affect the number of nuclear divisions (Ji et al. 2004). Second, the inhibitory phosphorylation of T14Y15 sites of Cdk1 are pairwise regulated by maternally supplied kinases Wee1/Myt1 and phosphatase Cdc25/Twine (Edgar and O'Farrell 1989; Edgar et al. 1994; Price et al. 2000; Stumpff et al. 2004; Jin et al. 2005; Blythe and Wieschaus 2015a). Therefore, Cdk1 is timely activated and inactivated by controlling T14Y15 inhibitory phosphorylation sites (Ayeni et al. 2014).
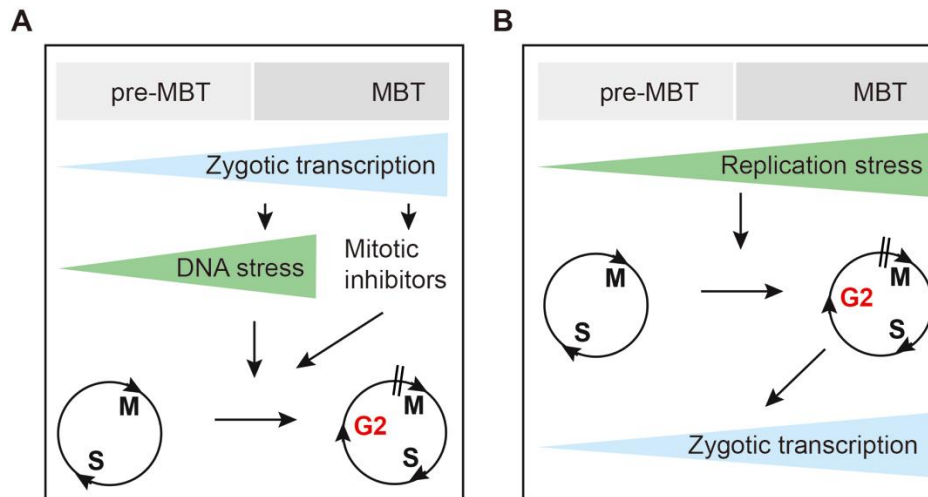
Figure 14: Models for the control of cell cycle remodeling during MBT. (A) The onset of zygotic transcription leads to activation of the DNA checkpoint due to interference of transcription and replication as well as expression of mitotic inhibitors. These two processes lead to the cell cycle remodeling. (B) Activation of the DNA checkpoint, caused by limiting amounts of replication factors, for example, triggers a slowdown and subsequent pause of the cell cycle. The longer interphase promotes zygotic transcription.

Cdc25/Twine degradation at the MBT

In NC14 and to a certain degree already in NC12 and 13, S phase lengthens and a G2 phase is introduced. Central to these changes is the induced degradation of the phosphatase Cdc25/Twine (Di Talia et al. 2013; Farrell and O'Farrell 2013) (Fig. 15). *Drosophila* Cdc25/Twine is a dual specificity phosphatase that activates cyclin:Cdk1 complexes by removing inhibitory phosphates from the ATP binding sites T14 and Y15 (Alphey et al. 1992; Sigrist et al. 1995; Edgar and Lehner 1996; Farrell et al. 2012). Twine protein is present in high levels during the pre-MBT cycles. Twine protein localization is dynamic with a nuclear accumulation during interphases and uniform dispersal during mitosis (Di Talia et al. 2013). The half-life of Twine was estimated to about 20 min during pre-MBT cycles (Di Talia et al. 2013). Yet with the beginning of NC14, Twine becomes destabilized as indicated by the shortening of its half-life to only about 5 min (Di Talia et al. 2013). Degradation of Twine is required for the cell cycle switch because embryos expressing a stable version of Twine

protein (Twine[106-180]) undergo an extra mitotic division (Di Talia et al. 2013). This rapid destabilization is the key to the cell cycle switch during MBT, as it depends on the N:C ratio and on zygotic transcription (Di Talia et al. 2013).
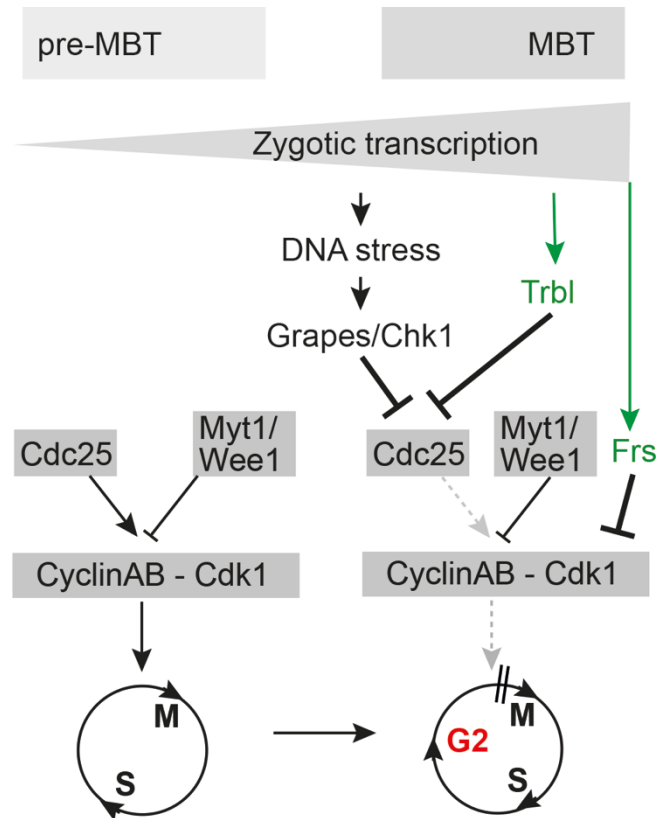

Figure 15: Model of cell cycle remodeling in Drosophila. Cyclin:Cdk1 is activated by the phosphatase Cdc25 and inactivated by the kinases Myt1/Wee1. In pre-MBT Cyclin:Cdk1 activity is high and promotes fast cell cycles. During MBT the balance of Cyclin:Cdk1 control is shifted towards low activity. Cdc25 is inhibited by the DNA checkpoint, which is activated by DNA stress caused by interference of DNA replication and zygotic transcription. In addition, the zygotic mitotic inhibitors, Tribbles and Frühstart, promote Cdc25 degradation and inhibition of the Cyclin:Cdk1 complexes, respectively.

Prior to MBT, the steady-state level of Twine is relatively stable due to balanced synthesis and degradation. The link of zygotic transcription and the switch-like decrease in the half-life of Twine suggests that zygotic factors may be involved. One of these factors is the pseudokinase Tribbles (Grosshans and Wieschaus 2000; Mata et al. 2000; Rorth et al. 2000), as induced RNAi-mediated depletion of *tribbles* accelerates Twine degradation (Farrell and O'Farrell 2013). However, *tribbles* is not essential for the MBT cell cycle switch, since embryos deficient for maternal and

zygotic *tribbles* do not undergo an extra nuclear cycle (Grosshans and Wieschaus 2000; Mata et al. 2000). The mechanism of how *tribbles* induces Twine degradation remains unknown, but in other organisms such as yeast, *Xenopus*, and human cells, Cdc25 (or Cdc25C) degradation is induced by phosphorylation due to multiple pathways (Frazer and Young 2012; Sung et al. 2013; Murphy et al. 2015). In addition to induced destabilization of Cdc25/Twine at NC14, additional mechanisms control pre-MBT levels and activity of Twine. The number of pre-MBT cell cycles is rather insensitive to changes in *twine* gene dose. A tripling of *twine* gene dose to 6×*twine*[+] induces an extra nuclear division in only a few embryos (Edgar and Datar 1996), suggesting that mechanisms exist that make Twine protein levels independent of gene dose.

The second *Drosophila* homologue of Cdc25, String, has distinct developmental functions in cell cycle control (Edgar and O'Farrell 1990; Chen et al. 2007). String but not Twine is required for mitotic entry in zygotically controlled cycles 14–16. In contrast to these later stages, *string* is not required for progression of the syncytial cell cycles (Edgar and O'Farrell 1990). Premature expression of *string* is sufficient to trigger mitotic entry during later stages of embryonic development but not in pre-MBT stages (Edgar and O'Farrell 1990). Although both *string* and *twine* mRNAs are destructed in interphase 14 (Edgar and Datar 1996), String protein stability gradually decreases during syncytial cycle without a sharp switch before MBT (Farrell and O'Farrell 2013). String protein turnover is due to increased checkpoint activity (Di Talia et al. 2013).

DNA replication checkpoint at NC13

Before the switch in cell cycle mode in NC14 in *Drosophila*, S phases show a progressive lengthening from 3.4 min in NC8 to 14 min in NC13 (Blumenthal et al. 1974; Shermoen et al. 2010). A critical regulator of the slow-down of replication is the *Drosophila* homologue of checkpoint kinase Chk1, Grapes (Sibon et al. 1997). Grapes starts to inhibit cyclin:Cdk1 activity by promoting the activity of kinases Wee1/Myt1 and suppressing the activity of phosphatase Cdc25, thereby adding the inhibitory phosphorylation of Cdk1 from NC11 onward (Fogarty et al. 1997; Sibon et al. 1997). Grapes mediates the DNA replication checkpoint and ensures that cells do not enter mitosis while replication is ongoing. *grapes* mutants prematurely enter

mitosis during syncytial divisions, which leads to mitotic catastrophe, as incompletely replicated chromosomes cannot be segregated in anaphase (Fogarty et al. 1997; Sibon et al. 1997). The checkpoint kinase, ataxia telangiectasia and Rad3-related (ATR, Mei-41 in *Drosophila*), acts upstream and activates Chk1/Grapes similar as in *Xenopus* (Sibon et al. 1999; Shimuta et al. 2002). *mei-41* mutants show a similar phenotype during syncytial divisions as *grapes*, indicating a functional replication checkpoint is required at the MBT (Blythe and Wieschaus 2015b).

In *Drosophila* the DNA checkpoint is triggered by ZGA. Blocking transcription by α-amanitin in *Drosophila* pre-MBT embryos does not suppress lethality of *mei-41* mutant (Blythe and Wieschaus 2015b). Nonetheless, embryos from *mei-41 Vfl/Zld* double mutant mothers could partially suppress the mitotic catastrophe, indicating that replication has been finished in time (Blythe and Wieschaus 2015b). These observations are consistent with the model that zygotic transcription reduces replication speed and induces DNA stress, leading to DNA checkpoint activation at ZGA (Sung et al. 2013; Blythe and Wieschaus 2015b).

Other regulators

In *Drosophila*, cyclin-dependent kinase inhibitor (CKI) Frühstart is another zygotic regulator, which functions to inhibit cyclin:Cdk1 activity by binding the hydrophobic patch of cyclins, thereby interfering with Cdk1 substrate recognition (Grosshans and Wieschaus 2000; Grosshans et al. 2003; Gawlinski et al. 2007). Together with large-scale ZGA, *frühstart* starts transcription immediately after mitosis 13, and generates a uniform cell cycle pause in cycle 14 (Grosshans et al. 2003). In the absence of Frühstart, embryos enter an extra round of nuclear division especially in embryos with extra copies of *twine*[+] (Grosshans et al. 2003) The expression of Frühstart depends on the N:C ratio, suggesting that Frühstart is involved in the link of N:C with cell cycle regulation (Lu et al. 2009). Wee1 and Myt1 kinases are Cdk1 inhibitors that oppose functions to Cdc25 phosphatases (Campbell et al. 1995; Price et al. 2000; Bettencourt-Dias et al. 2004; Stumpff et al. 2004; Jin et al. 2005) (Fig. 15). Wee1 can be activated by Grapes, and inhibits Cdk1 activity by adding inhibitory phosphorylation at T14 and Y15 sites (Royou et al. 2008; Fasulo et al. 2012; Farrell and O'Farrell 2014). Cyclin:Cdk1 activity is also influenced by some other factors such as Aurora-A and acquisition of late-replicating heterochromatin domains (Kang

et al. 2014; Blythe and Wieschaus 2015a).

In summary, the switch of the cell cycle from a fast syncytial mode to a slow embryonic mode is controlled on two levels of inhibition: (1) indirectly by interference of zygotic transcription with DNA replication and subsequent activation of the DNA checkpoint, (2) directly by expression of zygotic genes encoding mitosis inhibitors.

What is the trigger for MBT?

The MBT cell cycle switch depends on ZGA (Fig. 14). First, injection of α-amanitin, a Pol II inhibitor, before MBT induces an extra synchronized mitotic division, indicating that widespread zygotic transcription is required for the cell cycle switch in *Drosophila* (Edgar and Datar 1996). Second, ZGA correlates with DNA stress. About 80% of the RpA-70-GFP binding sites in early MBT cycles also have RNA Pol II bound (Blythe and Wieschaus 2015b). RpA70-GFP marks sites of DNA stress (Zou and Elledge 2003). This indicates that ZGA causes DNA stress and activates the DNA checkpoint (Blythe and Wieschaus 2015b). Third, a precocious onset of zygotic transcription is sufficient for an earlier MBT (Sung et al. 2013). Forth, dependent on ZGA, Tribbles and other factors trigger Twine destruction in NC14, resulting in inhibition of Cdk1 activation, thereby pausing the cell cycle (Grosshans and Wieschaus 2000; Mata et al. 2000).

The essential role of the DNA checkpoint for triggering MBT was initially shown by the analysis of the checkpoint mutants, *grapes*/Chk1 and *mei-41*/ATR, in *Drosophila* (Sibon et al. 1997; Sibon et al. 1999). Embryos from *grapes* females do not switch the cell cycle mode and do not enter MBT, indicating that the DNA checkpoint is required for MBT in *Drosophila* (Sibon et al. 1997; Blythe and Wieschaus 2015b). Based on the observation that *grapes* embryos would not express zygotic genes, the authors concluded that the checkpoint would be upstream of ZGA (Sibon et al. 1997). Recent data clearly show, however, that ZGA is normal in checkpoint deficient embryos and that the initial observation was probably due to technical difficulties in detecting expression of early zygotic genes (Blythe and Wieschaus 2015b).

An alternative source for checkpoint activation beside interference of replication and transcription are limiting amounts of replications factors. Experiments from mostly

Xenopus support this model (Fig. 14). In *Xenopus* embryos slowdown of DNA replication has been proposed to be upstream of ZGA (Collart et al. 2013). The replications factors Cut5, RecQ4, Treslin and Drf1 become limiting in MBT, what leads to an activation of the DNA checkpoint, slowdown of the cell cycle and ZGA (Collart et al. 2013).

In summary, in vivo and genetic experiments provide strong evidence for the model that ZGA is the trigger for MBT in *Drosophila*. ZGA acts upstream of cell cycle control, including the DNA checkpoint and degradation of Cdc25/Twine. First, ZGA is required for MBT and timely cell cycle pause; second, ZGA is associated with induction of replication stress in time and space (on the chromosome); third, precocious ZGA leads to precocious MBT. In other organisms experimental evidence mainly in *Xenopus* speak in favor of the alternative model, i. e., that cell cycle control acts upstream ZGA. However not all three criteria are fulfilled in vivo: the mechanism should be necessary, sufficient, and temporally and spatially associated with MBT.

What is the timer for MBT?

A central unresolved question concerning MBT is the timing mechanism for the associated processes including ZGA and number of pre-MBT cell cycles. Tight control of the cell cycle is important for further embryonic development, since the number of divisions determines the cell number and size. Too few cells may be incompatible with the formation of stripes of pair-rule gene expression, for example, as stripes should be at least one cell wide.

Molecular clocks

With the onset of embryonic development, fertilization may trigger a molecular clock, on which MBT and its associated processes may depend. A conceivable mechanism is translation of certain maternal mRNAs, which would lead to a time-dependent accumulation of the product following onset after fertilization. Translational regulators such as FMRP are required for MBT regulation in *Drosophila*, through dynamically regulating RNA metabolism and controlling the availability of specific transcripts, as well as mediating the *frühstart* mRNA activation level (Monzo et al. 2006; Papoulas et al. 2010). A target for translational regulation may be Vfl/Zld, whose protein level

increases during blastoderm concomitantly with activation of zygotic transcription (Nien et al. 2011; Harrison and Eisen 2015).

Maternal RNA degradation may represent a second such a mechanism constituting a molecular clock. A large fraction of these maternal RNAs is degraded following egg activation and independent of zygotic transcription. For some RNAs at least, the degradation proceeds with a constant speed (Tadros et al. 2007; Sung et al. 2013), and may in this manner constitute a molecular clock. It has been proposed that the speed of RNA degradation affects the number of nuclear divisions, as expression levels of *smaug* affect the timing of MBT (Semotok et al. 2005; Benoit et al. 2009). Distinct from Vfl/Zld, Smaug reaches its peak expression level at NC10, and performs downregulation at the MBT (Tadros et al. 2007; Benoit et al. 2009). Smaug is functional to mRNA clearance, and times the ZGA through inducing the destruction of maternal transcriptional inhibitor (Laver et al. 2015b).

N:C ratio as a clock

In contrast to a molecular clock as an absolute timer, more evidence speaks in favour of a regulatory process. The morphologically visible MBT depends on genome ploidy, because haploid embryos undergo one more division and tetraploid embryos, one less division (Kane and Kimmel 1993). It has been proposed that the N:C ratio represents the timer for MBT. Nuclear content is determined by the amount of DNA or chromatin, which doubles with every cell cycle, whereas cytoplasmic content remains constant during cleavage divisions. The embryo may measure the N:C in that the increasing amount of chromatin titrates a constant cytoplasmic factor until this becomes rate-limiting (Newport and Kirschner 1982a; Pritchard and Schubiger 1996). Potential cytoplasmic factors are repressors of transcription, replication or the cell cycle, for example. In *Xenopus* embryos, DNA content is important for MBT (Gerhart 1980; Newport and Kirschner 1982b). Injection of purified DNA leads to precocious onset of zygotic transcription, as measured by total transcription rate (Newport and Kirschner 1982b). However, the amount of DNA seems not to be the only determinant, since an increased or decreased nuclear volume, while keeping the DNA content unchanged, leads to a precocious or delayed MBT including zygotic activation and corresponding cell cycle remodeling (Jevtic and Levy 2015). Similar findings come from zebrafish that the timing of ZGA is governed by the N:C ratio

(Zhang et al. 2014a).

It is unclear what is titrated by the exponentially increasing amount of DNA and chromatin, but maternal histones proteins H3/H4 may be central factor (Amodeo et al. 2015). Depletion and overexpression of H3/H4 delay the cell cycle switch, and also induces premature transcriptional activation (Amodeo et al. 2015). In *Drosophila* embryos, the maternal form of the linker histone H1 dBigH1 has been implicated in the timing of MBT (Perez-Montero et al. 2013). Maternal dBigH1 is replaced by the somatic form in early embryogenesis. Embryos with half of the maternal contribution and lacking zygotic expression show increased levels of activated Pol II and zygotic gene expression. However, the link of dBigH1 to MBT remains unclear as mutant defects and embryonic genotypes were not analyzed with high temporal resolution and with respect to MBT and ZGA.

The replication factors Cut5, RecQ4, Treslin and Drf1 have been found to be limiting for replication initiation during MBT in *Xenopus* embryos (Collart et al. 2013). Titration of the maternal pool of these replications factors by the exponentially increasing chromatin leads to slower replication initiation, ZGA, longer interphases, and DNA checkpoint activation.

Other cytoplasmic factors may also be titrated, such as metabolites. It has been proposed that deoxynucleotides may serve as a marker for the cytoplasm (Vastag et al. 2011). The maternal pool may be incorporated in the exponentially increasing amounts of DNA. The existence of such a maternal pool is well known, as inhibition of zygotic synthesis by hydroxyurea (HU), which inhibits the NDP reductase, causes a cell cycle arrest only briefly before MBT (Vastag et al. 2011).

Although it is clear that ploidy determines the number of pre-MBT cell cycles in all model organisms, it is much less clear whether all of the MBT-associated processes, including ZGA, cell cycle, RNA degradation, are controlled by the N:C ratio. Haploid *Drosophila* embryo*s* switch the cell cycle mode only after an extra division 14 in NC15 (Edgar et al. 1986; Lu et al. 2009). In contrast, ZGA does not depend on the N:C ratio in *Drosophila*. Although older data indicated a link of ploidy and ZGA in *Drosophila* (Pritchard and Schubiger 1996), genome-wide analysis of embryonic transcripts with carefully staged *Drosophila* embryos revealed that the majority of

zygotic transcripts (127 out of 215 genes) show an expression profile comparable between haploid and diploid embryos (Lu et al. 2009). These data suggest that ZGA timing is controlled by a molecular clock in *Drosophila*. However, a small set of zygotic transcripts (88 out of 215 genes) shows clearly delayed expression in haploid embryos (Lu et al. 2009). This small gene set includes genes encoding mitotic inhibitors such as Frühstart (Grosshans et al. 2003), which are involved in the MBT associated remodeling of the cell cycle.

1.2 Protein phosphatase V

Function of PpV

The *Drosophila* Protein phosphatase V (PpV, FlyBase ID FBgn0003139) has been first reported by its functional complementation to *Saccharomyces cerevisiae SIT4* mutant (Mann et al. 1993), and later been identified as the orthologue of human Protein Phosphatase 6 (PP6), rat PPV and *Schizosaccharomyces pombe* ppe1 (Bastians and Ponstingl 1996).

PpV is a serine/threonine protein phosphatase which encodes 303 amino acids with a molecular mass of 34.7 kDa (Mann et al. 1993; Morrison et al. 2000). It belongs to Phosphoprotein phosphatases (PPP) family and PP2A subfamily, and shares highly conserved catalytic subunits with PP2A (microtubule star, mts) and PP4 (Morrison et al. 2000; Miskei et al. 2011). These phosphatases are assumed to function as dimers/trimers with a catalytic and regulatory subunits (Wera and Hemmings 1995). PpV is highly conserved among species. Data from Flybase Orthologs Search show 79% similarity to human PP6C, 89% to mouse Ppp6c, 89% to *Xenopus tropicalis* ppp6c, 89% to *Danio rerio* ppp6c, 76% to *C. elegans* pph-6 and 81% to *Saccharomyces cerevisiae* SIT4 (http://flybase.org/).

High-throughput expression data from Flybase show PpV is expressed throughout development and in adult flies (http://flybase.org/). Importance for my study is the high expression of PpV in 0–2 h early embryo as well as in female ovary, indicating PpV is maternally supplied.

Compared to other phosphatases, very few studies have been done for PpV. Human homologue PP6 is relatively well known because of its function in tumorgenesis, including melanoma tumors (Hodis et al. 2012; Krauthammer et al. 2012; Hammond et al. 2013), breast cancer (Zhong et al. 2011) and cancer therapy (Stefansson and Brautigan 2007; Zeng et al. 2010). PP6 is also involved in inflammation (Yan et al. 2015) and DNA damage (Douglas et al. 2010). PP6 homologues have been shown functional in *Drosophila* mitosis (Chen et al. 2007), *C. elegans* cortical contractility (Afshar et al. 2010), mouse oocyte meiosis and embryonic viability (Hu et al. 2015; Ogoh et al. 2016).

PpV in *Drosophila* cell cycle control

As discussed in the introduction, central of cyclin:Cdk1 control is the positive regulator Cdc25/Twine (Edgar and Datar 1996; Di Talia et al. 2013). The instability of Cdc25/Twine during MBT is due to the onset of zygotic gene expression, that zygotic inhibitors like Tribbles induce its degradation (Grosshans and Wieschaus 2000; Seher and Leptin 2000; Grosshans et al. 2003). How PpV/PP6 regulates cell cycle mode is still underexplored. From an RNAi screen of 117 protein phosphatases in S2 cell line it showed that PpV RNAi blocks G2/M and causes arrest in S Phase, meaning PpV could promote entry into anaphase (Chen et al. 2007). The cell size was not affected however (Chen et al. 2007). On the molecular level Quantitative phosphoproteomic analysis is being used as a systematic tool to investigate global kinase-phosphatase networks in vivo (Bodenmiller et al. 2010). By using this approach together with gene-depletion and RNAi, respectively, potential mitotic substrates of PP6 and PpV have been identified (Sopko et al. 2014; Rusin et al. 2015). However, there is no physiological relevance of these substrates in cell cycle regulation so far.

Potential catalytic target of PpV/PP6

AuroraA is a key mitotic serine/threonine kinase which has functions in centrosome separation and spindle assembly, and its homologue in human is oncogenic (Bischoff et al. 1998). *Drosophila* embryos from *auroraA* female mutants show phenotypes with abnormal distribution of centrosomes on mitotic spindles (Glover et

al. 1995). In larval neuroblasts the hypomorphic *auroraA* mutants lead to polyploid and circular mitotic figures (Glover et al. 1995).

AuroraA is activated at mitotic centrosomes and its activation requires autophosphorylation of the T-loop at Thr-288 residue (Ertych et al. 2016). PP6 is an AuroraA T-loop phosphatase which comprises both catalytic and regulatory subunits, therefore mediates inactivation of AuroraA (Stefansson and Brautigan 2007; Zeng et al. 2010). It has also been reported that human Cdc25B is a phosphorylation target of AuroraA (Dutertre et al. 2004). Specifically, Cdc25B can be phosphorylated by AuroraA and its phosphorylated form is located at the centrosome during mitosis (Dutertre et al. 2004). These evidences lead us to refer AuroraA as the potential target of PpV/PP6.

Cdc25 phosphatase catalytic domain

Cdc25 family is conserved among species. The function of Cdc25 can be controlled via two ways, including steady-state level, for example transcription/synthesis and degradation, and activation level, for example phosphorylation by other kinases or phosphatases (Bouldin and Kimelman 2014). Studies of mammalian Cdc25 crystal structure revealed a rhodanese–like domain which may act in catalytic function (Fauman et al. 1998; Hofmann et al. 1998). However, when aligning reported phosphorylation sites of human Cdc25C with residues of rhodanese–like domain in human Cdc25A, only one phosphorylation site Y416 could match to VLKGG**Y**KEF region of Cdc25A rhodanese–like domain (http://www.phosphosite.org; Hofmann et al. 1998). Majority of the phosphorylation sites in human Cdc25A/B/C were found exclusively prior to rhodanese–like domain (Frazer and Young 2012), suggesting that Cdc25 phosphatase catalytic activity may be regulated under a relatively complex mechanism.

1.3 Aims of this project

Cell cycle is an important aspect of biological processes for organism growth, renewing and development. The mode of cell cycle is variant among different cell and tissue types (Fig. 16). Canonical mode contains gap phase G1, DNA synthesis

phase S, gap phase G2 and mitosis M phase. G1, S and G2 phases are named together as interphase. In cultured cells, such kind of mode with continuous cell growing and proliferation is often observed. In vivo, cells which do not divide further enter gap phase G0. Some tissues undergo endo-replication which consists only S phase and gap phase, so that cells eventually become polyploidy. For example mouse liver cells and *Drosophila* salivary gland (Edgar et al. 2014). During oogenesis, meiosis is involved to produce haploid gamete, where DNA replication is followed by two rounds of cell divisions. As a consequence, daughter cells contain only half the number of chromosomes.
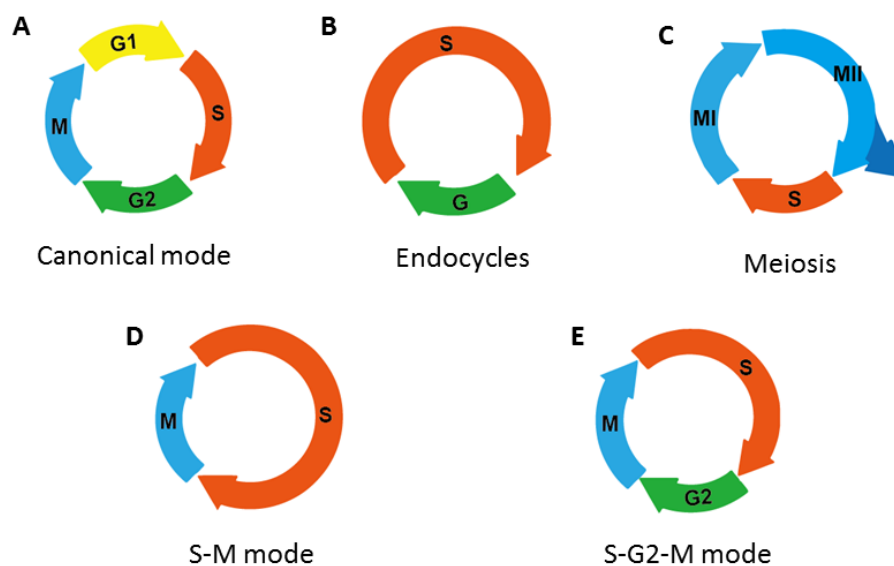
Figure 16: Variant modes of the cell cycle. (A) Canonical mode consisting of G1, S, G2 and M phase. (B) Endocycles consisting of S and G phases. (C) In meiosis, the chromosomes duplicate in S phase and undergo meiosis I and meiosis II, to form haploid gametes. (D-E) In pre-MBT, early embryogenesis reveals S-M mode in fast cleavage cycles. In post-MBT, cell cycle mode switches to S-G2-M. This developmental switch is cell cycle remodeling.

In *Drosophila*, during the MBT, a gap phase is added and the cell cycle mode is transited from S-M to S-G2-M (Lee and Orr-Weaver 2003) (Fig. 16). Cdc25/Twine is timely decayed and thus leads to the introduction of G2 phase. The mechanisms of how the degradation of Cdc25/Twine is induced are unclear. Zygotic transcription and zygotic genes (e. g. *tribbles*) induce Twine destabilization with change in half-life from 20 min to 5 min (Di Talia et al. 2013). Premature expression of *tribbles* is

sufficient to pause nuclear division cycles and to promote Twine degradation (Grosshans and Wieschaus 2000; Farrell and O'Farrell 2013). However, embryos lacking any Tribbles (maternal and zygotic null) have normal timing of MBT and undergo normal number of nuclear divisions (96% of the embryos, N=28). Tribbles is not exclusive as other zygotic genes or consequences of zygotic transcription are also involved.

The model that Twine instability induces cell cycle mode switch predicts a strong dependence on the expression levels of Twine (Di Talia et al. 2013; Farrell and O'Farrell 2013). However this was not observed. It has been reported that 1×*twine*[+] and 6×*twine*[+] are almost like WT, and only a very small fraction from 6×*twine*[+] females undergo extra division (Edgar and Datar 1996). One explanation of the apparent contradiction would be a mechanism that makes Twine protein level independent of *twine* gene dose.

In order to identify new regulators of the MBT cell cycle control, a set of X chromosome-linked mutations with early embryonic phenotypes was screened for cell cycle phenotypes (Luschnig et al. 2004; Vogt et al. 2006; Grosshans unpublished). In addition, a new Ethyl methanesulfonate (EMS) mutagenesis and screen for blastoderm phenotypes were conducted for the third chromosome (Part I). The X9 mutant which was being utilized in this work is a null mutation of *PpV* that a non-sense mutation has been identified in the 7th amino acid of PpV. Embryos from X9 germline clone undergo frequently an extra nuclear division with otherwise apparently normal development until gastrulation. Moreover, four alleles of *PpV* mutant are present in the Bellen collection of X-linked lethal, with point mutations of H112L, I117F, G162S and W203R (Haelterman et al. 2014). These four strains are severe alleles as the mutations cause the lethality in all cases. However, the expression profiles of PpV protein and the embryonic phenotypes in these alleles are unknown.

In this study, following critical questions could be addressed:

1) How is PpV involved in the MBT cell cycle remodeling?

2) What is the mechanism underlying control of Cdc25/Twine protein expression at the onset of MBT?

Besides that, a method fluctuation analysis was established and employed to detect temporal dynamic profile of Twine protein with precisely established time axis. We validated the novel application of fluctuation analysis in protein dynamics in *Drosophila* embryo.

2 Results

2.1 X9 mutants are lethal and frequently undergo an extra nuclear division prior to MBT

2.1.1 Embryos from X9 germline clones do not develop to larvae

In order to identify novel maternal candidate genes, which are essential for *Drosophila* early embryogenesis, a collection of Ethyl methanesulfonate (EMS)-induced mutants were generated in Tübingen, Germany (Luschnig PhD dissertation 2000; Luschnig et al. 2004; Vogt et al. 2006). Stocks with embryonic lethality were kept and mapping and sequencing were performed. Among them, X chromosome mutation X9 was found to be interesting as it showed frequent defects in remodeling of the cell cycle at the MBT (Grosshans unpublished).

Observation of DAPI stained germline clone X9 embryos by fluorescent microscopy revealed a high proportion of non-development (~50%, N=105), indicating functional defects during oogenesis, meiosis or fertilization. Mutant embryos that developed and did not hatch survived until latest stage 8. When crossing females of X9 germline clones to males, lethality was not zygotically rescued in heterozygous female embryos, demonstrating potential zygotic expression is not sufficient to substitute a lack of maternally supplied gene products.

Time-lapse imaging with differential interference contrast microscopy (DIC) was conducted to record phenotypes of X9 germline clones. In most cases, cellularization accomplishes properly but pole cells shift gets stuck either at the beginning or shortly before completing of gastrulation. Cephalic furrow formation was observed occasionally.

Oogenesis appeared also abnormal in X9 mutants. Roughly 80% of the ovaries from X9 germline clone females showed degenerated egg chambers (Fig. 17 and Tab. 7), resulting in very low egg laying rate. Moreover, about 10% of egg chambers had 32-cell germline cysts, suggesting one additional cystocyte division (Fig. 17 and Tab.7).

To determine if X9 mutant has defective early pattern formation, Even skipped (Eve) antibody was used for immunostaining of X9 germline clone embryos (Frasch and Levine 1987). Similar to WT, seven marker stripes distributed evenly in X9 embryos in interphase 14, suggesting normal gap and pair-rule gene localizations in anterior-posterior patterning (Fig. 18A). Cuticle preparation of germline clone derived X9 embryos showed differentiated structure with normal number of denticle bands, although appeared 'ugly', meaning normal early developmental morphology (Fig. 18B).
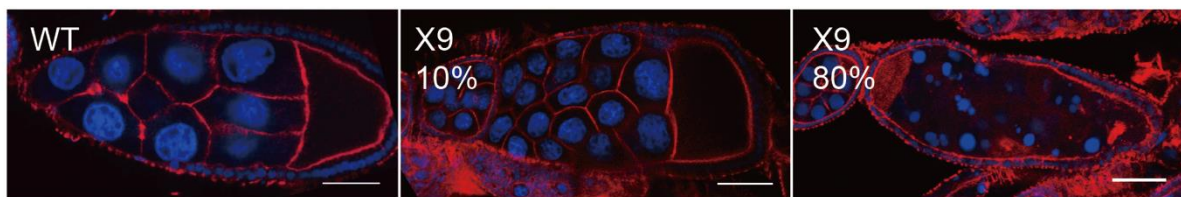
Figure 17: Phenotypes of ovariole from X9 germline clone adult females. Approximately 10% of the egg chambers from X9 females have 32 germ cells, resulting from one additional cystocyte division. Approximately 80% showed degenerated egg chambers. Egg chamber DNA was stained with DAPI (blue). Actin cytoskeleton was stained with Phalloidin (red). Scale bar represents 50 μm.
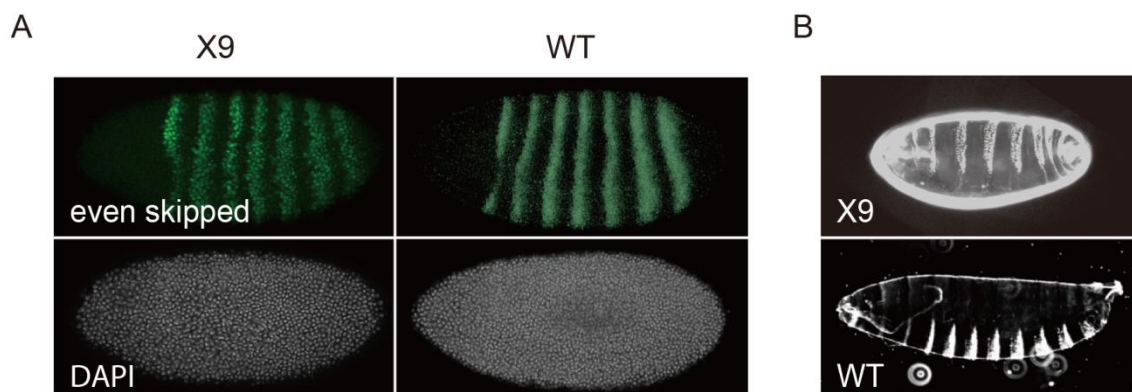
Figure 18: Pattern formation is not affected in X9 embryo. (A) Fixed WT and X9 embryos were stained for pair-rule protein Even skipped (green) and DNA (white). Seven even stripes appeared in both WT and X9 embryos in interphase 14. (B) Cuticle preparation of WT and X9 embryos. Anterior is to the left throughout.

2.1.2 X9 germline clones show blastoderm defects

Cell cycle defect

X9 embryos showed defects in late blastoderm stage. Approximately 30–50% of the embryos underwent a round of extra mitotic division, either comprising the entire embryo or only part of it. Further observation revealed irregular nuclear elongation. Some nuclei started to fallout into the embryonic core during later phase of the last nuclear cycle (Fig. 19). Germline clone embryos labelled with fluorescent histone-RFP gave a closer look into chromosomal modeling by using live-imaging (Fig. 20A). The lengths of the early cell cycles were comparable to WT embryos, although a little longer (Fig. 20B) (Tab. 6 and Supplemental Tab. 1). Additionally, X9 embryos had very slow mitotic waves with average speeds of 3.1±0.9 µm/min (N=4) as compared to 12±3 µm/min (N=4) in WT embryos in the last mitosis. This causes difficulty in measuring the cell cycle length.
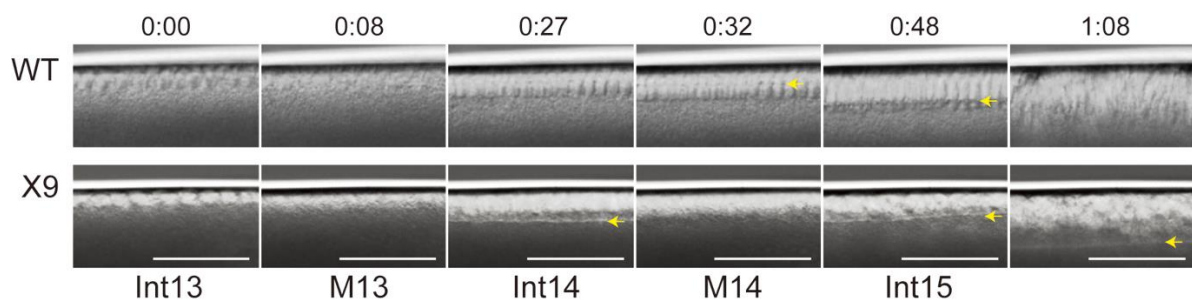
Figure 19: Time-lapse images of DIC microscopy reveal a cell cycle phenotype. Images from time lapse recordings of embryos show the cortical part of the WT and germline clone derived X9 mutant embryos. Yellow arrows point to the invaginating furrow front. Int: interphase; M: mitosis. Scale bar represents 50 µm.

Chromosome segregation defects

A mitotic phenotype was detected beside the additional cleavage cycle. During syncytial divisions NC10–13, a low frequency of reproducibly chromosome segregation defects was observed (3% of the nuclei (N>100), three embryos). Delayed chromosome separation i.e. chromosome bridges in telophase was often observed (Fig. 21A and 21C). In addition, although the arrangement of the

centrosomes with single centrosomes at spindle poles appeared normal, some mis-segregated chromatins were pulled toward to the neighboring spindles (Fig. 21B).
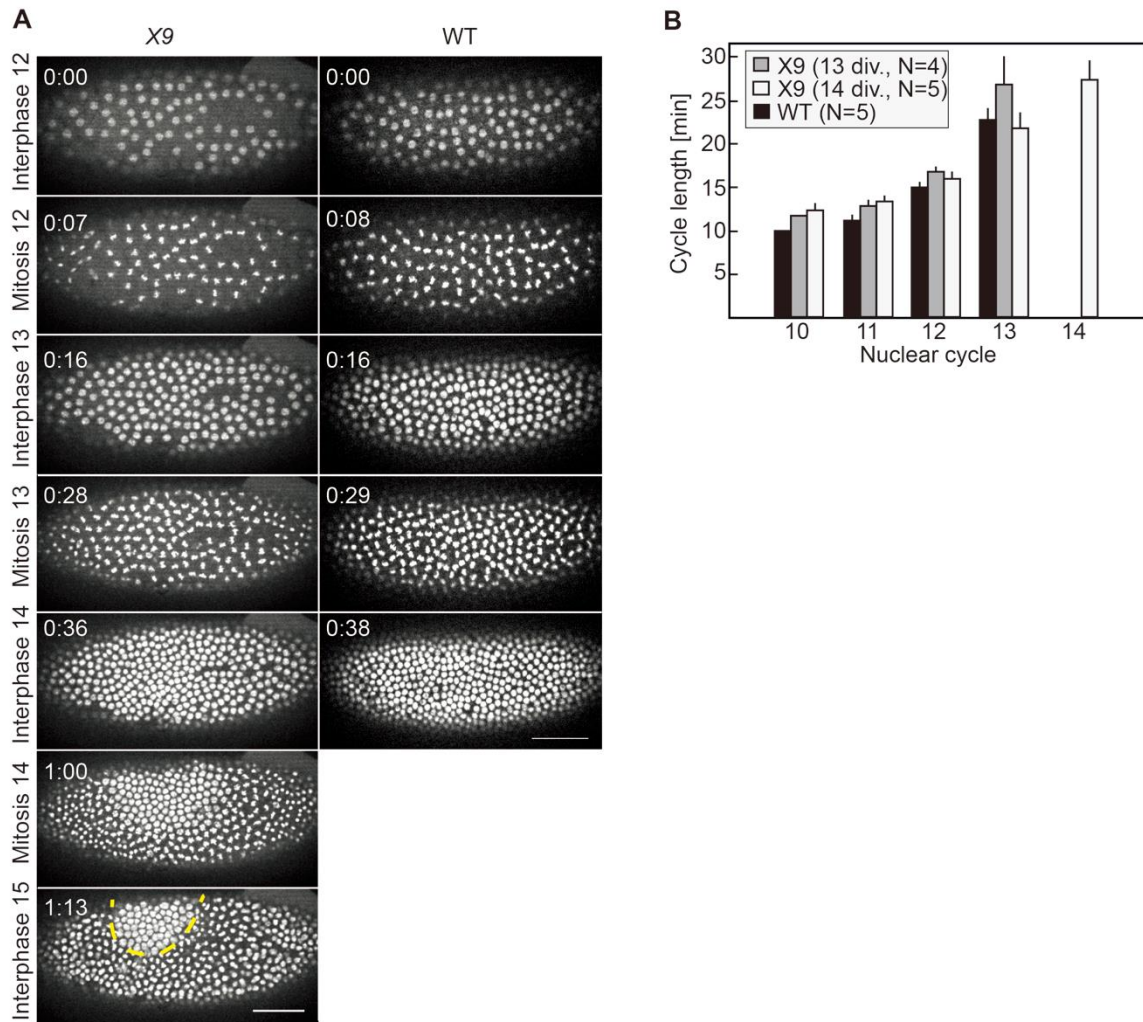

Figure 20: X9 germline clone embryos undergo extra mitotic division. (A) Fluorescent time-lapse imaging of WT and X9 embryos expressing Histone2Av-RFP. Yellow dashed line encircles respective nuclear densities. Scale bar represents 50 µm. (B) Quantification of the cell cycle lengths with time-lapse recordings of WT embryos and embryos from X9 germline clones expressing Histone2Av-RFP. X9 embryos were grouped in ones with normal cell cycle number (13 divisions) and ones with at least a partial extra cycle (14 divisions).

Table 6: Cell cycle lengths in WT and X9 embryos expressing Histone2Av-RFP

Genotype	Cycles	N	Cell cycle length (min)				
			10	11	12	13	14
X9	13	4	12.0	13.0±1.0	17.0±1.0	26.8±3.3	
X9	14	5	12.5±1.5	13.6±1.5	16.0±1.2	21.8±2.6	27.4±2.1
WT	13	5	10.0	11.5±1.0	14.8±1.0	22.4±1.8	

Corresponding to Supplemental Table 1.
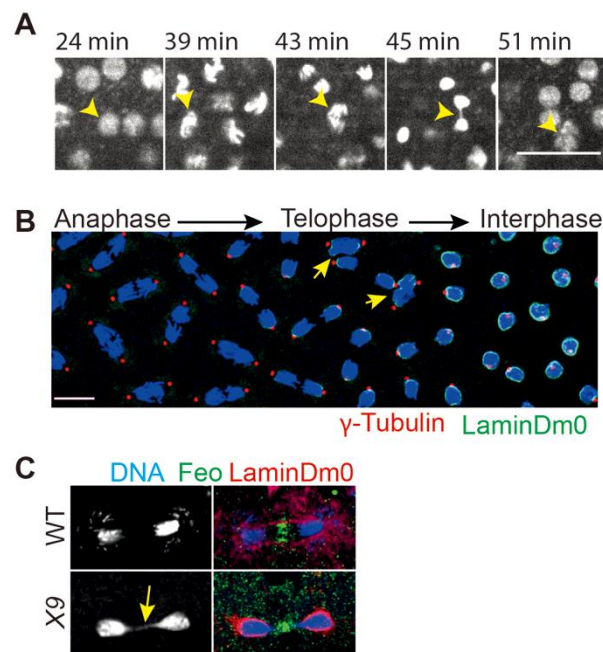
Figure 21: X9 mutants show chromosome segregation defects during syncytial divisions. (A) Images from time-lapse recordings of X9 germline clone embryos expressing Histone2Av-RFP. Yellow arrow heads point to nucleus with abnormal chromosome segregation. Scale bar represents 20 µm. (B) Fixed embryos from X9 germline clones were stained for centrosomes (γ-Tubulin, red), nuclear lamina (LaminDm0, green) and DNA (DAPI, blue). As a mitotic wave passed over the embryo, multiple mitotic stages were covered in a single embryo. Yellow arrows point to mis-segregating nuclei. Scale bar represents 10 µm. Imaging was carried out by Sung. (C) Fixed WT and X9 embryo stained nuclear lamina (LaminDm0, red), mid body (Fascetto, green) and DNA (DAPI, blue). Yellow arrow points to delayed chromosome separation in telophase. Imaging was carried out by Sung.

Cell proliferation of larval and adult tissues

To clarify if X9 mutants have defect in cell proliferation, induction of X9 clones in female follicular epithelium cells was performed and their proliferation was analyzed. Females containing Flipase recognition target 18 (Frt18) and heat-shock promotor Flipase (hs-Flp) in control and X9 backgrounds were crossed with nuclear localization signal-GFP (nls-GFP) Frt18 males (Chou and Perrimon 1996). After heat-shock, recombination occurred between the Frt sites, resulting in depletion clone cells without GFP (X9/X9) and twin clone cells with two copies of GFP (nls-GFP/nls-GFP). By counting the number of each genotype of follicular cells, it can be compared how many cell divisions underwent in depletion clones and their neighboring twin clones. If cell proliferation is affected in X9 mutants, different cell numbers were expected to be observed between X9/X9 and nls-GFP/nls-GFP clone cells.
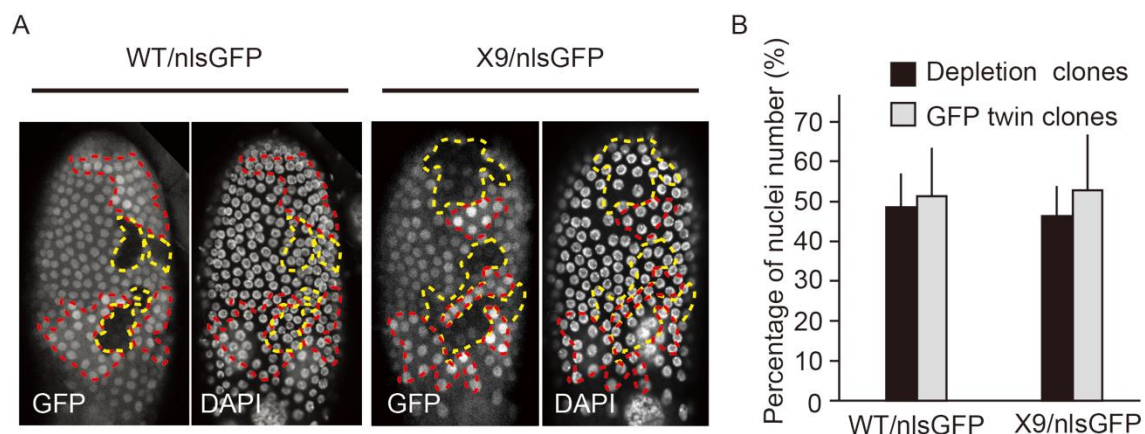
Figure 22: Induction of X9 clones in follicle epithelium does not affect cell proliferation. (A) Follicle epithelium cells of WT and X9 stained with GFP-booster and DAPI. The proliferation of X9 clones (GFP depletion area, encircled by dashed yellow line) and GFP twin clones (two times GFP signal, encircled by dashed red line) were compared by counting the number of nuclei (DAPI). Scale bar represents 50 µm. (B) Quantification of depletion clones percentage in control and X9 female flies. N=10 egg chambers in X9. N=8 egg chambers in WT.

When comparing the number of depletion clones and nls-GFP twin clones in control follicular epithelium cells, the ratio of WT/WT and nls-GFP/nls-GFP was close to 1:1. While in X9 mutant follicular cells, the number of X9/X9 and nls-GFP/nls-GFP clones were also similar (Fig. 22A and 22B), suggesting cell proliferation in follicular epithelium cells was not affected in X9 mutants.

2.2 X9 is a null mutant allele of *PpV*

2.2.1 Mapping, cloning and genomic rescue

The X9 mutant was mapped by meiotic recombination and complementation with duplications and deficiency kits from Bloomington Drosophila Stock Center. By using meiotic recombination with marker chromosomes, two lethal mutations were identified. The distal lethal is associated with the early embryonic phenotype. Germline clones of the proximal lethal developed normally. Complementation test with duplications showed lethality rescue in Dp5279, Dp5281 and Dp948 strains, indicating the lethality was located to the X:4–6 region in lethal 1. Smaller deficiencies in 5F3–4 region restricted the mutation loci of X9 to Ex6239. Under the breakpoint Ex6239, only the duplication Dp(1;3)DC155 rescued lethality and the germline clone phenotype, so that the mutation point was narrowed in this region (Fig. 23).

This region contains four annotated genes: *swallow pseudogene* (*swaPsi*), *swallow* (*swa*), *Mitochondrial assembly regulatory factor* (*Marf*), *Protein phosphatase V* (*PpV*) and one unannotated code CR44816 (Fig. 23). Mapping of the X9 mutant was carried out by Prof. Dr. J. Großhans and Dr. H. Sung.

Sequencing of the genes in the mapped region was performed in comparison to the isogenic X238 chromosome, which was isolated in the same mutagenic background. Sequencing revealed a nonsense mutation in the seventh codon of the *PpV* gene, which induced a premature stop codon in X9 rather than Tryptophan in WT (W7Stop) (Fig. 24). The *PpV* gene has four transcript variants RA, RB, RC and RD with 1,599–1,675 bp mRNAs, whereas different isoforms encode same 303 amino acids. *PpV* gene contains three exons and 2–3 introns, with 664 bp 3' UTR. Four alleles of *PpV* mutant exist in Flybase, with point mutations of W203R (*PpV^A*), I117F (*PpV^C*),

G162S (PpV^X) and H112L (PpV^Y), respectively (Haelterman et al. 2014) (Fig. 25A). Time-lapse imaging revealed that embryos from PpV^A germline clone females were defective during cellularization and gastrulation. Whereas PpV^C germline clone derived embryos showed 50% extra mitotic nuclear division (N=10), with cellularization and gastrulation defects comparable to X9. Immunostaining of fixed PpV^A and PpV^C embryos with the lateral membrane marker Discs large 1 (Dlg), pattern formation marker Even skipped (Eve) and DNA dye DAPI showed apparent normal (Fig. 25B).
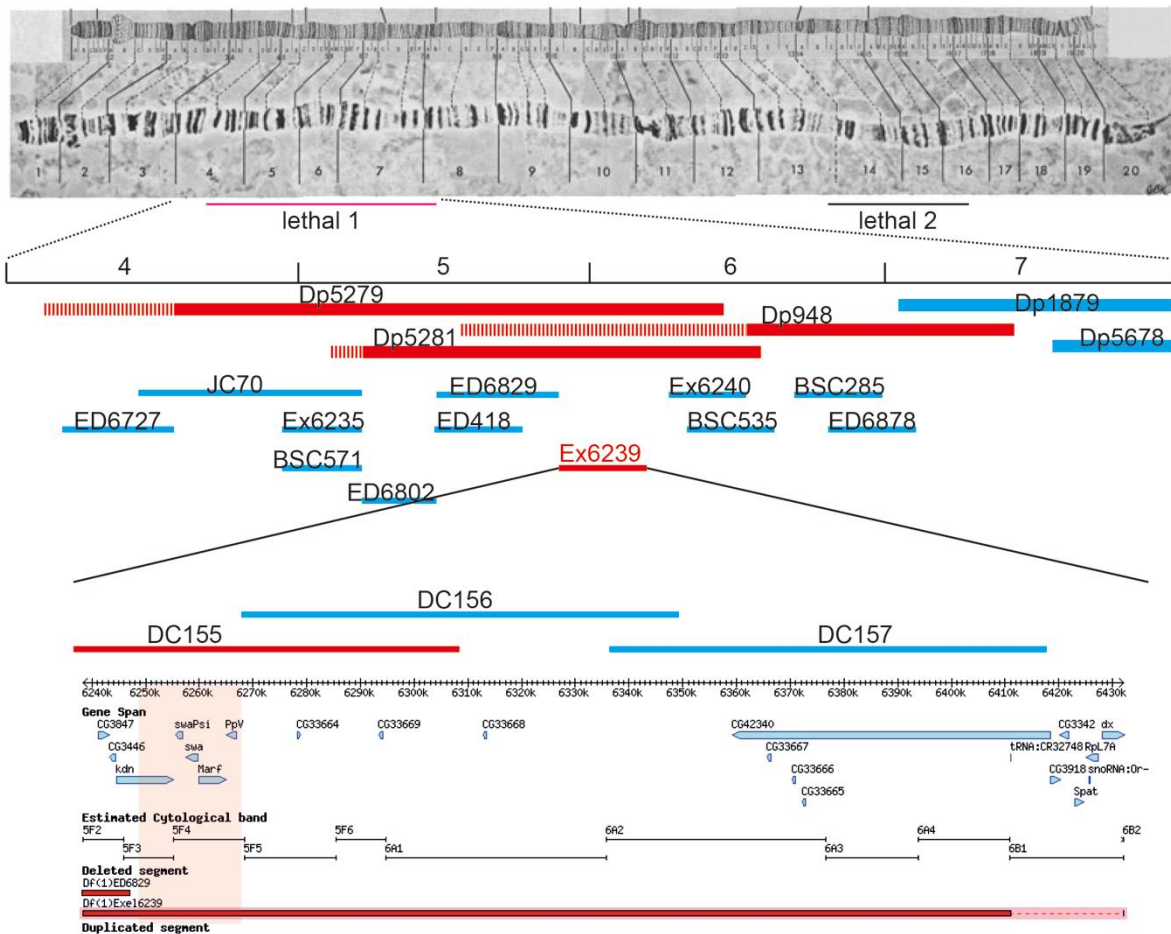
Figure 23: Mapping of X9 mutant. Image of the X chromosome with the position of the mapped lethal mutations and mapped region by the closest breakpoints (distal Df(1)ED6829, proximal Dp(1;3)DC156). The distal lethality was mapped by complementation with indicated duplication and deficiency chromosomes. Dashed regions indicate uncertainty of the breakpoints. Complementing duplications and non-complementing deficiencies are marked in red. Mapping was carried out by Großhans and Sung.
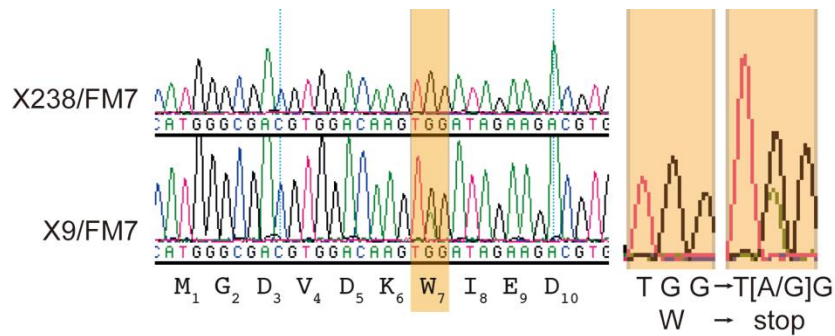
Figure 24: Sequencing and cloning of X9 mutant. Sequence traces of DNA amplified from heterozygous X9/FM7 and in comparison X238/FM7 with a related genetic background. The double peak in the X9 trace reveals the non-sense mutation in codon 7 (TGG to TAG). Sequencing was carried out by Großhans and Sung.

The genomic rescue construct was employed for complementation. The 2,679 bp full-length genomic rescue construct PpV-rescue was cut by EcoRI from BAC clone 18C-18 (BACPAC Resources Center) and cloned into the pattB vector (Fig. 26). PpV-rescue transgenic flies were generated by microinjection of genomic rescue construct into embryos of phiX-86Fb line, and then were crossed to X9 heterozygous flies. The PpV-rescue complemented the lethality of X9 and the embryonic phenotype of germline clones.

Unexpectedly, homozygous X9 and PpV-rescue transgenic flies X9/X9;PpV+/PpV+ are female sterile. This raises the question if part of the endogenous promotor is missing in the PpV-rescue construct. It seems not to be the case, since a large duplication Dp(1;3)DC155 which covers ~90 kb whole genomic region of the *PpV* locus also rescues lethality and the germline clone phenotype, but not the female sterility of X9 homozygous females. This suggests that an additional mutation of a gene which is required for follicle function and for egg formation exists on X chromosome of X9. Nonetheless, female sterility of *PpV*[A] and *PpV*[C] alleles, as well as their lethality and phenotypes were successfully rescued by PpV-rescue construct, verifying the causality of the phenotypes.
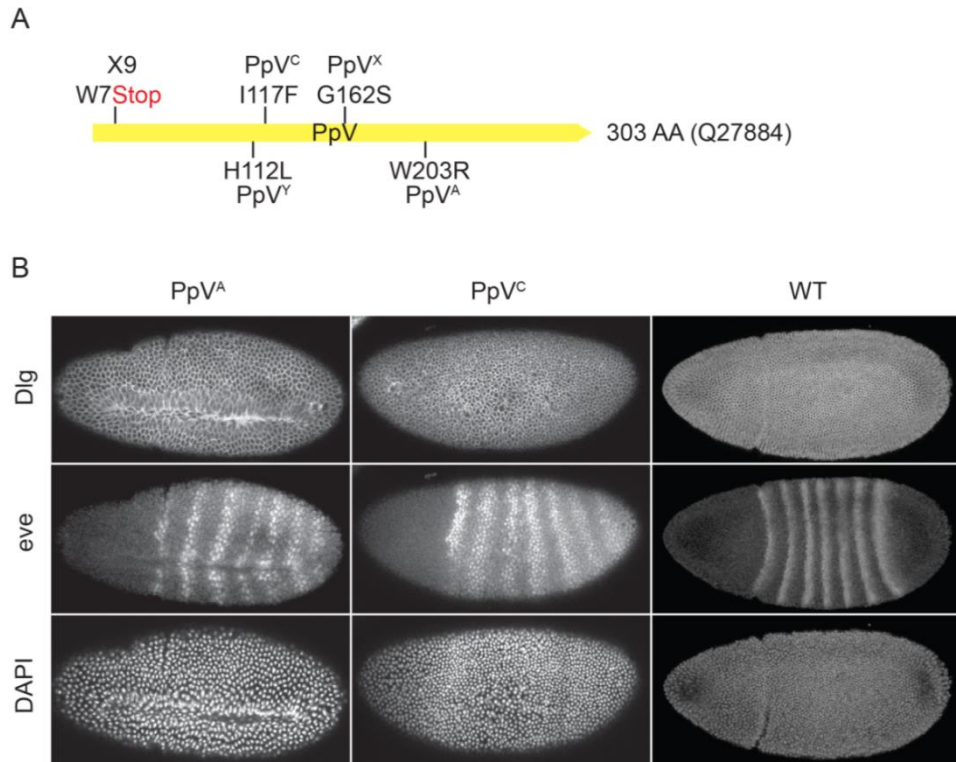
Figure 25: Phenotypes of *PpV* mutant alleles. (A) Scheme of five *PpV* mutant alleles. The mutation of X9 leading to a stop codon at position 7 is indicated (W7stop). Alleles *PpV^A*, *PpV^C*, *PpV^X* and *PpV^Y* induce missense mutations (Haelterman et al. 2014). (B) Immunostaining of fixed *PpV^A* and *PpV^C* germline clone embryos. Localization and morphology of Discs large 1 (Dlg), Even skipped (eve) and DAPI showed apparent normal.
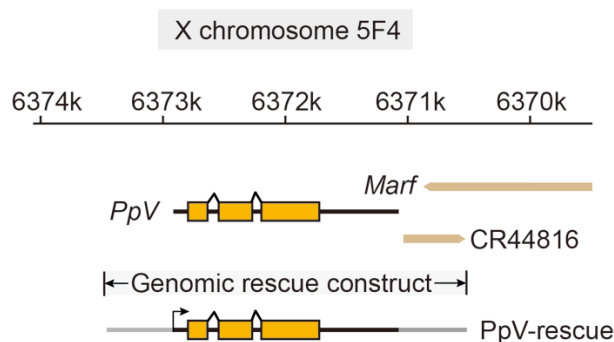

Figure 26: Identification and genomic rescue of X9 mutant. Region surrounding the *PpV* locus on X chromosome. Exons of *PpV* transcript are indicated in orange, and introns in black lines. Neighboring loci are marked in brown. Region of genomic rescue construct PpV-rescue is depicted in grey.

2.2.2 Embryonic expression level of PpV

To generate a PpV antibody, a peptide corresponding to the non-conserved PpV C-terminus DAERVIPKQNTTP was synthesized for immunization (Charles River Laboratories, Kißlegg). However this peptide proved to be non-immunogenic in two rabbits, despite the promising computer prediction. Thus the full-length *PpV* coding sequence was cloned into an expression vector with a C-terminal His-tag. The His-PpV protein was purified under denaturing conditions (Trenzyme, Konstanz) (Fig. 27A). Rabbits were immunized with the purified denatured protein (BioGenes, Berlin). The anti-rabbit serum was utilized in the following Western blot.

In order to detect PpV expression level in X9 mutants and rescue transgenic flies, Western blot was performed with proteins extracted from WT, X9 germline clone and X9;PpV+ embryos. The result of Western blot showed a major band with a size of approximately 35 kDa in WT lane corresponding to the estimated molecular weight of PpV (34.7 kDa). In X9 mutant lane, however, there was no band present at the predicted PpV position, indicating X9 is an apparent null allele of PpV. Introducing PpV-rescue construct in X9 homozygous background restored a band at PpV position, but with weaker protein level compared to WT (Fig. 27B). This result confirmed X9 mutants can be rescued by exogenous expression of PpV.

To test if zygotic PpV is expressed during late embryonic development, embryos from X9 germline clone were staged as 0–4 h, 4–8 h and 8–12 h, and used for Western blot. Proteins from staged embryos were extracted and loaded onto SDS-PAGE gel, and detected by PpV antibody. The result showed the absence of a PpV band in all the stages, meaning no zygotic expression of PpV protein was detected (Fig. 27C). This is consistent with the genetics, since no zygotic rescue was observed.
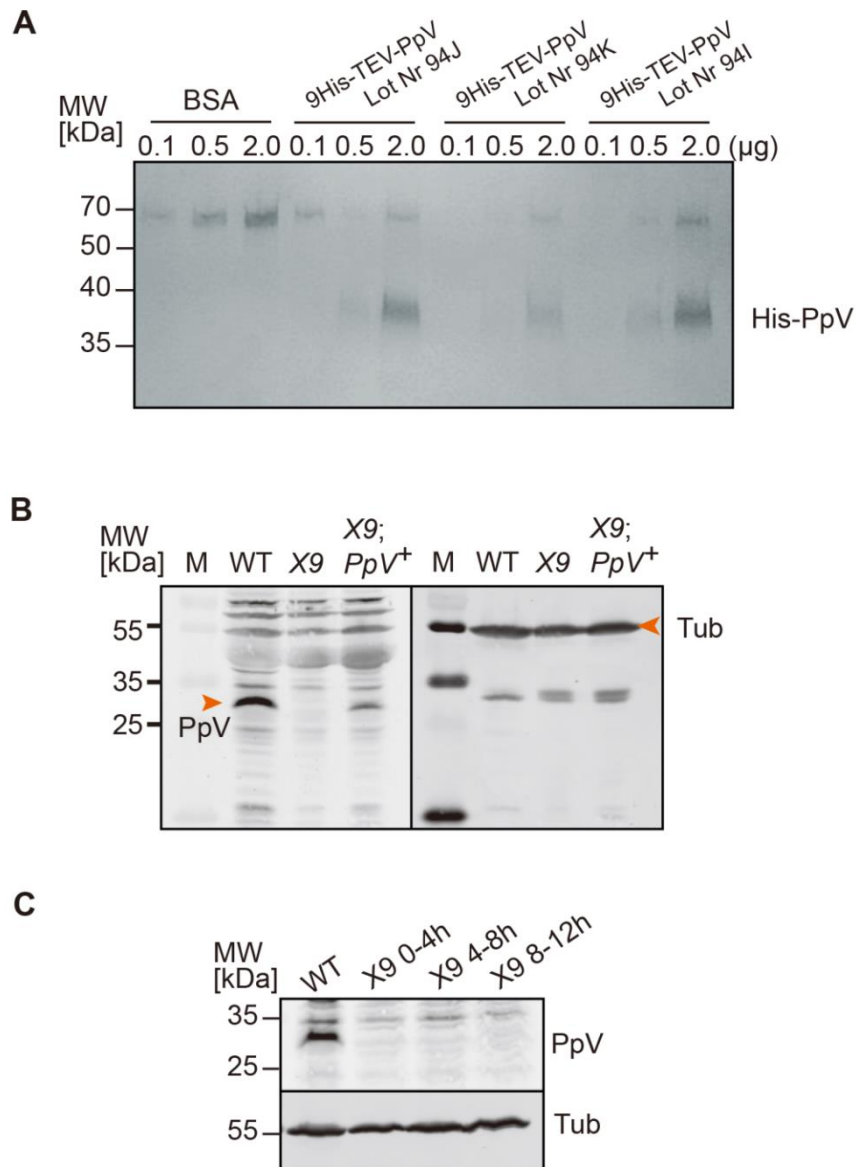
Figure 27: Expression level of PpV. (A) Coomassie blue staining of three different purified His-PpV proteins. Concentration gradient of BSA serves as reference. (B) Western blot with extracts of WT embryos, X9 germline clone embryos and transgenic rescue X9; PpV+ embryos. Red arrows point the positions of PpV and Tub. (C) Western blot with extracts of WT and staged embryos from X9 germline clones. Loading control with α-Tubulin (Tub).

2.2.3 PpV protein is distributed throughout the cells with a weak cytoplasmic enrichment

To reveal protein subcellular localization of PpV in *Drosophila* early embryogenesis, immunostaining of PpV antibody was utilized. The antiserum led to an indistinguishable staining in WT and X9 germline clones. This indicates that the unspecific reactivity of the antibody is stronger than the specific binding. This is consistent with the high cross reactivity observed in the Western blots. As a so far not characterized UAS-GFP-PpV line was available from the Bloomington Drosophila Stock Center, embryos from UAS-GFP-PpV females and maternally expressed Gal4 transgenic males mat67;mat15 were generated by using UAS/Gal4 system (Duffy 2002). GFP fluorescent signal in the fixed F2 generation embryos was observed exclusively localized in the cytoplasm (Fig. 28). In stage 11, GFP signal can be seen highly enriched in the yolk (Fig. 28). With this experimental approach GFP-PpV was most likely ectopically expressed as compared to endogenous levels, making interpretation of the data difficult.
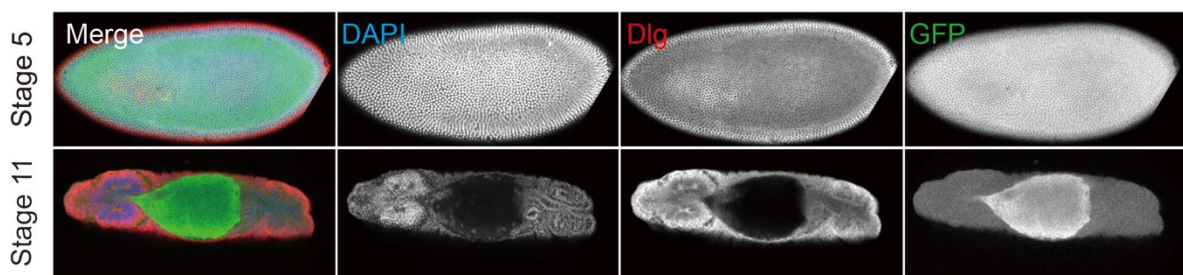

Figure 28: GFP signal of fixed embryos from maternally expressed UAS-GFP-PpV. Embryos were immunostained with Discs large 1 (Dlg), GFP-booster and DAPI. GFP signal was observed exclusively localized in the cytoplasm (stage 5) and the yolk (stage 11).

To avoid the complication of cross reactivity, a GFP-tagged version of PpV under control of the endogenous promoter was generated. The 5' terminal 444 bp (a HindII/EcoRI-BspM1 fragment) were replaced by a corresponding 1,229 bp fragment with codon optimized GFP and a linker inserted at the start codon (Fig. 29A). The GFP-PpV-rescue plasmid was introduced into transgenic flies by microinjection. The GFP-PpV-rescue flies also rescued lethality and the cell cycle phenotype of germline

clones. PpV protein was specifically detected by the immunostaining of GFP-booster. It has been clarified that GFP-PpV was uniformly distributed in early embryos spatially and temporally, from syncytial blastoderm to MBT (Fig. 29B). Closer observation revealed slightly lower GFP levels in the nucleus. There was no obvious difference among embryos in different embryonic stages, indicating the expression levels of PpV protein do not change much through embryonic development (Fig. 29B).
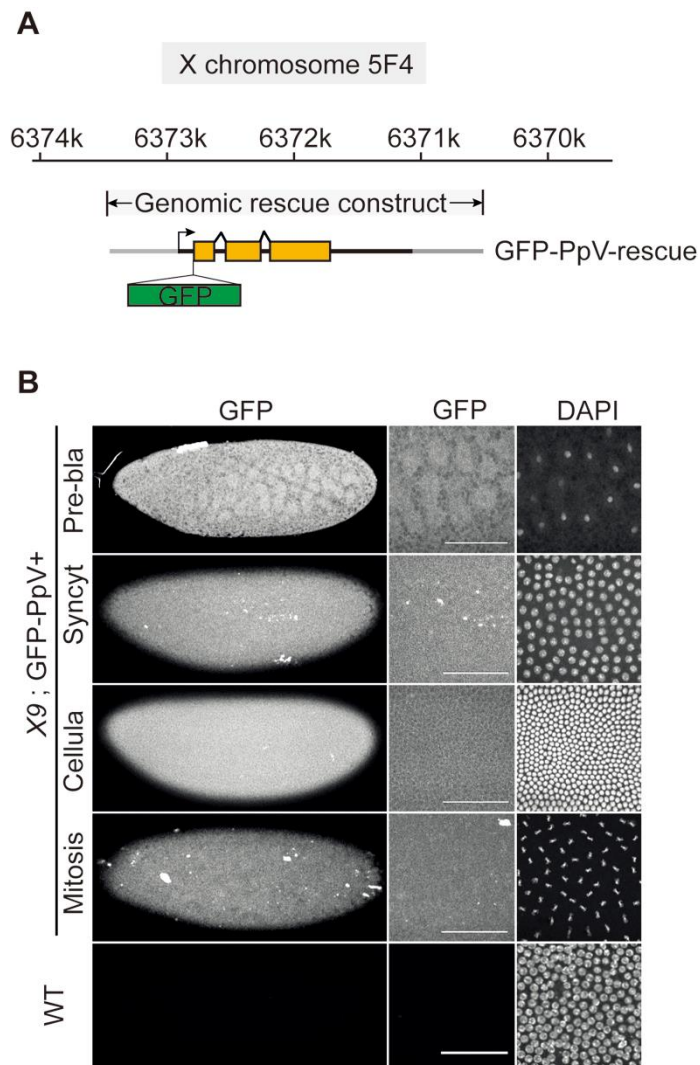

Figure 29: Subcellular localization of GFP-PpV. (A) Scheme of the genomic rescue construct GFP-PpV-rescue. Exons of PpV transcript are indicated in orange, and GFP insertion is in green. Position in genomic region is depicted in grey. (B) Fixed embryos with and without a genomic rescue construct GFP-PpV were stained for GFP and DAPI. Magnified view was recorded by 40× objective. Pre-bla: pre-blastoderm; Syncyt: syncytium; Cellula: cellularization. Scale bar represents 50 μm.

2.3 Physical and genetic interactions of PpV

2.3.1 Physical binding partners of PpV

Two-hybrid screening was performed to identify physical interactions of PpV protein. PpV bait (aa 2–303) was conducted by Hybrigenics Company. In the low sensitivity screen only one type of interactor was isolated, namely Two A-associated protein of 42 kDa (Tap42) (Supplemental Tab. 2). Tap42 is the *Drosophila* homologue of human Alpha4, which constitutes the common regulatory subunit of the PP2A family, including PP6 (Chen et al. 1998; Nanahoshi et al. 1998; Cygnar et al. 2005). It has been reported that FLAG immunoprecipitations of Tap42 appeared strong interaction with *Drosophila* PP2A family members PP2A (microtubule star, mts), PP4 and PpV in vitro (Stefansson and Brautigan 2007; Wang et al. 2012), which consist with our two-hybrid screening results. In a second screen with higher sensitivity, additional potential binding partners were isolated (Supplemental Tab. 3). The list included Chorion protein 38 (Cp38), Hsp70/Hsp90 organizing protein (Hop) and like-AP180 (lap). However, none of these potential binding partners have an obvious link to the mutant phenotypes of embryos from X9 germline clones.

2.3.2 Genetic interactions of PpV

Beside the physical interaction partners, physiological functional interactions of PpV in vivo were characterized by genetic interaction tests. By overviewing regulatory processes of *Drosophila* early cell cycles, multiple regulators including Checkpoint kinase 1 (Chk1), Wee1, Myt1, Frühstart, Tribbles and Cdc25/Twine are potential targets of PpV. Viabilities of double mutants were first tested for genetic interactions. Two of these experiments revealed genetic interactions with *Tribbles* and *Cdc25/Twine*. X9;*tribbles* double mutants did not lay any eggs, indicating an additive or synergistic genetic interaction during oogenesis. A different genetic interaction was detected with *Twine*. Germline clone of X9 with heterozygous *twine* mutant X9/ovo;*twine*/+ was semi-fertile, since few hatching larvae cases were observed (<5%, N>1,000), contrary to absolute 0% hatching rate of sole X9 mutant. The formal description for this interaction is that *twine* is a dominant suppressor of *PpV*. This indicates that PpV and Twine act in an antagonistic manner.

Genetic interactions on wing imaginal discs

Zygotic regulators Tribbles and Frühstart control blastoderm nuclear cycles through distinct pathways. Tribbles is implicated due to its function in degradation of Twine (Grosshans and Wieschaus 2000; Seher and Leptin 2000; Farrell and O'Farrell 2013), whereas Frühstart interferes with Cdk1 substrate recognition (Grosshans and Wieschaus 2000; Grosshans et al. 2003; Gawlinski et al. 2007). To address the relationship between Tribbles, Frühstart and PpV, effects on wing imaginal discs were assessed by using the UAS/Gal4 system and tissue-specific ms-Gal4 driver. In positive controls, overexpression of *cyclinE* and *string* suppressed the wing phenotypes of overexpression of *frühstart* and *tribbles*, respectively (Fig. 30A). In contrast, overexpression of *PpV* failed to suppress either *frühstart* or *tribbles* overexpressing phenotypes. So did *PpV* mutant X9 (Fig. 30A). These data exhibited PpV may be a tissue or developmental specific regulator.

Genetic interactions on ovaries

We employed the *tribbles* null mutant *tribbles*^{EP1119}, which contains a P-element inserted in the 5'UTR of *tribbles* locus. Embryos from deficiency version *tribbles*^{EP1119}/Df(3L)ri-79c females have undetectable *tribbles* mRNA (Mata et al. 2000). *tribbles*^{EP1119} is rescued by a genomic rescue transgene of the *tribbles* locus and can be regarded as a strong allele of *tribbles*. Homozygous *tribbles* flies are (semi-)viable and fertile, and the embryos develop normally with 13 nuclear division cycles prior to MBT (96%, N=28). Although *tribbles* loss-of-function homozygous females are fertile, the ovarioles of both *tribbles/ tribbles* and the *tribbles*/Df(3L)ri-79c revealed constantly abnormal (Fig. 30B). In contrast to literature reported frequent 8-cell germline cysts (Mata et al. 2000), the phenotypes of big nuclei, multiple or single, from nurse cells drop into oocyte was observed quite often (35%, Tab. 7).

Females from *PpV* and *tribbles* double mutant X9/ovo;*tribbles*/Df(3L)ri-79c were sterile. The ovaries of these females displayed multiple defects including egg chambers with an increased number of nurse cells, two nuclei shared one nurse cell and rarely even enlarged single nurse nucleus (Fig. 30B and Tab. 7). As both X9 and *tribbles*^{EP1119} are null alleles, it can be speculated that PpV and Tribbles may act

additively because the phenotype in the double mutants is stronger than that in the single mutants (Fig. 30B).
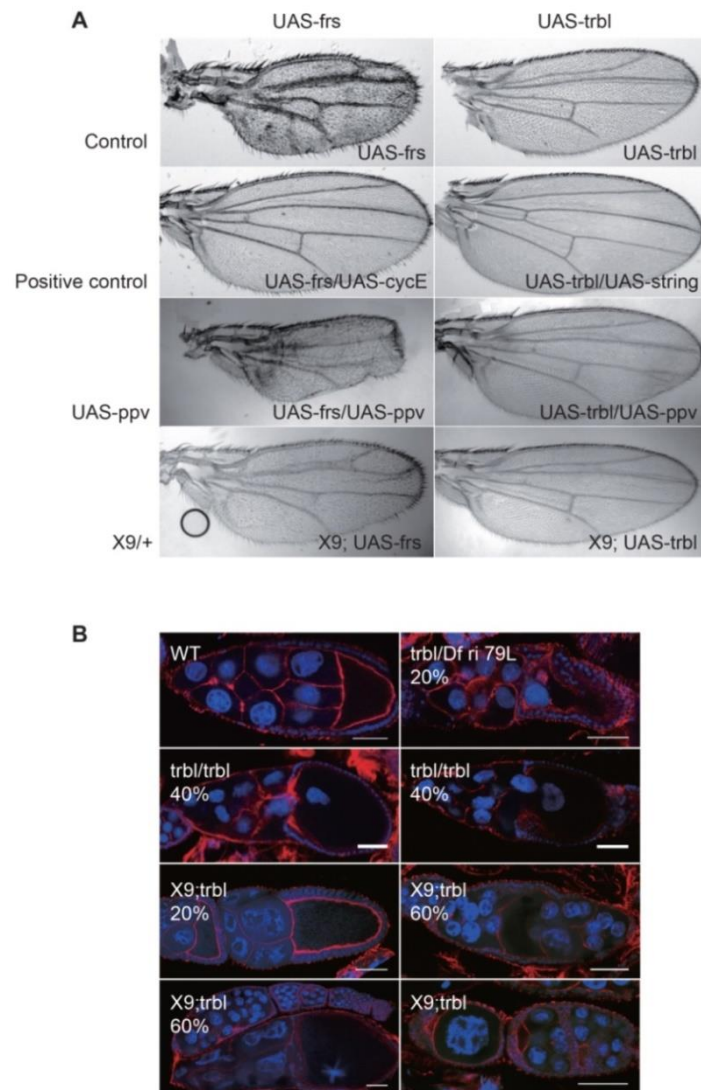

Figure 30: Genetic interactions on wing imaginal disc cells and ovaries. (A) Wings from UAS-frühstart and UAS-tribbles blank controls (top); UAS-frühstart/UAS-cyclinE and UAS-tribbles/UAS-string positive controls (second row); UAS-frühstart/UAS-PpV and UAS-tribbles/UAS-PpV (third row); X9;UAS-frühstart and X9;UAS-tribbles (bottom). (B) Phenotypes of fixed ovarioles. WT cysts contain 16 cells including 15 nurse cells and a single oocyte (top left). About 20% of the egg chambers from *tribbles* loss-of-function *tribbles*[EP1119]/Df ri 79L and 40% of *tribbles*[EP1119] homozygous showed the nurse cells drop into oocyte (top right and second row); double mutants X9;*tribbles*[EP1119]/Df ri 79L appeared 20% of two nuclei in one nurse cell, 60% of 32-cell and occasionally single putative cyst (third row and bottom). Egg chamber DNA was stained with DAPI (blue), and actin cytoskeleton was stained with Phalloidin (red), respectively. Scale bar represents 50 μm.

Table 7: Phenotypes of ovaries

Genotype	Phenotype				
tribbles/Df ri 79L	Big nuclei in oocyte			Normal	Total Nr.
	5			23	28
tribbles/*tribbles*	Big nuclei in oocyte	8-cell		Normal	Total Nr.
	25	1		41	67
X9	32-cell	Degenerated egg chamber		Normal	Total Nr.
	2	23		5	30
X9; *tribbles*/ Df(3L)ri-79c	32-cell	1 cell	2 nuclei in 1 cell	Normal	Total Nr.
	10	1	4	3	18

Epistasis of *Tribbles* and *PpV*

To investigate the functional interaction between Tribbles and PpV in early embryogenesis, the transcripts of *tribbles* were depleted by RNAi in early embryos. It has been reported that RNAi against *tribbles* slightly delays Twine degradation, but it is not clear yet if it could also induce additional mitosis. After microinjection of *tribbles* dsRNA, WT embryos developed normally until cellularization, indicating Tribbles is not required for cell cycle pause (Fig. 31B and 31C). Meanwhile, a slightly increased proportion of X9 mutant embryos with an extra nuclear division revealed comparable with water control injection case (Fig. 31B and 31C).

Tribbles mRNA was then injected to test if the ability of Tribbles to induce a precocious cell cycle pause depends on PpV. In WT, it has been confirmed that injection of *tribbles* mRNA leads to a precocious cell cycle pause (~70%), like previously reported (Fig. 31B and 31C) (Grosshans and Wieschaus 2000; Farrell and O'Farrell 2013). In X9 mutants, the proportion of paused cell cycle cases were similar to WT (~60%), showing that Tribbles can pause the cell cycle even in the absence of PpV. Microinjection of *PpV* mRNA in both WT and X9 embryos before MBT did not change or rescue the cell cycle phenotype. It may be due to expanding

the amount of *PpV* mRNA cannot immediately drive its translation (Fig. 31B and 30C). These experiments may conclude that PpV and Tribbles have redundant functions in controlling the cell cycle pause during the MBT.
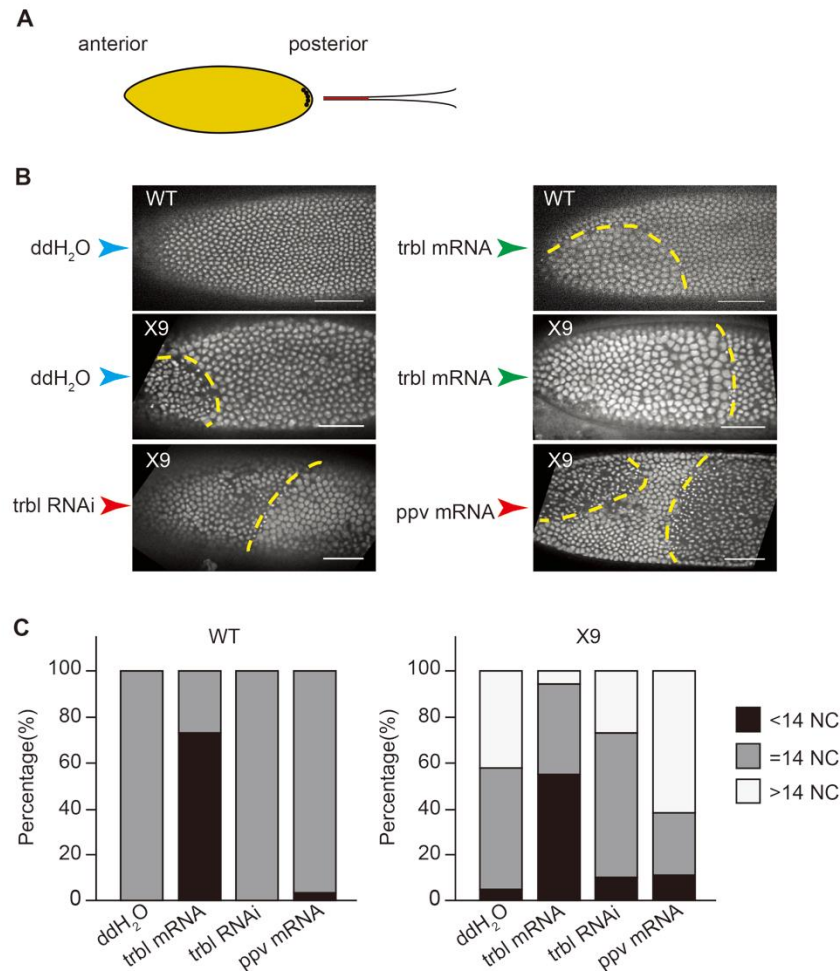

Figure 31: Functional interactions of PpV and Tribbles. (A) Scheme of microinjection from the posterior pole. (B) WT embryos and embryos from germline clones derived X9 expressing Histone 2Av-RGFP were microinjected with water, *tribbles* mRNA, *tribbles* dsRNA (RNAi) and *PpV* mRNA (indicated by arrow heads in different colors). Yellow dashed lines encircle respective nuclear densities. Scale bar represents 50 μm. (C) The numbers of syncytial nuclear divisions were scored from the time-lapse movies of injected embryos. Partial NC15 was scored as >14 NC, incomplete NC13 was <14 NC. In WT group, the numbers of embryos which were injected with water, *tribbles* mRNA, *tribbles* dsRNA (RNAi) and *PpV* mRNA were 21, 26, 9 and 30, respectively. In X9 group, the numbers of corresponding embryos were 19, 27, 34 and 19, respectively.

Functional interaction between AuroraA and PpV

As mentioned in the introduction, human PP6 has been shown to be an inhibitory regulator of AuroraA kinase, by controlling the T-loop phosphorylation state of AuroraA in human colon carcinoma cell lines (Zeng et al. 2010; Ertych et al. 2016). To research if this is conserved in *Drosophila* embryogenesis, embryos of 4×GFP (*w; Resille::GFP(117GFP); Spider::GFP*) and X9 germline clones were mixed and immunostained with AuroraA antibody. AuroraA normally localized and distributed at the centrosomes with similar expression levels in both 4×GFP and X9 embryos, no matter during mitosis or in interphase (Fig. 32), and the number of centrosomes per mitotic cells revealed bipolar in X9 mutants. This result indicates absence of PpV does not affect expression level or cellular localization of AuroraA. One would expect an AuroraA gain-of-function phenotype in X9 mutants.
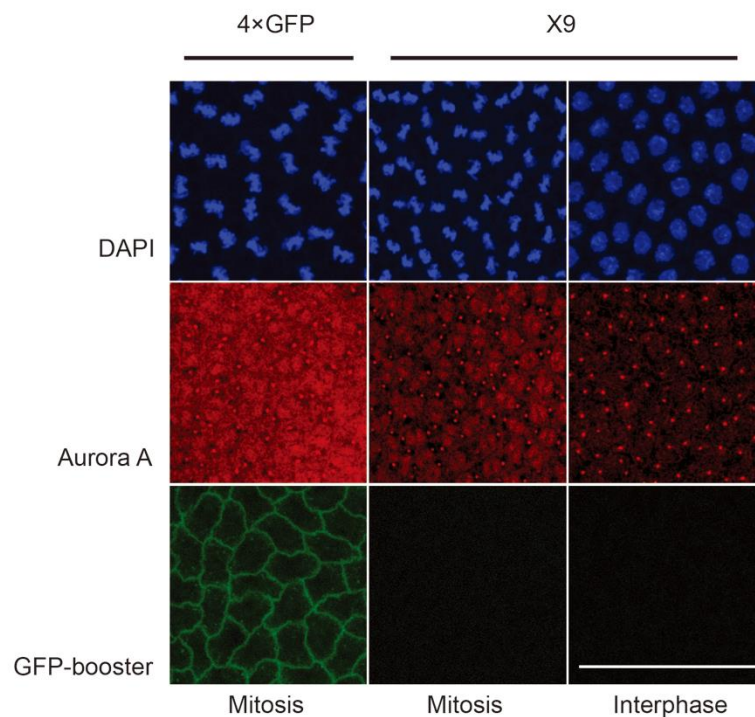

Figure 32: The embryonic expression and localization of AuroraA does not change in X9 mutants. Embryos from 4×GFP control and X9 germline clone were mixed in one tube and immunostained with DAPI, AuroraA and GFP-booster. The expression levels and the subcellular localization of AuroraA do not change in mitosis and interphase of X9 embryos. Scale bar represents 50 μm.

To test if the cell cycle phenotype in X9 mutants depends on AuroraA, double mutants of *PpV* and *aurA* is advisable to generate. However, embryos from hypomorphic *auroraA* females are characterized by severe and asynchronous mitotic defects (Glover et al. 1995) (Fig. 34), which prevents counting the number of nuclear divisions. Therefore, to circumvent this complication, we employed a chemical inhibitor of AuroraA. MLN8054 is being used as an efficient AuroraA kinase activity inhibitor and has been validated in *Drosophila* (Manfredi et al. 2007; Gottardo et al. 2015). To eliminate the activity of AuroraA, MLN8054 was injected into WT embryos expressing Histone 2Av-RFP shortly before the MBT, and then the concentration-dependent penetrance of *auroraA*-like segregation phenotypes was observed. Injection at 1 µM or 5 µM MLN8054 led to low frequency of spindle defects (Fig. 33B). When increasing the concentration of MLN8054 to 20 µM, 49% showed mitotic defects, 40% aggregated cell degeneration and fallout, and only 6% WT-like (N=33, Fig. 33A and 33C). Embryos showed frequent defects in chromosome segregation in anaphase and telophase of syncytial cycles, consistent with the *auroraA* loss-of-function phenotypes (Glover et al. 1995). Therefore, 20 µM concentration of MLN8054 was adopted in this experiment to address if AuroraA is involved in promoting the mitosis after NC14. By scoring the nuclear density and the number of nuclear division cycles, injected WT embryos did not impair the counting of division number besides chromosomal segregation defects, that all the embryos went through 13 divisions (N=20). In X9 injection cases, 44% embryos underwent additional division cycles (N=18), which was comparable to water injected control embryos (Fig. 33C). Above data suggested AuroraA may not be required for the extra nuclear division in X9 mutant embryos.

Despite this, AuroraA may still act as substrate of PpV in *Drosophila*. Since AuroraA is activated by autophosphorylation in mitosis, extracts from WT and X9 germline clone embryos were stained with DAPI dye and manually sorted in blastoderm interphase and mitosis under microscopy, and then loaded in Western blot for activity detection. As reported previously (Giet et al. 2002), Western blot of AuroraA detected a single band at approximately 47 kDa in WT (Fig. 35A). In X9, however, a weaker second band with a slightly increased apparent molecular weight beside the major band was detected in both interphase and mitotic embryo extracts (Fig. 35A), which may represent a phosphorylated form, thereby indicating hyperactivity status

of AuroraA with absence of PpV. Commercial phosphorylated Aurora antibody Phospho-Aurora A (Thr288)/ Aurora B (Thr232)/ Aurora C (Thr198) is a mammalian based polypeptide. Western blot with Phospho-Aurora antibody detected a band in mitosis, however with a different apparent molecular weight as AuroraA (Fig. 35B). This band may represent AuroraB, as the expression level was low in interphase and peak in mitosis, consistent with Aurora kinases attribute. In addition, the size of this protein was around 35 kDa, also corresponding to AuroraB (329 amino acids, estimated 38.3 kDa).
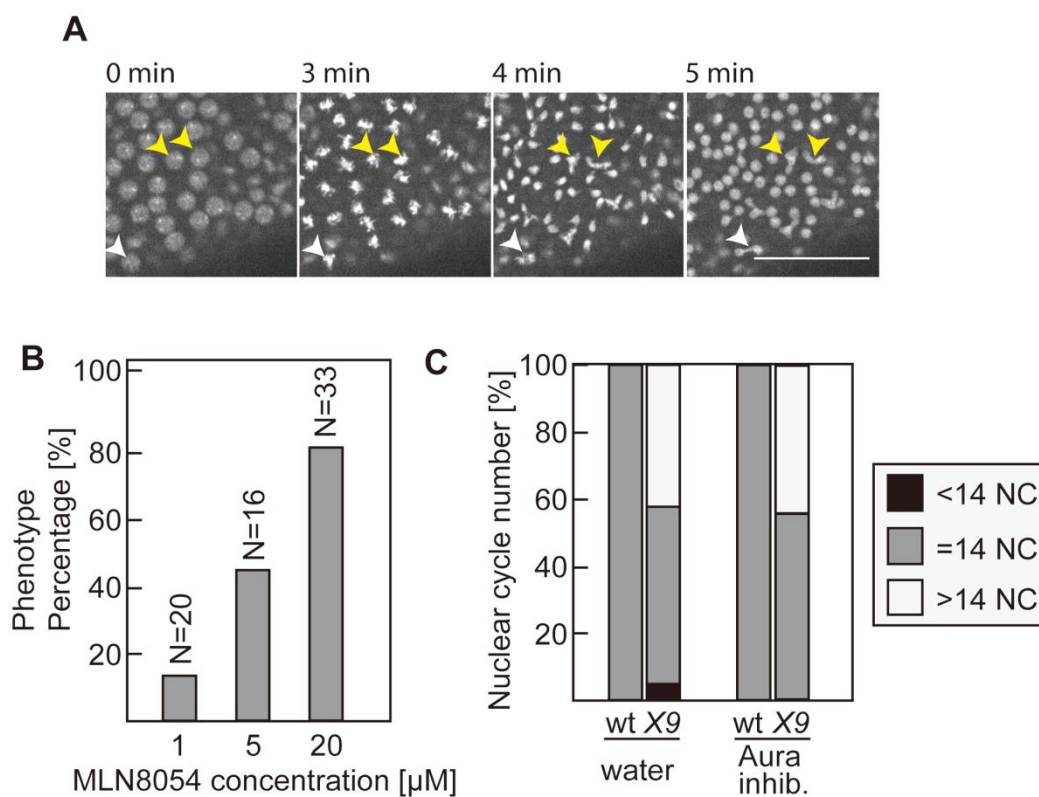
Figure 33: Microinjection of AuroraA kinase activity inhibitor MLN8054. (A) Images from time-lapse recording of a WT embryo expressing Histone 2Av-RGFP injected with 20 µM AuroraA inhibitor MLN8054. Arrow heads point to nuclei with failing segregation. Scale bar represents 50 µm. (B) Dose dependence of mitotic phenotype following MLN8054 injection. (C) Movies of injected embryos were scored for the number of nuclear divisions. Partial NC15 was scored as >14 NC, incomplete NC13 was <14 NC.
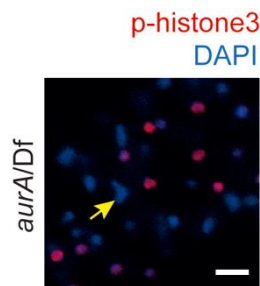
Figure 34: Embryos from hemizygous *auroraA* females show segregation defects. Image from fixed embryos from *auroraA*/Df females stained for mitotic nuclei (p-histone3, red) and DNA (blue). Arrow in yellow points to nucleus with mis-segregated DNA. Scale bar 20m.
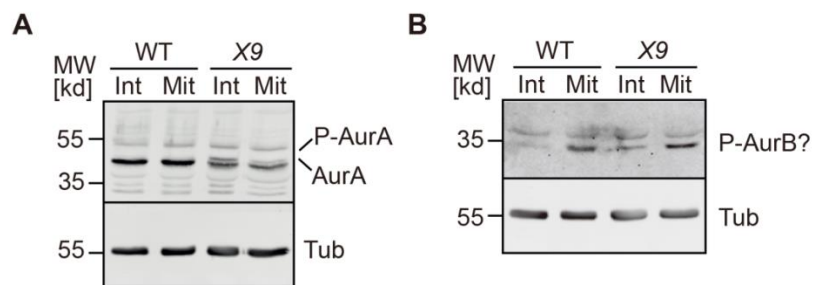

Figure 35: Western blot of AuroraA and Phospho-Aurora. (A) AuroraA Western blot of extracts from WT and X9 germline clone embryos. Embryos were manually staged for syncytial mitosis (Mit) or interphase (Int) (NC11–13). (B) Western blot with Phospho-Aurora A (Thr288)/ Aurora B (Thr232)/ Aurora C (Thr198) antibody. Suspected Phospho-AuroraB was detected due to the molecular weight and its activity during mitosis. Loading control with α-Tubulin (Tub).

2.4 Twine is a direct or indirect target of PpV

Summarizing results above, PpV and Tribbles act in parallel, and Twine is negatively controlled by Tribbles. Moreover, Twine is a dominant suppressor of PpV as *PpV* and *twine* double mutant partially rescued embryonic lethality of X9 germline clones. These evidences lead to the hypothesis that PpV may act directly or indirectly upstream of Twine.

2.4.1 Twine protein levels are increased in *PpV* mutant

Detection of Twine embryonic expression level

Degradation of Twine phosphatase in interphase 14 triggers the cell cycle switch at MBT (Di Talia et al. 2013; Farrell and O'Farrell 2013). qPCR of total *twine* RNA measurement resulted similar transcription levels of *twine* in WT and X9 embryos (1: 0.94, Tab. 8). The embryos cultured from 1 to 3 hours were then heat-fixed and immunostained for Twine antibody, and roughly staged by the morphology marker of the cellularization furrow and nuclear length (Fig. 36A). When comparing individual embryos from WT and X9 germline clone, Twine appeared more stable in X9 embryos than in WT because X9 embryos at a late stage still showed Twine staining (Fig. 36B). Direct comparison of the staining is problematic, as WT and mutant embryos were not stained in one tube and the imaging was performed side by side. The highest signal intensity was simply normalized as 100, so this does not allow a comparison of the absolute fluorescent levels.

Embryos from WT and X9 mutant were then stained with DAPI and carefully staged by different nuclear cycles (NC12, 13, 14 early and 14 late) based on nuclear density and length. Western blot of Twine was performed with extracts form exactly staged embryos. There were no obvious deviations between WT and X9 (Fig. 37). Similar to histological staining, the Western analysis is complicated. The embryos were staged by morphology but not absolute time, resulting in an experimental variance. X9 embryo collection represents a mixture of phenotypes with only 30–50% penetrance of the extra mitosis. Therefore, analysis of individual embryos would reflect differences between WT and mutants. We need a better assay which could detect individual embryo with precisely defined time axis.
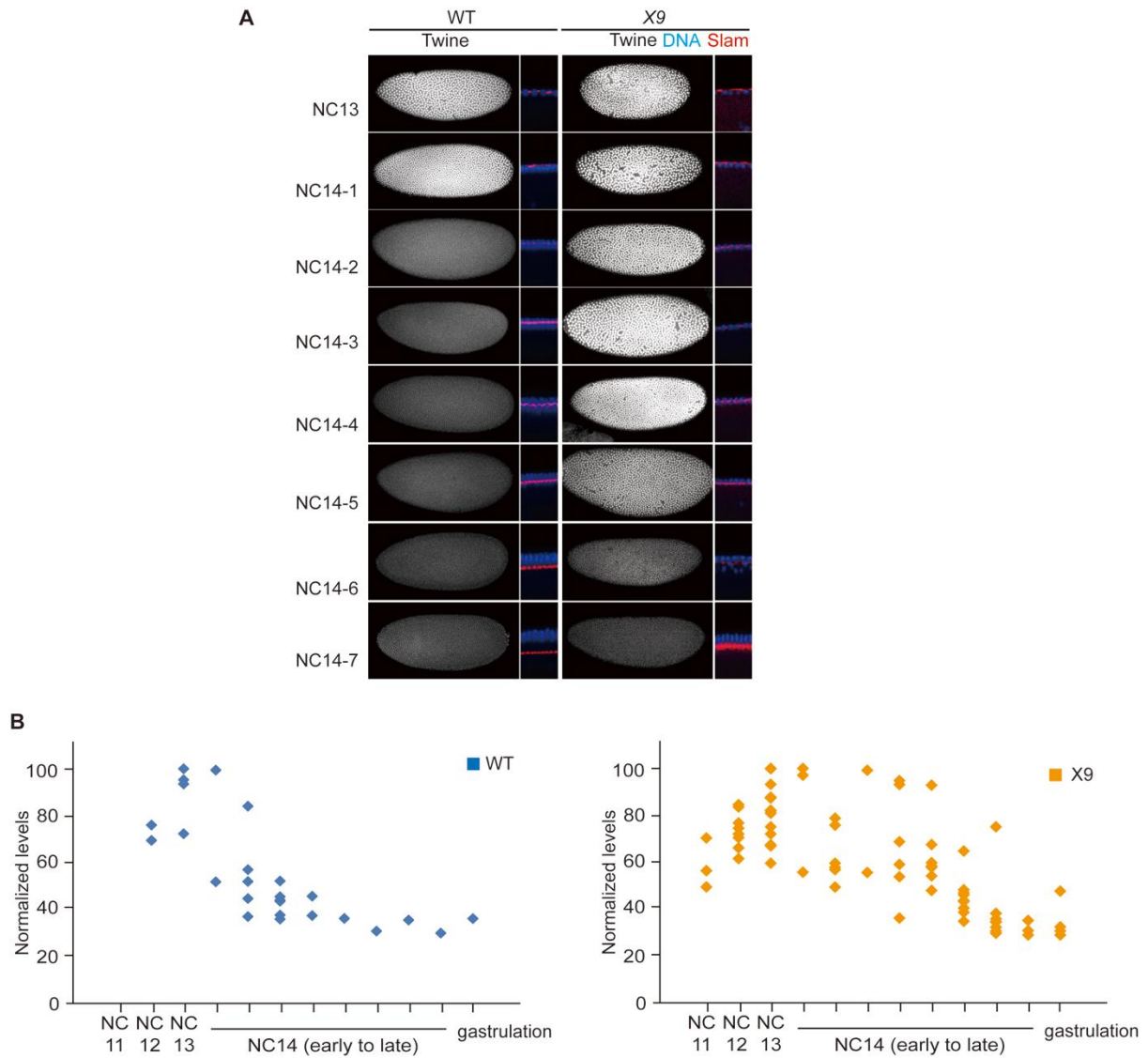
Figure 36: PpV modulates Twine protein expression. (A) Fixed representative WT embryos and embryos from germline clones derived X9 stained for Twine (white), Slam (red) and DAPI (blue). Sagittal sections with Slam staining and nuclear morphology allows approximate staging. Staging was based on the relative position of cellularization furrow (Slam) and nuclear length (DAPI). NC11 to NC14 were staged based on the nuclei density. NC14-1 to NC14-5 are corresponding to 3.5–6.5 μm of nuclear length. NC14-6 to NC14-8 are defined according to the degree of furrow tip invagination along nucleus. (B) Quantification of Twine protein level according to Twine signal intensity. The strongest protein signals in interphase 13 were normalized as 100.
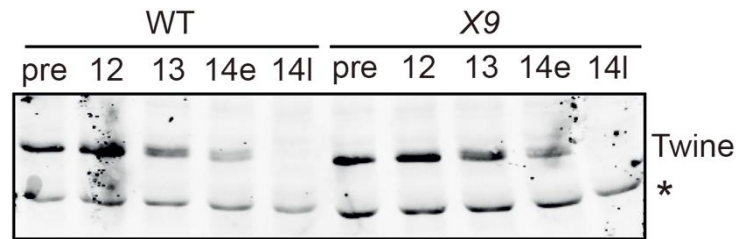
Figure 37: Twine expression profile of nuclear cycle 12 to 14 in WT and X9 embryos. Western blot of Twine with extracts of WT embryos and embryos from germline clones of X9 manually staged by the nuclear density. 10 embryos were loaded on one lane. Pre-blastoderm embryos (pre), NC12, 13, 14 early (14e) and late (14l). Cross-reacting band (marked by *) serves as loading control.

Table 8: qPCR of total *twine* RNA level in WT and X9 embryos

Sample	Target	Cq value	Mean Cq value
WT	*GAPDH* 1	19.83	19.81
	GAPDH 2	19.79	
	Twine 1	17.18	17.19
	Twine 2	17.20	
	WT *GAPDH/ Twine* ratio		1.152
X9	*GAPDH* 1	20.36	20.40
	GAPDH 2	20.43	
	Twine 1	18.79	18.79
	Twine 2	18.79	
	X9 *GAPDH/ Twine* ratio		1.086

Glyceraldehyde 3 phosphate dehydrogenase (*GAPDH*) serves as reference. Cq value: quantification cycle value.

Fluctuation analysis

To carefully analyze the dynamic profile of Twine protein in individual embryos with absolute time, we turned to fluctuation analysis which is a simple version of fluorescence correlation spectrometry (FCS, Schwille 2001). This approach has been used extensively, for example in determining the number of ion channels (Zingsheim and Neher 1974). The principle of fluctuation analysis is shown in Figure 38. When one fluorescence signal is passing through the focal volume, the signal is collected and recorded as a trace (Fig. 38A and 38B). Multiple fluctuation traces are computed as time average (i) and variance (σ), which allows calculation of average molecular brightness and average number of molecules within the focal volume (Fig. 38C). The calculation equations have been previously established (Chen et al. 2002; Digman et al. 2008). The advantage of this approach is that the frequency of these traces are dependent on the number of fluorescent signal, independent on the intensity, as how often but not how strong the protein signal is, can be addressed by this measurement. Importantly, this approach shows great potential to investigate developmental processes in vivo, but has not been applied in *Drosophila* syncytial blastoderm embryos before.

The method was validated by embryos expressing one or two copies of nuclear localization signal GFP (nls-GFP) driven by the ubiquitin promoter. Western blot with extracts from these embryos demonstrated that the protein levels of GFP corresponded to gene copy number (Fig. 38D and Supplemental Tab. 4). Western blot was performed triplicated with three biological independent samples for quantification. However, quantification by densitometry revealed large error bars in both 1× and 2× nls-GFP transgenic extracts (1±0.32 and 3.3±2.0, respectively. Mean±SD). By using fluctuation analysis with embryos in early NC14, an increase from c(1×GFP)=102.3±17.3 to c(2×GFP)=213.7±49.1 was revealed, and thus a two-fold higher absolute concentration of nls-GFP in embryos with two transgenes as compared to embryos with one nls-GFP transgene (Fig. 38E and Supplemental Tab. 5).

Having validated the method, embryos expressing Twine-GFP were exploited for fluctuation analysis. Transgenic Twine-GFP attP2 construct contains a 3,614 bp genomic fragment with a copy of exogenous *twine*, a linker sequence and a

Drosophila codon optimized EGFP, and the transgenic flies can be kept as homozygous stock (Fig. 39A). When introducing transgenic Twine-GFP into *twine* homozygous mutant, the female sterility was rescued, meaning exogenous Twine-GFP is functional in vivo.

In one recording, focal volume was defined in one spot of nucleus from an individual embryo (Fig. 39C), and the highest intensity of Twine-GFP at the beginning of interphase 14 (WT) or 15 (X9) was defined as the starting point. Following the last mitosis, multiple time points for every 3 min intervals in interphase 14/15 were recorded for each spot, that five times 10 s measurements were recorded for each time points (Fig. 39B). From the traces of Twine-GFP fluorescence, the average molecular brightness and the number of molecules per optical volume were calculated. Embryos from Twine-GFP/+ and Twine-GFP/Twine-GFP were used as control, and embryos from X9/ovo;Twine-GFP/+ were used as *PpV* mutant samples.

Curves of Twine-GFP levels were obtained corresponding to average particle number and measurement time. Exponential fitting of the curves provides two parameters: initial particle number (N_0) and the decay time (t) (Fig. 40A and Supplemental Fig. 1). Specifically, the initial particle number corresponds to the concentration of Twine at the onset of interphase 14/15, and it is dimensionless as an absolute molar concentration was not given in the focal volume setting; the decay time reflects synthesis and degradation rate of protein, which is different than the half-life. Quantification data showed in embryos with one or two copies of Twine-GFP that little variation around the mean value appeared, meaning this approach is robust (Fig. 40B and 40C, Tab. 9). However, in X9 mutants, a statistically significant change of the initial particle number was shown. The mean value of Twine-GFP initial particle number grew up from less than 40 in WT background to almost 60 in X9 background (Fig. 40B). In terms of the decay time, it was found approximately 10 min in both control (1× and 2×) Twine-GFP and X9;Twine-GFP (Fig. 40C). Interestingly, consistent with observation in X9 phenotype and Twine immunostaining, a high variation between X9 individual embryos in both initial particle number and decay time were demonstrated. Closer look revealed Twine-GFP initial particle number in X9 distributed in two subgroups, with an average number of 70–80 in one group with 8 embryos, and an average of 40, which is

comparable to WT cases, in another group with 9 embryos. This may explain why 30–50% of X9 mutants, not all, undergo an extra embryonic nuclear division. These evidences indicate that maternal PpV may act as a controller that maintains a low embryo-to-embryo variation of Twine protein in pre-MBT.
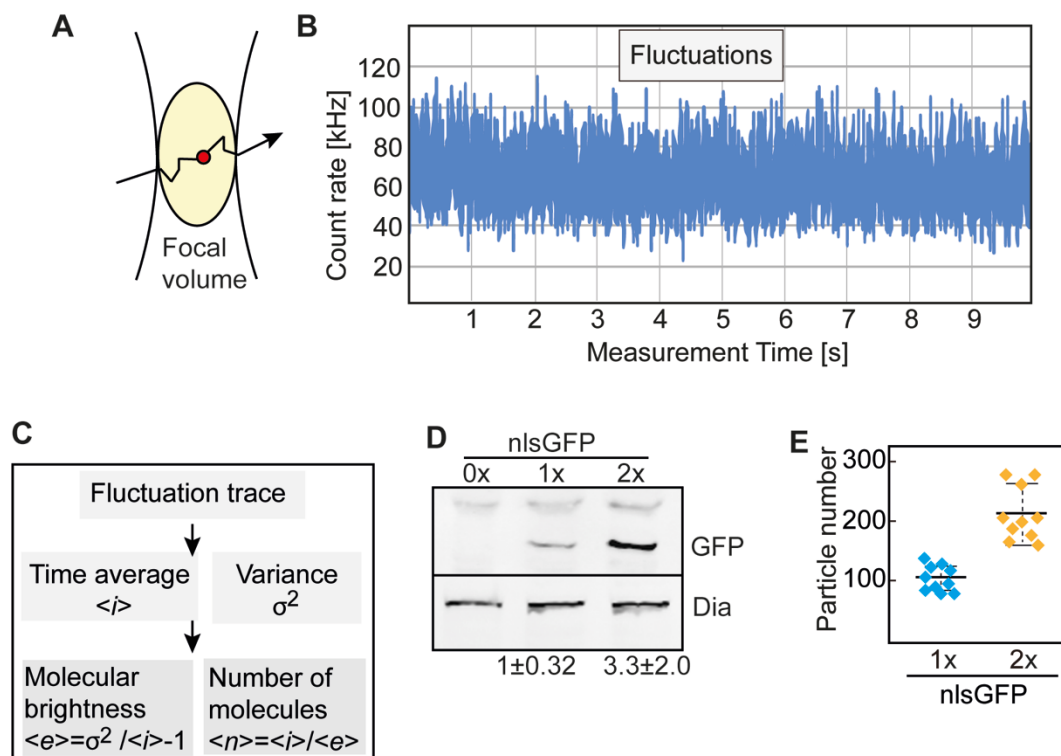

Figure 38: Fluctuation analysis for absolute concentration dynamics. (A) Principle of fluctuation analysis. Passing through the focal volume leads to changes in the fluorescence signal. The frequency of these changes depends on the concentration. (B) Fluctuation trace of a measurement. (C) Time average and variance are computed from the fluctuations trace, which allows calculation of average molecular brightness and average number of molecules within the focal volume. (D) Western blot with extracts of the embryos (0–3 h) with 0×, 1×, and 2× copies of an nls-GFP transgene. Quantification by densitometry (N=3). (E) Particle number per focal volume as determined by fluctuation analysis of GFP fluorescence. Mean, bold line; standard deviation, dashed line.
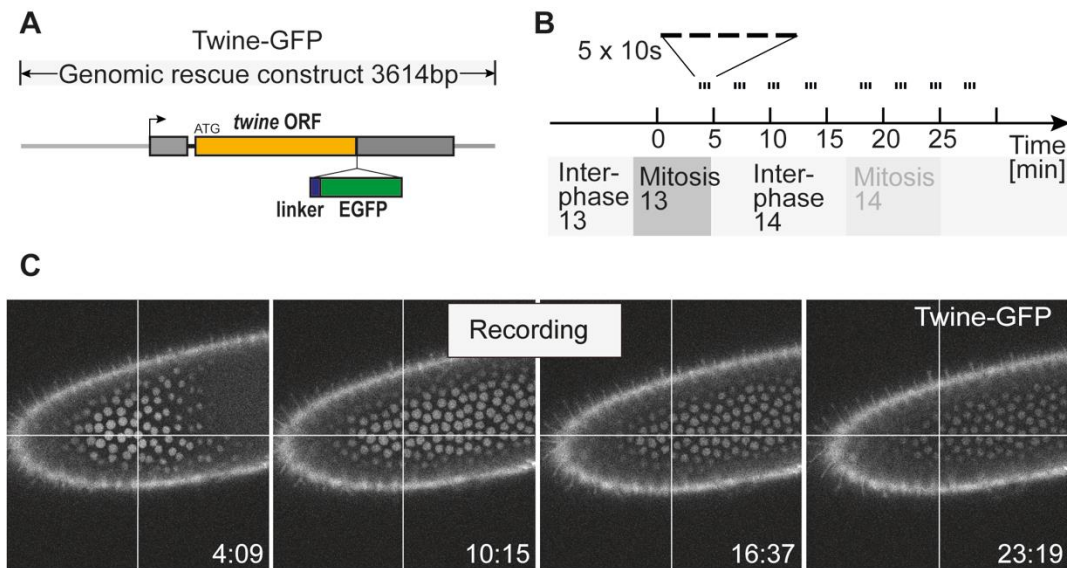
Figure 39: Experimental scheme of fluctuation analysis. (A) Scheme of Twine-GFP genomic rescue construct. *twine* open reading frame (ORF) is indicated in orange. Linker sequence (Stuffer) is indicated in blue box and EGFP is in green box. Untranslated regions (UTR) are indicated in grey box. 3,614 bp genomic region is depicted in grey line. (B) Experimental scheme. Five 10 s measurements are recorded for each time point (every 3 min). Multiple time points in interphase 14/15 are recorded for each embryo. (C) Images from a recording.

As it has been reported that zygotic Tribbles modulates Twine turn over at MBT (Farrell and O'Farrell 2013), *tribbles* mutant may induce longer Twine decay time. To generate *tribbles* mutants with Twine-GFP insertion, lines of *tribbles*[EP1119] (P-element on chromosome 3L, 77C1) and Twine-GFP attP2 (insertion on chromosome 3L, 68A4) were crossed and heat-shocked to induce recombination. Recombinant embryos containing *tribbles*[EP1119] and Twine-GFP were identified by PCR (data not shown). When employing embryos of *tribbles*,Twine-GFP/*tribbles* to fluctuation analysis, similar initial particle number was comparable to control embryos (Fig. 40B). However, in contrast to X9;Twine-GFP, the decay time was significantly longer (13 min) than the control (Fig. 40C). These data confirmed that Tribbles is involved in the induced degradation of Twine during MBT in molecular terms, through mildly enhancing the decay rate.

Surprisingly, when generating flies with *tribbles*[EP1119] and Twine-GFP, homozygous of *tribbles*,Twine-GFP/*tribbles*,Twine-GFP revealed lethal. This may be due to an additive effect, that because of the maternal and zygotic elimination of *tribbles* together with four copies of *twine*, the balance of developmental regulatory network was totally broken. However, why reduction of one copy Twine-GFP weakens the lethality and how *twine* gene dose influences its expression are still unclear.
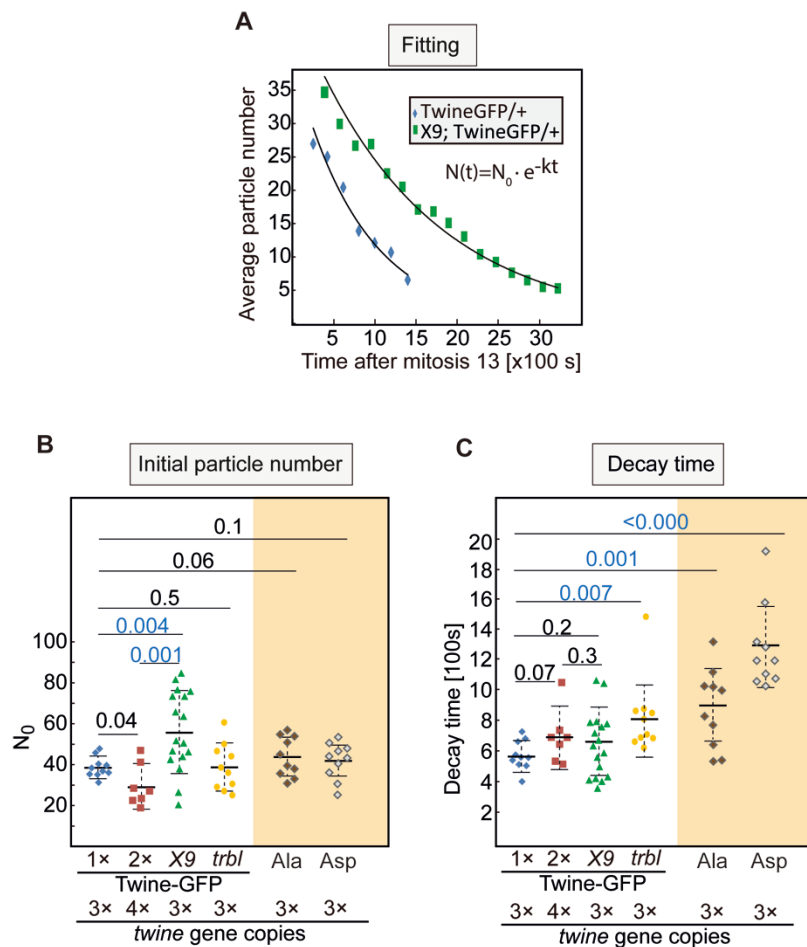

Figure 40: Expression profile of Twine-GFP measured by fluctuation analysis. (A) Representative time courses for a WT and mutant embryo. Exponential fitting provides two parameters for each embryo: initial particle number (N_0) and the decay time. (B, C) Distribution of calculated initial particle number and decay time for WT embryos with one or two copies of Twine-GFP, embryos from X9 germline clones with one copy of Twine-GFP and maternal and zygotic homozygous *tribbles* embryos with one copy of Twine-GFP. Lanes with orange background indicate one copy of mutated Twine-GFP with wild type endogenous Twine. The numbers indicate the statistical significance (p value) for the difference between two distributions. Number of total *twine* gene copies (endogenous + transgene) are indicated below.

Table 9: Initial particle number and decay time measured by fluctuation analysis

Genotype	N	Initial particle number Mean ± SD	Decay time (100s) Mean ± SD
Twine-GFP/+	10	38.5±5.0	571.7±95.6
Twine-GFP	7	29.8±10.4	691.6±176.1
X9; Twine-GFP/+ [1]	17	56.7±19.5	640.1±213.7
tribbles, Twine-GFP/ *tribbles* [2]	10	38.9±11.2	809.2±256.1
Twine-GFP-Ala/TM3	10	44.3±9.6	902.8±264.4
Twine-GFP-Asp/TM3	10	42.0±8.5	1291.7±285.4

(1) Females with *PpV* germline clones: X9 Frt18 hsFlp / ovoD Frt18 ; Twine-GFP / +

(2) Females with this genotype were crossed to *tribbles*/*tribbles* males

Corresponding to Supplemental Figure 1.

2.4.2 Twine is hyperphosphorylated in *PpV* mutant

PpV as a serine/threonine protein phosphatase may affect Twine protein pre-MBT level directly by dephosphorylation or indirectly via other factors. To assess a potential control of Twine protein stability by phosphorylation, Twine was isolated from WT and X9 mutant embryos and the phosphopeptide of Twine was analyzed by mass spectrometry (MS).

Isolation of Twine-GFP

Twine-GFP was pulled-down from extracts of Twine-GFP and X9;Twine-GFP syncytial embryos by GFP-Trap binder beads (Fig. 41A). Coomassie blue staining and silver staining of isolated proteins were performed to estimate the amounts of Twine-GFP by the reference protein BSA (Fig. 41B and 41C). The amount of extracted Twine-GFP protein from 5,000 embryos was in a range of 15 ng. In total, extracts from a scale of approximately 50,000 embryos for each group were isolated and run as samples.

Phosphopeptide analysis of Twine

Isolated Twine-GFP was loaded onto a SDS-PAGE gel and cut from defined area (Fig. 41B, white box) based on its predicted molecular weight. Purified Twine-GFP

was digested by trypsin and the amino acid sequence was analyzed by Protein ID using mass spectrometry. Twine protein peptides were identified from both WT and X9 Twine-GFP extracts.
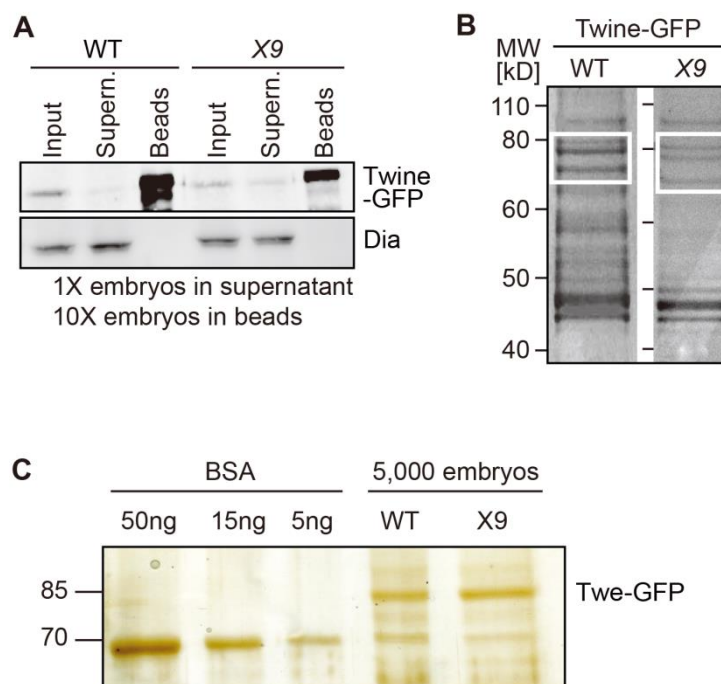

Figure 41: Isolation of Twine-GFP by GFP-pulldown assay. (A) Twine-GFP was isolated with GFP-Trap binder beads from extracts of staged (0–1.5 h) WT embryos or embryos from X9 germline clones. Western blot with GFP and Diaphanous (Dia) control antibodies showed strong Twine-GFP signal in beads-binding lanes. (B) Images of Coomassie blue stained SDS-PAGE gel. White boxes indicate the area where the bands were analyzed by mass-spectrometry. (C) Silver staining for estimating the amount of isolated Twine-GFP. Concentration gradient of BSA serves as reference.

Phosphopeptide enrichment of Twine was achieved with the coverage of 59.4% and 70% in WT and X9 mutants, respectively (Fig. 42A). Peptides in wild type were detected 1.8 fold more frequently than in the X9 mutants, indicating the phosphorylation sites which are found in the mutants should also be found in WT (Tab. 10). Two dual phosphorylation sites were identified in WT: Thr203+Ser205 and Thr394+Ser396 (Fig. 42A and Supplemental Tab. 6). Meanwhile, three additional

sites were found from X9 mutants, although these peptides were within the coverage in WT: Ser41, a cluster of five sites between Ser59 to Thr67, and Ser405+Ser412 at the C-terminal part (Fig. 42A and Supplemental Tab. 6). However, the five suspected phosphorylation sites Ser59 to Thr67 were too close to each other, so the spectra of this phosphopeptide were very noisy. Therefore, this analysis was ambiguous to assign the phosphorylation site in this cluster. We assumed at least one phosphorylated residue among the five phospho-sites.

Table 10: Comparison of non-phospho peptides in MS analysis of wild type and X9 mutant

Peptide	mass	AA (WT)	AA (X9)	AA ratio (WT/X9)
ALGDEPELIGDLSK	728.8799	18358242	8486655	2.16
LIQGEFDEQLGSQGGYEIIDCR	843.0633	2797579	1879327	1.49
YPYEFLGGHIR	676.3420	40374669	22168420	1.82
IYVFHCEFSSER	787.3584	8807155	5181341	1.7
GQIQEAFPTLTSNQENR	966.9741	44055348	25160476	1.75

The average peak area of five peptides were determined by XIC (extracted ion chromatograms) and compared between the wild type (WT) and the X9 mutant samples. The AA ratio of WT/X9 averages at 1.78 indicating that non-phosphopeptides were consistently about 1.8-fold more abundant in the wild type compared to X9 mutant samples.

To analyze if these phosphorylation sites are conserved among different model organisms, Twine and Cdc25C homologues from mouse, *Xenopus* and human were aligned and analyzed. The phosphorylation sites Thr203+Ser205 and Thr394 which were detected in both WT and X9 are conserved in mouse, *Xenopus* and human (Fig. 42B).

Nonetheless, data from phosphopeptide analysis indicated that Twine is phosphorylated to a higher degree in X9 mutants than in WT (Supplemental Tab. 6), suggesting these phosphorylation sites may contribute to the higher pre-MBT steady-state levels of Twine in X9 mutants.
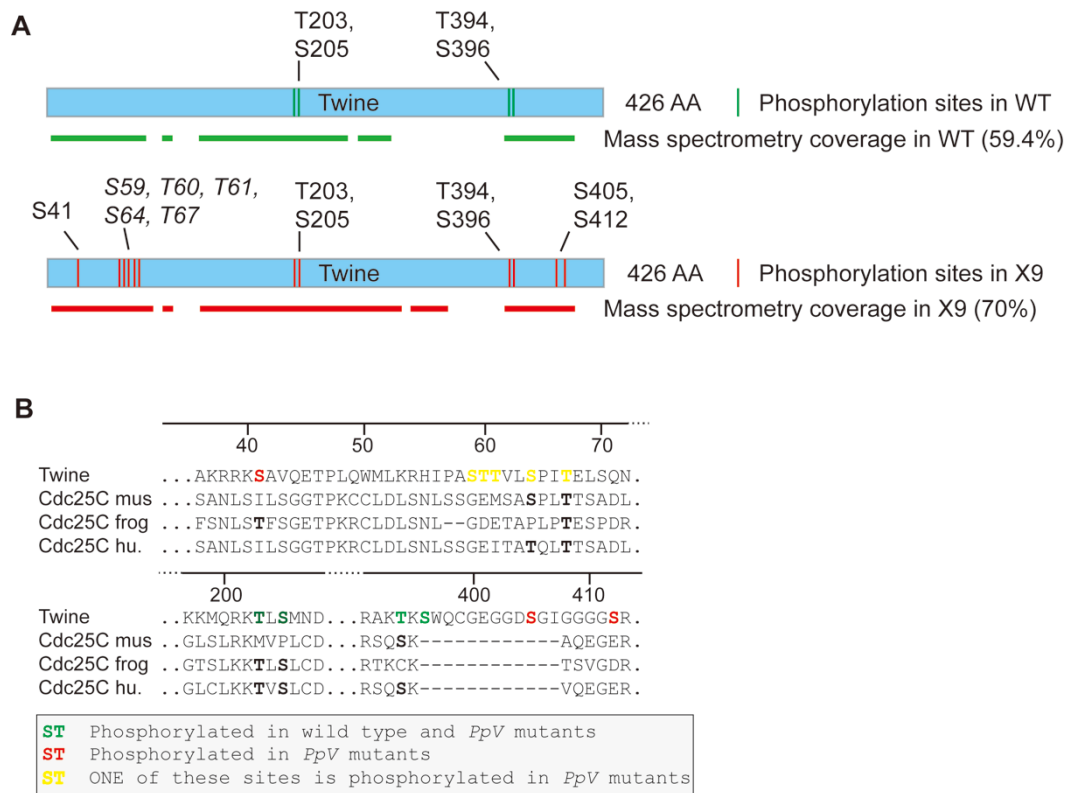
Figure 42: Identification of PpV dependent phosphorylation sites in Twine. (A) Schematic diagram showing the position of Twine peptides covered in the analysis and the identified phosphorylation sites. Italic types indicate ambiguous phosphosites. Coverage in WT and X9 are shown in green and red, respectively. (B) Alignment of Twine and Cdc25 homologue sequences (mus-mouse, frog-*Xenopus lav*., hu-human). Phosphorylation sites are marked in color. Conserved residues are printed in bold.

Transgenic flies with Twine-GFP phosphosites and phosphomimetic mutations

To test the relevance of the identified residues, we generated Twine-GFP constructs and corresponding transgenes, in which these residues were mutated (Fig. 43). We generated phosphosite (Twine-GFP-8×Ala) and phosphomimetic (Twine-GFP-8×Asp) mutants in the context of a genomic rescue construct (Fig. 43). When crossing these two types of mutated Twine-GFP into WT background, with the expression of two copies of endogenous *twine*, the phosphomimetic mutant showed a dominant effect that the homozygous Twine-GFP-8×Asp led lethality.
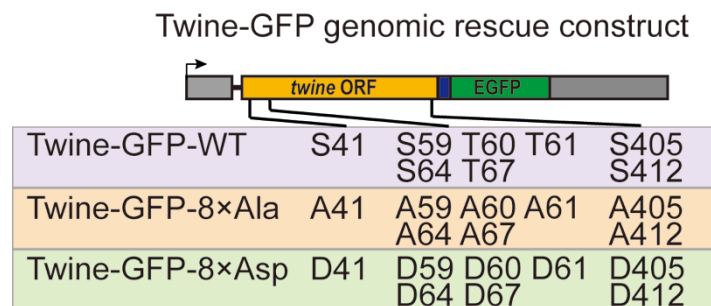

Figure 43: Transgenic Twine-GFP construct with phosphosites and phosphomimetic mutations. Eight PpV-dependent residues are shown in the box of Twine-GFP-WT. Phosphosites mutant Twine-GFP-8×Ala indicates the replacement of the eight phosphorylation residues to alanine/A. Phosphomimetic mutant Twine-GFP-8×Asp indicates the replacement of the eight phosphorylation residues to aspartic acid/D.

When applying fluctuation analysis to test the Twine-GFP profiles in heterozygous Twine-GFP-8×Ala and Twine-GFP-8×Asp transgenic flies with endogenous Twine, the initial particle numbers were comparable to WT version of Twine-GFP, whereas the decay times were significantly longer (Fig. 40B, 40C, Tab. 9 and Supplemental Fig. 1). The interpretation of these data would be questionable as the dominance of endogenous Twine and Twine-GFP transgene is not clear. An explicit way to overcome this complication is to introduce the two mutated Twine-GFP transgenes into *twine* null background.

Both mutated transgenes complemented the *twine* female sterility similar to the wild type Twine-GFP transgene. The dominant lethal phenotype also exists in homozygous Twine-GFP-8×Asp, indicating new activities such as new substrates are affected by mutated phosphorylation sites. We measured Twine protein levels and their decay by fluorescence fluctuation analysis in embryos containing no endogenous Twine but the transgenic Twine-GFP. The phosphosite mutant contained a strongly increased amount of initial Twine levels (Fig. 44A, Tab. 11 and Supplemental Fig. 2). We detected this increase in embryos with one copy of the transgene as well as in embryos with two copies. The decay rate was slightly lower in embryos with the phosphosite mutation than with the WT allele (Fig. 44A and Tab. 11). Consistent with the higher Twine levels we observed a cell cycle phenotype. Amazingly, embryos with one or two copies of Twine-GFP-8×Ala frequently underwent an additional nuclear division (Fig. 44B). Embryos with the phosphomimetic mutation showed distinct expression profile. The initial particle number is similar to WT but the decay time is longer (Fig. 44A). Meanwhile, this induced Twine stability did not result more embryos undergoing extra embryonic cleavage cycle (Fig. 44B).

In summary, we detected developmentally relevant phosphorylation sites in Twine by our mass-spectrometric analysis. Mutation of the PpV-dependent phosphorylation sites leads to higher pre-MBT protein expression and importantly a corresponding extra embryonic nuclear division comparable to PpV mutants. We conclude that PpV controls Twine phosphorylation state, ensures low expression levels and prompt decay of Twine, and thus timely remodeling of the cell cycle.

Table 11: Initial particle number and decay time measured by fluctuation analysis

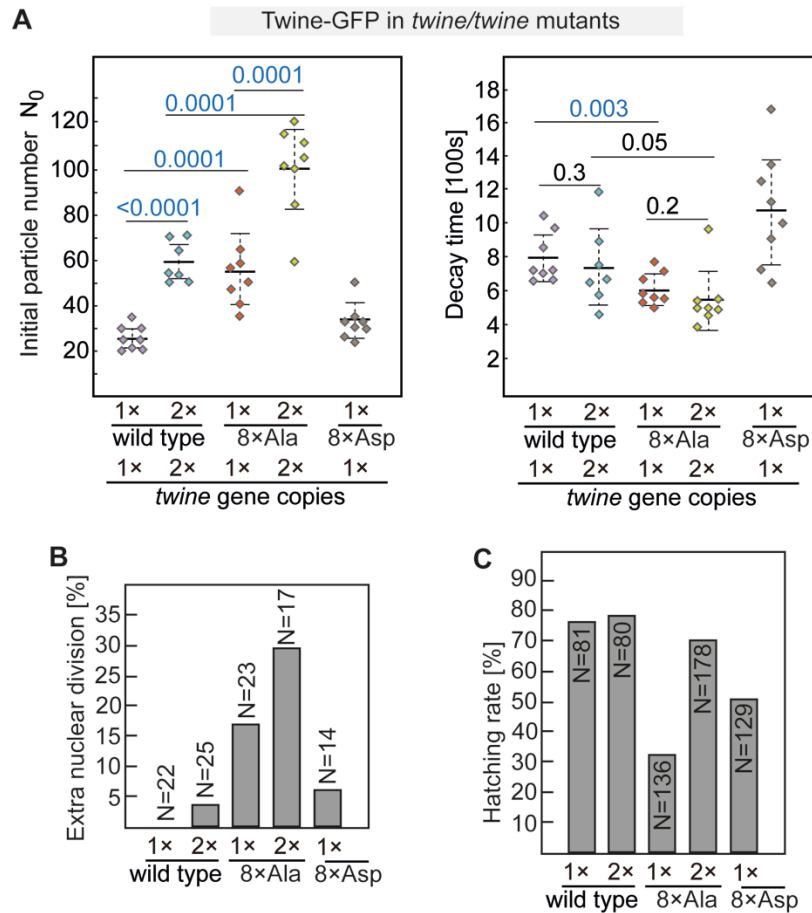| Genotype	N	Initial particle number Mean ± SD	Decay time (100s) Mean ± SD
twine; Twine-GFP-WT/TM3	8	26.3 ± 4.7	799.9 ± 131.9
twine; Twine-GFP-WT	7	59.7 ± 8.7	736.0 ± 221.4
twine; Twine-GFP-Ala/TM3	8	56.6 ± 16.2	601.9 ± 87.8
twine; Twine-GFP-Ala	8	99.9 ± 18.6	544.2 ± 173.2
twine; Twine-GFP-Asp/TM3	8	33.4 ± 7.7	1072.1 ± 316.5

Figure 44: Expression profile of Twine-GFP with phosphosites and phosphomimetic mutations. (A) Distribution of calculated initial particle number and decay time for embryos with one or two copies of wild type Twine-GFP and Twine-GFP-8×Ala, all of which are in twine mutant background. Mean, bold line; standard deviation, dashed line. The numbers indicate the statistical significance (p value) for the difference between two distributions. (B) Frequency of additional nuclear division in the embryos of wild type and mutated Twine-GFP. (C) Hatching rate of the embryos of wild type and mutated Twine-GFP. Number of total *twine* gene copies (endogenous + transgene) are indicated below.

3 Discussion

Cell cycle remodeling during the MBT is a universal developmental process in species with large eggs. After a series of rapid nuclear cycles with only S and M phases, cell cycle slows down dramatically and a gap phase arrests. This cell cycle remodeling has a biological importance as the following developmental stages are dependent on this induced cell cycle pause. There is still lack of knowledge regarding the timer of the MBT. In *Drosophila*, Cdc25/Twine phosphatase is key to the cell cycle mode switch, and its degradation is controlled by the onset of zygotic transcription and the N:C ratio (Di Talia et al. 2013; Farrell and O'Farrell 2013). Phosphorylation of human Cdc25A has also been proved to be critical for mitotic entry (Mazzolini et al. 2016).

The *Drosophila* Protein phosphatase V (PpV) is a serine/threonine protein phosphatase, which is maternally deposited in eggs. The human homologue PP6 is an important gene for tumorigenesis that has been found associated to multiple oncological processes (Zhong et al. 2011; Hammond et al. 2013). In this study, a *PpV* null mutation X9 was isolated and characterized, and was reported for its phenotypes and biological/biochemical profiles. It was revealed that an essential function of PpV is in controlling the number of fast nuclear cleavage cycles during *Drosophila* early embryogenesis. PpV is required for a robust switch in the cell cycle mode by regulating and maintaining of Cdc25/Twine level in pre-MBT. Our results facilitate a better understanding of PpV function in cell cycle control and its interaction with oncogenes Cdc25 and AuroraA, which may provide a perspective of cancer research.

PpV is essential for *Drosophila* early development

Absence of maternally supplied PpV leads to 100% embryonic lethality. Live-imaging by confocal microscopy revealed X9 embryos underwent frequently (30–50%) an additional syncytial mitotic cycle. Furrow invagination occurs firstly along with incomplete nuclear elongation in interphase 14 and retracts in few minutes, later occurs again in extra interphase 15 and goes through to finish cytokinesis (Fig. 19). The other 50–70% embryos undergo 13 regular syncytial mitosis, but eventually stop

development before completing gastrulation, suggesting additive function of PpV in late stages. However, no matter if the embryos had 13 or 14 nuclear cycles, the last cell cycle lengths were approximately 3 min extended compared with WT (Fig. 20). It is conceivable that the checkpoint activation is stronger in X9 mutants than in WT, due to the mitotic defects. An achieved checkpoint may supress entry into mitosis even Twine levels are higher in *PpV* mutants.

Previous study showed in S2 cells, RNAi of PpV blocked G2/M transition, meaning PpV could promote entry into mitosis (Chen et al. 2007). This seems contradictive to our conclusion. However, cell cycle in S2 cell line is canonical and cells perform continuous division in petri dish without developmental control. During the MBT in vivo, cell cycle mode is controlled by multiple factors, where PpV induces G2 phase directly or indirectly via Cdc25/Twine.

An additional phenotype of *PpV* mutant is the chromosome segregation defect. Low penetrance of nuclei revealed chromosome bridges in telophase, indicating PpV is also required for faithful chromosome segregation. When browsing literatures, a maternal kinase mutant *greatwall* was reported as similar phenotype in neuroblasts as what we observed in X9 embryos. Mutants in *greatwall* also cause longer cell cycle progression like X9, but the delays occur in mitotic transition, including G2-prophase and metaphase-anaphase (Yu et al. 2004). The function of Greatwall pathway in the segregation phenotype needs further investigation.

PpV and Tribbles have redundant function in embryonic cell cycle remodeling

We first attempted to answer how PpV is involved in cell cycle remodeling. Zygotic pseudokinase Tribbles and mitotic inhibitor Frühstart may be targets as cell cycle remodeling is robust and timely triggered by the onset of zygotic transcription. Genetic interactions between Tribbles, Frühstart and PpV on wing imaginal discs did not show potent evidence on either suppressing or promoting. Females from double mutant of *PpV* and *tribbles* revealed severe defects on ovaries (Fig. 30B), meaning PpV may have fundamental function in egg activation or oogenesis. Microinjection of *tribbles* mRNA in X9 mutant embryos exhibited similar proportion of precocious cell cycle pause as WT (Fig. 31), indicating Tribbles regulates Cdc25/Twine

independently of PpV. Recent study revealed that in human cells, Cdc25C is a direct target of human Tribbles homolog 2 (TRIB2) (Liang et al. 2016).

PpV controls Cdc25/Twine level in pre-MBT whereas Tribbles induces Cdc25/Twine degradation during MBT

Next we resolved the question what is the mechanism of Cdc25/Twine controlling during early mitotic divisions. We proposed a hypothesis that Cdc25/Twine may be the substrate of PpV, based on following observations: First, PpV acts in parallel with Tribbles, so that it may target Cdc25/Twine as a complementary inhibitor; second, X9 *twine* double mutants partially suppressed the embryonic lethality of X9, suggesting an antagonistic effect between PpV and Cdc25/Twine.

Immunostaining of roughly staged embryos and its quantification revealed Twine protein level persisted longer in X9 mutant than in WT, suggesting a more stable form of Twine in X9. However this is rather misleading because the quantification was based on normalized signal intensity of Twine, where we can see Twine level sustained as maximum 100 from NC13 to NC14-3 (Fig. 36B). As a matter of fact, the resolution of fluorescent confocal microscopy failed to distinguish subtle changes among highest signals, therefore giving an impression that PpV may affect Twine instability. Moreover, roughly staging by morphological markers was not able to precisely establish the time axis of dynamic protein levels. Western blot of carefully staged embryos also did not give us a better solution, since mixture of many embryos with high individual variation resulted homogenous protein level. Only 30–50% of the X9 embryos had an extra division and only in there high levels of Twine are expected, so that the mixture was not able to reflect actual individual behavior (Fig. 37).

We developed an approach fluctuation analysis, which has not been used in *Drosophila* yet. By applying this approach two parameters were extracted from the profiles, the initial particle number at onset of NC14/15 and the decay time. In the control of one or two copies Twine-GFP, the relative initial particle number of Twine was in a range of 30–40, and the decay time was approximately 10 min (Fig. 40B). This is reasonable since the half-life of Twine decreases from more than 20 min during pre-MBT to 5 min in interphase 14 (Di Talia et al. 2013), and this was

measured excluding new synthesis. However, the cell cycle remodeling may mainly depend on Twine degradation rather than synthesis, as destruction of *twine* transcripts before NC12 did not induce the cell cycle slowing (Farrell and O'Farrell 2013). Another argument is that the behavior of embryos with 3× or 4× total gene copies of *twine* appeared not significantly differently (Fig. 40B and 40C). Actually, increasing the gene dose of *twine* to six copies caused only 5% of the embryos underwent an extra division, even though the mRNA of *twine* increased substantially (Edgar and Datar 1996). This also confirmed our presumption that Twine synthesis by its mRNA has limited effect to cell cycle mode, thus the induced degradation is more important.

In X9 mutants, fluctuation analysis showed statistically significant higher initial particle number of Twine, but the decay time appeared similar to WT (Fig. 40B and 40C). This indicates Twine protein is expressed in higher levels during pre-MBT stage with the absence of PpV, and the entry into mitosis occurs only when Twine levels fall below the critical mitosis threshold (Fig. 45). It can be expected the homeostasis of Twine pre-MBT level is regulated by a feedback mechanism, that Cdk1 is activated by Twine during mitosis and then gives an inhibitory signal to Twine directly or through PpV. Only excess Twine is degraded, which is timely controlled by the feedback loop from PpV or Cdk1 activation levels. Meanwhile, there was a wide variation of Twine initial particle number among individual X9 embryos, consistent with the observation in immunostaining. In summary, PpV ensures low Twine steady-state levels in pre-MBT embryos, and narrows the embryo-embryo variation to a ground level.

Tribbles is relatively better understood that it regulates syncytial cell cycle mode switching by inducing Twine destruction in interphase 14 (Grosshans and Wieschaus 2000; Farrell and O'Farrell 2013). Tribbles is zygotically expressed and its expression is corresponding with ZGA. Fluctuation analysis of *tribbles* loss-of-function embryos resulted opposite to *PpV* mutant X9: The initial particle number of *tribbles* was similar to WT. However, a significantly longer decay time was observed, consistent with approved Tribbles-induced Twine degradation. Although Tribbles has an effect on Twine protein levels, its function is more than uncertain. Loss of Tribbles does not lead to any cell cycle defect.

Considering Tribbles is not an exclusive regulator of Twine, PpV may act complementary to Tribbles. We raised our model that maternal PpV controls pre-MBT levels of Twine, whereas Tribbles and other zygotic factors control the destabilization of Twine during MBT (Fig. 45 and 46).
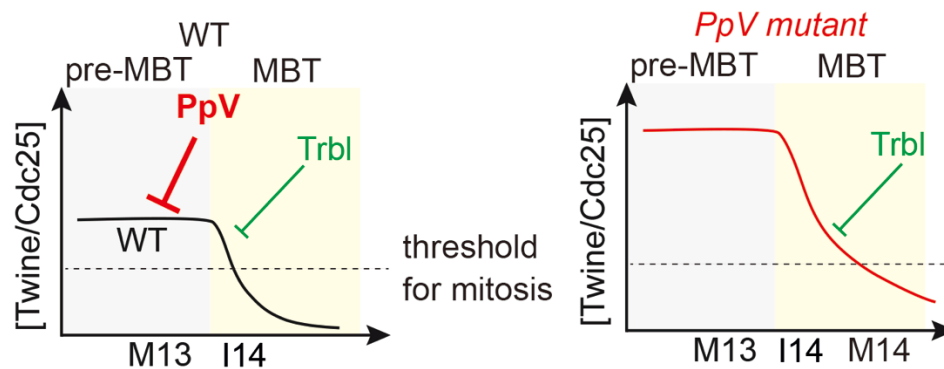

Figure 45: Model for the PpV function during MBT cell cycle control. Schematic temporal profile of Cdc25/Twine in WT (left) and X9 mutant embryos (right). PpV controls pre-MBT levels of Twine, whereas Tribbles (Trbl) and other zygotic factors control the destabilization of Twine during MBT. M: mitosis. I: interphase.

Is AuroraA involved in *Drosophila* cell cycle control?

Aurora kinases are highly conserved among species, and the activity of Aurora protein levels is peak in mitosis. AuroraA protein kinase is a target of PP6 in human tumorigenesis (Zeng et al. 2010; Hammond et al. 2013; Ertych et al. 2016). PP6 catalytic subunit PP6C together with Sit4-associated proteins SAPS3 inhibits AuroraA activity via removing its autophosphorylation Thr-288 (Ertych et al. 2016). In human cell lines, repression of *PP6* resulted AuroraA hyperactivity and frequent disordered chromosome segregation, similar to X9 phenotype (Zeng et al. 2010). In our study, *Drosophila* embryos lack of PpV caused hyperactivity status of AuroraA, suggesting PpV may inhibit AuroraA activity the same way as in human cells. The segregation defects of X9 mutants may also due to AuroraA gain-of-function.

However, this seems not an essential function, as only a minor portion of the nuclei are affected.

It has also been reported that Cdc25B is phosphorylated by AuroraA during mitosis in cultured human tumor cells (Dutertre et al. 2004). However, human Cdc25B is located at the centrosome during mitosis, and *Drosophila* Cdc25/Twine performs otherwise that accumulates at the nuclei during interphases and disperses into the cytoplasm during mitosis. Nevertheless, if this could also function in a similar way in *Drosophila* early embryogenesis, PpV may act directly on Twine, or indirectly via AuroraA. We prefer the direct model more because of the following reasons: Firstly, two of the three PpV dependent phosphorylation sites on Twine do not match the Aurora lenient consensus motif either [KR].[ST][^P] (Sardon et al. 2010) or [RKN].[R].[X].[ST].[MLVI] (Ferrari et al. 2005); Secondly, AuroraA acts and is activated during mitosis, whereas control of Twine protein levels is an interphase process; Thirdly, inhibition of AuroraA by chemical inhibitors in X9 mutants did not rescue the cell cycle phenotype, indicating that the entry into an extra cycle does not depend on hyperactive AuroraA.

How does PpV control Twine pre-MBT levels by dephosphorylation?

Phosphopeptide analysis of Twine detected two dual phosphorylation sites in WT and three additional sites in X9 mutants. Two dual phosphorylation sites Thr203+Ser205 and Thr394+Ser396 exist in both WT and X9. When aligning these sites with Cdc25 homologues from mouse, *Xenopus* and human, Thr203+Ser205 is conserved in *Xenopus* and human, and Thr394 is conserved in mouse and human (Fig. 42B). In terms of the three additional phosphorylation sites, Ser41 is conserved in *Xenopus*, but others did not show conservation to the representative species. Furthermore, Ser205 residue was also found phosphorylated in mouse, *Xenopus* and human (http://www.phosphosite.org; Frazer and Young 2012). Interestingly, the three PpV-dependent phosphorylation sites have not been reported previously in either *Drosophila* or other species, suggesting a novel mechanism of PpV-involved Cdc25 stability.

If Twine is the direct substrate of PpV, PpV may hydrolyze the phosphates at the detected PpV-dependent phosphorylation sites, thereby influences the stability of

Twine in pre-MBT embryos. Alternatively, PpV may indirectly maintain Twine pre-MBT level through dephosphorylating a protein phosphatase or kinase. *twine* mutant flies with mutated phosphosite transgenic Twine-GFP constructs showed significant higher initial Twine protein levels (Fig. 44A), corresponding with higher proportion of extra embryonic nuclear cycle (Fig. 44B). A constitutive activation mutant *Twine*[106-180] led to a higher initial Twine level at the beginning of NC14 and thus a high fraction of extra division (6 of 13 embryos) (Di Talia et al. 2013), consistent with our observation.

Full activation of Cdc25 can be due to the secondary phosphorylation by other kinases or phosphatases aside PpV (Wang et al. 2010). Mutated Twine-GFP transgenes modified all PpV-dependent phosphorylation sites concurrently and therefore blocked the mobility shift of catalytic activation. These phosphorylation sites can be functionally transient or orderly, hence raise the difficulties to trigger or inhibit the temporal catalytic activation.
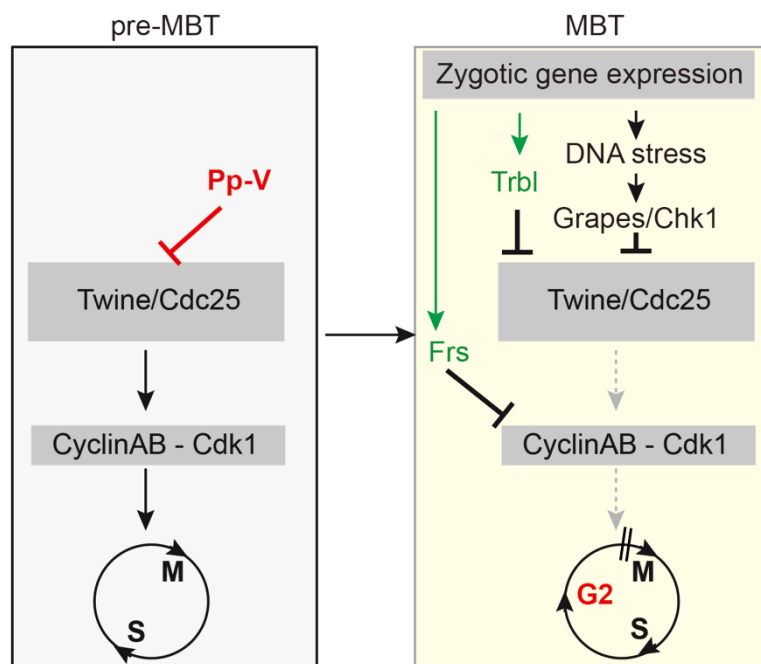

Figure 46: PpV is required for timely cell cycle remodeling during MBT. Activation of the zygotic genome leads to expression of the zygotic genes *frühstart* (*frs*), *tribbles* (*trbl*) and DNA replication stress, which activates the DNA checkpoint. PpV constitutes a forth negative element in controlling Cdc25/Twine and Cdk1-cyclin, therefore switches cell cycle mode from S-M to S-G2-M.

4 Materials and methods

4.1 Materials

4.1.1 Chemical reagents

All standard chemicals were purchased from AppliChem, Carl Roth, Gibco BRL, Invitrogen, Merck, Sigma-Aldrich, unless otherwise stated. RNase-free water was purchased from Ambion /Life Technologies.

4.1.2 Buffers, solutions and media for bacterial culture and flies

Unless otherwise mentioned, all buffers and solutions were prepared according to standard protocols (Sambrook and Russell 2001). Flies were kept and raised according to standard conditions and procedures. Fly recipes and protocols found in reference (http://flybase.org/).

Table 12: Buffers and solutions used in this study

Name	Composition
Buffers and solutions for immunostaining and western blot	
PBS	130 mM NaCl 7 mM Na_2PO_4 3 mM NaH_2PO_4 pH 7.4/HCl
PBT	1x PBS 0.1% Tween 20
TBST	50 mM Tris 150 mM NaCl 0.05% Tween 20 pH 7.6/HCl
FA fixation solution for embryos	4.5 ml 1× PBS 5 ml Heptane 0.5 ml 37% Formaldehyde

Heat fixation solution for embryos	0.4% NaCl
	0.03% Triton X-100
Fixation solution for imaginal discs	9.5 ml 1 × PBS
	0.5 ml 37% Formaldehyde
Fixation solution for ovarioles	9.5 ml 1 × PBS
	0.5 ml 37% Formaldehyde
Immunostaining blocking buffer	1× PBS
	5% BSA
Western blot blocking buffer	1× PBS
	5% milk powder
Western blot transfer buffer	25 mM Tris
	175 mM Glycine (pH 8.3)
	20% Methanol
Mild stripping buffer	15 g glycine
	1 g SDS
	10 ml Tween 20
	1 l ddH$_2$O
	pH 2.2/HCl
Lämmli buffer (2×)	0.09 M Tris
	0.6% bromophenol blue
	20% Glycerol
	6% ß-mercaptoethanol
	pH 6.8/HCl
Buffers for genomic DNA extraction from single adults flies	
Squish buffer	9.8 ml ddH$_2$O
	100 µl 1 M Tris
	20 µl 0.5 M EDTA
	50 µl 5 M NaCl
	200 µl 10 mg/ml Proteinase K (freshly added)
	pH 8.0/NaOH
Buffers and solutions for silver staining of SDS gels	

Fixing solution	2.4 ml acetic acid
	8.8 ml ethanol
	8.8 ml ddH$_2$O
Farmer reducer solution	a spatula tip of Kaliumhexacyanoferrate III
	a spatula tip of Sodiumthiosulfate
	250 ml ddH$_2$O
Silver solution	0.1% AgNO$_3$
Formaldehyde processing solution	0.1 % (v/v) 37% Formaldehyde
	2.5 % (w/v) Na$_2$CO$_3$
Stop solution	5 % acetic acid
Buffers for GFP-Pulldown of Twine-GFP from embryos	
Lysis and washing buffer	50 mM Tris
	500 mM NaCl
	1 mM DTT
	0.5 mM EDTA
	0.5% Tween 20
	1% Phosphatase inhibitor cocktail 3 (freshly added)
	1 Tablet /50 ml Protease Inhibitor Cocktail (freshly added)
	pH 7.4/HCl

4.1.3 Molecular genetics/biology procedures

Following kits were used, according to manufacturer's instructions:

MiniElute Gel Extraction Kit	(Qiagen)
Plasmid Midi Kit Nucleobond AX	(Macherey-Nagel)
In-fusion HD Cloning Kit	(ClonTech)
mMESSAGE mMACHINE SP6 Transcription Kit	(Ambion /Life Technologies)
MEGAscript T7 Transcription Kit	(Ambion /Life Technologies)

SYBR Green Real-Time PCR Master Mixes	(Thermo Fisher Scientific)
Qiagen Plasmid Midi Kit	(Qiagen)
RiboMAX Large Scale RNA Production Systems	(Promega)

Following non-restriction enzymes were used:

Taq Polymerase	(Expressed and purified in the lab)
Pfu Polymerase	(Expressed and purified in the lab)
Phusion DNA Polymerase	(Life Technologies)
T7 RNA polymerase	(Expressed and purified in the lab)
Transcriptor reverse transcriptase	(Roche)
DNaseI	(Roche)
Proteinase K	(Ambion /Life Technologies)
T4 DNA Ligase	(Fermentas /Thermo Fisher Scientific)
Alkaline Phosphatase, shrimp	(Roche)

4.1.4 Antibodies

Table 13: Primary antibodies used in this study

Antibody	Raised in	Dilution / working concentration		Source
		Immunostaining	Western blot	
Aurora A	Rabbit	-	1:5,000	Glover lab (Giet et al. 2002)
Diaphanous (Dia)*	Guinea pig	-	1:5,000	Grosshans lab (Grosshans et al. 2005; Wenzl et al. 2010)

Discs large 1 (Dlg)	Mouse	1:100 (~0.4 µg/ml)	-	Hybridoma Bank 4F3
Even skipped (Eve)*	Guinea pig	1:1,000	-	Grosshans lab
Fascetto (Feo)	Rabbit	1:100	-	Gatti lab (Verni et al. 2004)
GFP	Rabbit	-	1:10,000	Torrey Pines Biolabs
Lamin DmO	Mouse	1:500	-	Saumweber lab (Risau et al. 1981)
Phospho-Aurora A/B/C	Rabbit	-	1:2,000	Bastians lab
PpV*	Rabbit		1:200	Grosshans lab
Slow as molasses (Slam)	Rabbit	1:5,000	-	Grosshans lab (Acharya et al. 2014)
Tribbles	Rabbit	1:500	-	Grosshans lab
Twine	Rat	1:500	1:5,000	Wieschaus lab (Di Talia et al. 2013)
Tubulin (α-)	Mouse	1:5,000	1:50,000	Hybridoma bank B512
Tubulin (γ-)	Mouse	1:5,000	-	Sigma-Aldrich T6557

* Serum

Alexa-conjugated secondary antibodies for immunostaining were purchased from Life Technologies /Invitrogen and used at a dilution of 1:500 (4 µg/ml). DAPI (4',6-Diamidino-2-phenylindole dihydrochloride) was obtained from Sigma-Aldrich and used as DNA staining dye at a working concentration (0.2 µg/ml). Alexa Fluor 546 Phalloidin was purchased from Thermo Fisher Scientific and used at a dilution of 1:1,000. GFP-Booster Atto488 was purchased from Chromotek and used at a final

concentration of 2 µg/ml. Anti-Digoxigenin-peroxidase antibodies were purchased from Roche and used at a dilution of 1:200 (0.75 U/ml). Secondary antibodies for western blots, IRDye-800CW and IRDye-680, were purchased from LI-COR Biosciences and used at a dilution of 1:20,000 (0.05 µg/ml).

4.1.5 Oligonucleotides

All oligonucleotides were ordered from Eurofins Genomics.

Table 14: Oligonucleotides used in this study

Name	Sequence (5' - 3')	Description
BL1	GAGCCAATCGATTGGAACCT	*PpV* cloning forward primer
BL2	TGCAACTAATTTCGCTTGCCT	*PpV* cloning reverse primer
BL3	GTATACTTGGTGTGTACACACT	pattB-PpV colony PCR forward primer
FW16	GAT CAA CTA CCG CCA CCT	pattB-PpV colony PCR reverse primer
BL10	GTAATACGACTCACTATAGGGCG ATCAGCGCACAGCCTAGTCA	*Tribbles* dsRNA forward primer, designed based on Farrell 2013
BL11	GTAATACGACTCACTATAGGGCG ATGGCCATAGATGGTGCTCC	*Tribbles* dsRNA reverse primer, designed based on Farrell 2013
BL12	AGGTCGACGGTATCGATAAGCTT GATATCGAATTCAAAT	GFP-PpV In-fusion forward primer
BL13	AGCTTCTTCAGCTCGTTCTCCGG CAGGTACTTGCATTTCT	GFP-PpV In-fusion reverse primer
BL16	GAGTTCCTTGGCGGACACAT	*twine* qPCR forward primer
BL17	CAGGATAGTCCAGTGCCGGAT	*twine* qPCR reverse primer
MP37F	CACCAGTTCATTCCCAACTT	*GAPDH* qPCR forward primer
MP37R	CTTGCCTTCAGGTGACGC	*GAPDH* qPCR forward primer

4.1.6 Plasmid constructs

Table 15: Plasmids used in this study

Name	Description	Source
pCS2	in vitro transcription with SP6	Grosshans lab
CS2-tribbles	tribbles cDNA in pCS2	Grosshans lab
CS2-frühstart	frühstart cDNA in pCS2	Grosshans lab
pBABR-Twine-EGFP	Twine genomic DNA with optimized EGFP	gift of Blythe, Di Talia and Wieschaus
pattB	attB/phiC31 system	Grosshans lab
pattB-PpV	rescue construct of X9	generated in this study
pattB-GFP-PpV	rescue construct of X9	generated in this study
BAC-PR98-18C18	PpV genomic DNA	BACPAC Resources Center
BKSII(+)	Bluescript cloning vector	Grosshans lab
BKS-PpV	subcloning step to make pattB-PpV	generated in this study
BKS-GFP-PpV	subcloning step to make pattB-GFP-PpV	generated in this study
GFP-PpV	PpV genomic DNA with optimized EGFP	synthesized from Eurofins Genomics
Twine-GFP-8×Alanine	phosphorylated serine/ threonine are replaced by alanine (encoded by GCC)	synthesized from Eurofins Genomics
Twine-GFP-8×Aspartic acid	phosphorylated serine/ threonine are replaced by aspartic acid (encoded by GAC)	synthesized from Eurofins Genomics

4.1.7 Fly stocks

Table 16: Fly stocks used in this study

Name	Genotype	Source
oregon-R	+/+	Grosshans lab
GFPCad,HisRFP	ubi-ECadGFP{w+}His2AvRFP{w+}/*CyO*	Grosshans lab
PpV X9	*w* Pp-V[X-9-13-1] v Frt[9-2, 18E] Flp122{ry+} /FM7c, *y w[a] sn B*	Grosshans lab
ovoX18	ovo[D2]v[24]FrtX[9-2]{w+}/C(1)DX *y w f*	Tübingen collection
ovoX18; HisRFP,CadGFP	ovo[D1-18]hs-Flp *y w sn*, FrtX[19A]{neo}/C(1)DX,*y w f*; ubi-ECadGFP{w+}His2AvRFP{w+}/*CyO*	Grosshans lab
Frt18E	*y1 w*, FrtX[9-2]hs-Flp[122]{ry+}/FM7c	Grosshans lab
twine	*twn*[HB5] *cn bw* / *CyO*	Tübingen collection
tribbles	EP(3)1119{w+} *ry*	Grosshans lab
TM3 TM6B	*w* ; TM3, *Sb Ser* / TM6B, *Tb Hu*	Grosshans lab
phiX-86Fb	*y w* M(eGFP.vas-int.Dm)ZH-2A ; M(RFP.attP)ZH-86Fb	Basler lab
Twine-GFP	*y w*/*w*;Twine-EGFP attp2	gift of Blythe, Di Talia and Wieschaus
tribbles, Twine-GFP	*w*; EP(3)1119{w+} *ry* Twine-EGFP attp2/TM3	generated in this study
twine; Twine-GFP-8×Ala	*twn*[HB5] *cn bw;* Twine-EGFP-8×Ala{w+}/TM3	generated in this study
twine; Twine-GFP-8×Asp	*twn*[HB5] *cn bw;* Twine-EGFP-8×Asp{w+}/TM3	generated in this study
PpV rescue	*w*;attB[68A4]{PpV,w+}/TM3	generated in this study
GFP-PpV rescue	*w*;attB[68A4]{GFP-PpV,w+}/TM3	generated in this study
X9;Twine-GFP	*w* Pp-V[X-9-13-1] v Frt[9-2, 18E] Flp122{ry+} /FM7c, *y w[a] sn B*; Twine-EGFP attp2	generated in this study
X9; PpV+	*w* Pp-V[X-9-13-1] v Frt[9-2, 18E]	generated in this

	Flp122{ry+} /FM7c, *y w[a] sn B*; attB[68A4]{*PpV,w+*}	study
X9; GFP-PpV+	*w* Pp-V[X-9-13-1] v Frt[9-2, 18E] Flp122{ry+} /FM7c, *y w[a] sn B*; attB[68A4]{*GFP-PpV,w+*}	generated in this study
UAS-frühstart	*y w* ; pUASt- frühstart	Grosshans lab
UAS-tribbles	*w* ; pUASt-tribbles	Grosshans lab
UASp-PpV-GFP	*w**; P{UASp-PpV EGFP C}2	Bloomington Drosophila Stock Center
mat67;15	tub-Gal4-P16[67] {w+}; tub-Gal4-P16[15] {w+}	St. Johnson lab
tribbles/Df ri 79L	EP(3)1119{w+} *ry* /Df ri 79L	Grosshans lab
X9; *tribbles*	*w* Pp-V[X-9-13-1] v Frt[9-2, 18E] Flp122{ry+} /FM7c, *y w[a] sn B*; EP(3)1119{w+} *ry*	generated in this study
4×GFP	*w*; Resille::GFP(117GFP);Spider::GFP	Grosshans lab
nls-GFP,FrtX18E	*y w* ubi-nlsGFP{w+}[X1]FrtX[9-2]{w+}; hs-Flp[38]{ry+}	Luschnig lab
DC155	*w1118*; Dp(1;3)DC155, PBac{DC155}VK00033	Bloomington Drosophila Stock Center
PpV[A]	*y1 w** PpV[A] P{neoFRT}19A/FM7c, P{GAL4-Kr.C}DC1, P{UAS-GFP.S65T}DC5, *sn+*	Bloomington Drosophila Stock Center
PpV[C]	*y1 w** PpV[C] P{neoFRT}19A/FM7c, P{GAL4-Kr.C}DC1, P{UAS-GFP.S65T}DC5, *sn+*	Bloomington Drosophila Stock Center
auroraA[074-18]	Dp(1;Y)BS; *ru1 st1 aurA1 e1 ca1*/TM3, *Sb1*	Bloomington Drosophila Stock Center
Df AuroraA	w1118; Df(3R)Exel6162, P{XP-U}Exel6162/TM6B, Tb1	Bloomington Drosophila Stock Center

4.1.8 Microscopy

Spinning Disk microscope:	Zeiss Observer.Z1, CSU-X1 (2009)
Confocal microscope LSM780 mit Airyscan:	Zeiss AxioObserver.Z1 (2011)
Microinjection microscope:	Leica MZ125
	Zeiss Microinjection microscope
Fluorescence microscope:	Zeiss AxioPlan 2
Stereomicroscopes:	Zeiss Stemi 2000

4.1.9 Other materials

Aquapolymount	(Polysciences)
Amersham Protran 0.45 NC Nitrocellulose membrane	(GE Healthcare)
CDC25 Phosphatase Inhibitor II	(Merck Millipore)
cOmplete Protease Inhibitor Cocktail Tablets	(Roche)
GFP-Trap_A/M Beats	(Chromotek)
MassRuler DNA Ladder	(Thermo Fisher Scientific)
MLN8054 Aurora Kinase inhibitor	(Bastians lab)
PageRuler Prestained /Unstained Protein Ladder	(Thermo Fisher Scientific)
Phosphatase Inhibitor cocktail 3	(Sigma-Aldrich)
Ponceau S solution	(Sigma-Aldrich)
Ribolock RNAse inhibitor	(Thermo Fisher Scientific)
10S and 3S VoltaLef Halocarbon oil	(Lehmann & Voss)

4.1.10 Other equipment

arium pro Water Purification Systems	(Sartorius)
ChemiDoc Gel Imaging System	(Bio-Rad)
Concentrator 5301	(Eppendorf)
CFX96 Real-Time PCR System	(Bio-Rad)
FemtoJet Microinjector	(Eppendorf)

NanoDrop 2000c	(Thermo Scientific)
Odyssey CLx Infrared imaging system	(LI-COR Biosciences)
P-97 Micropipette Puller	(Sutter Instrument)
Thermocycler	(Biometra)
Trans-blot SD Semi-Dry Transfer Cell	(Bio-Rad)

4.1.11 Software

Adobe Acrobat Reader	(Adobe)
EndNote	(Thomson Reuters)
FIJI/ ImageJ	(NIH)
FileMaker Pro	(FileMaker)
Lasergene	(DNASTAR)
Illustrator CS6	(Adobe)
Microsoft Office	(Microsoft)
Photoshop CS6	(Adobe)
ZEN 2012	(Carl Zeiss)
MATLAB	(MathWorks)

4.2 Methods

Unless otherwise mentioned, all molecular procedures were carried out according to standard protocols (Sambrook and Russell 2001) and Grosshans' lab protocols.

4.2.1 Mapping and sequencing

The X9 mutant females were crossed to the males containing deleted segments on X chromosome from a collection of deficiency kits from Bloomington Drosophila Stock Center. Lethality was found in Dp5279, Dp5281 and Dp948 deficiencies. Smaller overlapping deficiencies were used to narrow down the region which contains the mutated gene. Ex6239 and further DC155 crosses were shown lethal and complement the mutation. Candidate genes in this region (*kdh*, *swaPsi*, *swa*,

Marf and *PpV*) were sequenced in genomic DNA from homozygous mutant embryos, and aligned to isolated fly strain with the same genomic background.

Mapping of the X9 mutants was carried out by Prof. Dr. J. Großhans and Dr. H. Sung. All genome and sequence data are from the FlyBase (http://flybase.org/) and the National Center for Biotechnology Information (http://www.ncbi.nlm.nih.gov/).

4.2.2 Generation of transgenic flies

For the *PpV* genomic rescue construct, *PpV* full length genomic DNA was obtained from BAC clone 18C-18 cutting by EcoRI, and 2,679bp fragment was cloned into pattB vector. GFP-PpV fragment was synthesized by Eurofins Genomics based on optimized GFP codon sequence, and cloned into pattB vector by In-fusion HD Cloning system. The constructs of mutated Twine phosphosites were synthesized by Eurofins Genomics and cloned into the KpnI/BamHI fragment of Twine-EGFP-pBABR plasmid (S. Blythe, S. Di Talia and E. Wieschaus).

The transgenic flies were generated with attB/phiC31 Integrase Vector System (Thorpe et al. 2000; Bischof et al. 2007). For microinjection, the embryos of yw;;M(RFP.attP)ZH-86Fb line were dechorionated with 50% Klorix bleach for 90 s, dried in a desiccation chamber for 5 to 10 min, then covered by halocarbon oil. Glass capillaries with internal filament were pulled as needles. The constructs with 0.1 µg/µl concentration were loaded into the needles and injected posteriorly prior to pole cell formation. Embryos were growing at appropriate condition until adults, and then crossed with TM3/TM6b double balancers. F1 single males with red eyes marker were collected and crossed with double balancers and setted as stocks.

4.2.3 Immunostaining

Formaldehyde or heat fixed embryos were rinsed thrice in PBT, and blocked in 5% BSA in PBT at 4°C overnight. The primary antibodies were added in the respective dilutions in 0.1% BSA with PBT and embryos were incubated 2 h with constant rotation at room temperature. Then the embryos were rinsed thrice and washed four times 15 min with PBT. Secondary antibodies were added in PBT and embryos were incubated for 2 h. Embryos were rinsed thrice and washed four times 15 min in PBT again. Embryos were then stained with DNA dye, rinsed thrice in PBT, washed in

PBT for 5 min and were mounted using aquapolymount mounting medium on glass slides.

4.2.4 Western blot

Manual staging was done when heat fixed embryos were stained with DAPI. Embryos were aligned on glass slide and covered with 50% glycerine in PBS, and staged with a fluorescence microscope according to nuclear density and chromatin structure. Embryos of the same nuclear cycle or stage (N=10–20) were pooled, dissolved in 1× Lämmli buffer and denatured at 95°C for 10 min. To facilitate homogenization, the lysates were gently triturated.

Embryo lysates and PageRuler Protein Ladder were loaded respectively on an 8% to 10% SDS-PAGE gel for Western blot. The gel was run at 20 mA constant current about 1 h. The proteins from the gel were transferred onto a nitrocellulose membrane either using a semi-dry transfer at 60 mA for 1 to 2 h or a wet transfer at 100 mA for 4°C overnight, depending on the size of the proteins. For loading control, the nitrocellulose membrane was stained in Ponceau S solution for a few minutes and washed several times with deionised water. The nitrocellulose membrane was then blocked in 5% milk powder in PBT or 3% BSA in TBS for 1 h. The primary antibodies were added in the respective dilutions in 0.5% BSA PBT and the nitrocellulose membrane was incubated overnight at 4°C. The nitrocellulose membrane was then rinsed thrice and given four times 10 minute washes in PBT, and was incubated with LI-COR secondary antibodies IRDye-800CW and IRDye-680 for 1 h at room temperature, protected from light. Then it was again rinsed thrice in PBT and washed 10 min. The blot was scanned with the Odyssey CLx Infrared imaging system and the bands were detected. 16-bit images were processed by Photoshop and FIJI/ImageJ.

4.2.5 Silver staining

Gel from SDS-PAGE was fixed into fixing solution for 30 min, and washed twice with deionised water. Fixed gel was incubated with Farmer Reducer solution for 2.5 min, and washed twice 5 min with deionised water. Silver solution was added for staining for 30 min. Stained gel was washed twice for 30 sec, and equilibrated with 2.5% Na_2CO_3 for 1 min. The processing was performed with Formaldehyde solution for 3–

5 min, until clear bands appeared. The gel was washed briefly and incubated with Stop solution for 15 min.

4.2.6 RNA isolation and quantitative PCR

Quantitative PCR and data analysis were carried out according to the protocols of SYBR Green Real-Time PCR Master Mixes and qPCR system software (Thermo Fisher Scientific). cDNA template was synthesized by reverse transcription of Drosophila total RNA, which was isolated by using TRIzol total RNA isolation protocol (Invitrogen). The following primer pairs were used: *twine* qPCR primers BL16 and BL17; *GAPDH* qPCR primers MP37F and MP37R.

4.2.7 Microscopy

Time lapse recording was carried out under Spinning Disk microscope. Embryos were dechorionated with 50% Klorix bleach for 90 s, aligned on a piece of apple-juice agar, glued on to a coverslip and covered with halocarbon oil. Live-imaging with DIC (differential interference contrast) optics was performed with a light intensity of 2.5–3.0 V, an exposure time of 80–100 ms and a frame interval of 0.5–1 min. Fluorescent live imaging was performed with 30–50% laser intensity, 100 ms exposure time and a frame interval of 30 sec to 1 min.

Imaging for immunostained samples was taken under confocal microscope LSM780. The settings were manipulated based on optimal imaging conditions and each channel was recorded separately. 25× oil/water/glycerol, 40× water and 63× oil/water/glycerol immersion objectives were utilized to record the images.

4.2.8 Preparation and imaging of ovaries and wings

Ovaries were collected from female adult flies and transferred in tubes on ice, and fixed with 9:5 ml of PBS and 0.5 ml of 37% formaldehyde for 20 min. Fixed ovaries were transferred into an Eppendorf tube and rinsed thrice with PBT. For staining nurse cells, Phalloidin was added as 1:1,000 into 1 ml PBT for 30 min at RT, protected from light. The ovaries were then rinsed thrice with PBT, and stained with DAPI for 1 min, rinsed thrice in PBT, washed in PBT for 5 min and were mounted using aquapolymount mounting medium on glass slides. For staining follicular epithelium cells of nls-GFP females, GFP-booster (1:500) was added for 1 h, then

rinsed thrice and washed four times 15 min in PBT. The ovaries were stained with DAPI for 1 min and washed in PBT for 5 min, mounted in aquapolymount mounting medium.

Wings were collected on glass slides and covered by Hoyer's mountant. The slides were incubated at 60°C in oven for 6–8 h.

4.2.9 Microinjection experiments

Embryos with fluorescent Histone-RFP signal were injected as previously described (4.2.2). mRNAs were synthesized through in vitro transcription. CS-tribbles plasmid template was linearized by XhoI and transcribed by mMESSAGE mMACHINE SP6 Transcription Kit. dsRNAs were produced by RiboMAX RNA Production T7 System, using tribbles cDNA template CS2-tribbles and dsRNA primers BL10 and BL11. The CS2-tribbles plasmid template was linearized by XhoI. mRNAs were injected at concentration of 800 µg/µl. dsRNAs were injected at concentration of 1–2 mg/ml (Farrell and O'Farrell 2013). MLN8054 Aurora Kinase inhibitor was injected at concentration of 20 µM.

4.2.10 Fluctuation analysis

Twine-GFP/Twine-GFP, Twine-GFP/+, X9;Twine-GFP/+, tribbles Twine-GFP/tribbles fly lines were generated and used in fluctuation analysis of Twine (gift of Blythe, Di Talia and Wieschaus). Confocal microscope LSM780 was used as Fluorescence Fluctuation Spectroscopy, 63✕ oil immersion objectives (Planapochromat, NA 1.4/oil) and a GaAsP detector were used as optical element. Settings and analysis were performed according to previous reported (Chen et al. 2002; Digman et al. 2008). The intensity traces were analyzed using the number and brightness analysis. In summary, we compute the time average $<i>$ and variance σ^2 of each trace. From these values we obtain the average brightness per molecule as $<e> = (\sigma^2/<i>) -1$ and the average number of molecules as $<n>=<i>/<e>$ (MATLAB code showing in Supplemental Tab. 7). The mathematical calculation of the fluctuation analysis was carried out by Dr. I. Gregor. The statistical significance (p value) of differences between the measured distributions was calculated by Student's t-test.

4.2.11 Isolation of Twine protein and phospho-sites analysis

Twine-GFP/Twine-GFP and X9;Twine-GFP/+ embryos were used in GFP-Pulldown and mass spectrometry. Approximately 50,000 to 80,000 embryos (assuming 100 embryos/mg wet weights, Ashburner 1989) were staged to 0–1.5 h, dechorionated, collected into Eppendorf tubes and snap-frozen in liquid nitrogen. Each 10,000 embryos were homogenized by glass dounce/grinder and pestle in 1 ml pre-cooled lysis and washing buffer. Embryo lysates were centrifuged at 14,000 rpm at 4°C for 15 min twice, and the supernatant was transferred into new pre-cooled Eppendorf tube. GFP-Trap_A agarose beads were washed thrice with lysis and washing buffer, added 20 µl into 1 ml embryo lysate. The embryo lysate and beads mixture were rotated on a wheel for 1 h at 4°C, and then spun down at 800 rpm for 2 min. Twine-GFP bounded beads were washed thrice with lysis and washing buffer, and protein was eluted from the beads in 50 mM Tris buffer.

For mass spectrometry, samples were run on SDS-PAGE 4–12% gradient 4–12% MOPS buffered system and bands excised and processed. Band slices were digested with trypsin over night at 30°C and the peptide extracted the next day. Samples were resuspended in 1% formic acid and a 15 µl Aliquots of each sample were run either before or after phosphopeptide enrichment. Phosphopeptides were enriched using Ti 4+ IMAC (ReSyn Biosciences) on an UltiMate 3000 RSLC nano system (Thermo Scientific) coupled to a LTQ OrbiTrap Velos Pro (Thermo Scientific). Peptides were initially trapped on an Acclaim PepMap 100 (C18, 100 µm × 2 cm) and then separated on an EasySpray PepMap RSLC C18 column (75 µm × 50 cm) (Thermo Scientific) over a 120 min linear gradient. The data was analyzed by Proteome Discoverer 1.4 (Thermo Scientific) using Mascot 2.4 (Matrix Science) as the search engine. Mass spectrometry of the phosphopeptide analysis was carried out by Prof. Dr. H.-A. Müller and the staff in Proteomics Facility, University of Dundee, UK.

Appendix

Supplemental Table 1: Quantification of nuclear cycle length in WT and X9

Embryo Nr	Nuclear cycle length (min)				
WT	**NC10**	**NC11**	**NC12**	**NC13**	**NC14**
1		10	16	20	
2	10	13	16	27	
3		12	14	21	
4			13	22	
5		11	15	22	
X9 (13 divisions)	**NC10**	**NC11**	**NC12**	**NC13**	**NC14**
1	12	14	18	21	
2				32	
3		12	16	26	
4				28	
X9 (14 divisions)	**NC10**	**NC11**	**NC12**	**NC13**	**NC14**
1	14	16	19	27	27
2		13	16	20	31
3	11	15	16	20	29
4		12	14	19	25
5		12	15	23	25

Supplemental Table 2: List of binding partners from yeast two-hybrid screen low sensitivity

Gene name	Copy	CDS	Global PBS
Tap42	3	full length	A
Tap42	10	partial	A
CG11873	1	partial	D
E(bx)	1	partial	D

PBS categories: A: Very high confidence in the interaction; B: High confidence in the interaction; C: Good confidence in the interaction; D: Moderate confidence in the interaction; E: Interactions involving highly connected (or relatively highly connected) prey domains, warning of non-specific interaction; F: Experimentally proven technical artifacts; N/A: The PBS is a score that is automatically computed through algorithms and cannot be attributed for certain reasons. Criteria by Hybrigenics, Paris. Bait: PpV (aa 2-303, full length).

Supplemental Table 3: List of binding partners from yeast two-hybrid screen high sensitivity

Gene name	Clone	CDS	Global PBS
Cp38	4	full length	A
Cp38	202	partial	A
Hop	10	partial	A
Aats-thr	5	partial	B
Tap42	5	full length	B
Tap42	11	partial	B
Dec-1	7	partial	B
Lap	1	full length	B
Lap	4	partial	B
Nahoda	5	partial	B
B4	4	partial	C
CG17446	3	partial	C
CG11873	1	partial	D
CG4538	1	partial	D
CG5642	1	partial	D
Nup54	1	partial	D
PpD3	1	partial	D
Retn	1	partial	D

PBS categories: A: Very high confidence in the interaction; B: High confidence in the interaction; C: Good confidence in the interaction; D: Moderate confidence in the interaction; E: Interactions involving highly connected (or relatively highly connected) prey domains, warning of non-specific interaction; F: Experimentally proven technical artifacts; N/A: The PBS is a score that is automatically computed through algorithms and cannot be attributed for certain reasons. Criteria by Hybrigenics, Paris. Bait: PpV (aa 2-303, full length).

Supplemental Table 4: Quantification of western blot with extracts from nls-GFP embryos by using FIJI densitometry measurement

Western blot Nr	Densitometry measurement by FIJI			
	Dia	Dia background	GFP	GFP background
Replicate1 1×nls-GFP	18351.205	16060.222	25987.116	20185.35
Replicate1 2×nls-GFP	17238.146	16063.215	28943.328	21607.828
Replicate2 1×nls-GFP	16271.889	15154.833	26397.362	20640.513
Replicate2 2×nls-GFP	16230.215	15059.201	45214.247	20935.35
Replicate3 1×nls-GFP	17960.276	16433.051	23096.737	19554.621
Replicate3 2×nls-GFP	17587.392	16429.984	37991.174	21498.9

Supplemental Table 5: Average particle number of nls-GFP expression profile by fluctuation analysis

	Average particle number					
1×nls-GFP	Repetition 1	Repetition 2	Repetition 3	Repetition 4	Repetition 5	Repetition 6
embryo1	75.45	82.45	82.66	86.02	84.29	88.23
embryo2	87.22	88.45	90.12	85.53	91.66	92.02
embryo3	105.16	108.13	110.23	108.54	107.22	112.54
embryo4	130.45	125.81	133.36	130.34	130.22	135.93
embryo5	118.26	128.37	118.71	121.52	123.42	126.44
embryo6	97.53	103.89	107.85	106.32	102.15	105.27
embryo7	88	87.1	91.08	85.36	89.79	87.72
embryo8	114.82	115.8	118.39	121.61	119.74	116.2
2×nls-GFP	Repetition 1	Repetition 2	Repetition 3	Repetition 4	Repetition 5	Repetition 6
embryo1	276	296.98	295.54	283.17	281.14	294.01
embryo2	207.65	197.15	200.77	209.09	198.96	195.58
embryo3	190.43	192.51	193.88	160.51	189.05	170.59
embryo4	201.15	201.62	213.43	208.27	205.26	211.69
embryo5	216.16	242.31	248.94	260.44	292.72	297.75
embryo6	171.68	157.86	167.96	157.44	137.07	136.82
embryo7	180.64	192.5	196.18	180.22	192.37	192.94
embryo8	162.21	157.57	155.72	161.87	151.43	164.61

Supplemental Table 6: Analysis of phosphorylation sites by mass spectrometry

Peptides	Position	M/Z	Mr (expt)	Mr (calc)	Ppm	Ion score	Expect
WT							
K.SWQCGEGGDSGIGGGGSR.G	S396	902.3405	1802.6665	1802.668	-0.83	46	4.40E-05
K.TKSWQCGEGGDSGIGGGGSR.G	T394, S396	1016.9122	2031.8099	2031.8106	-0.34	68	4.30E-07
K.TLSMNDAEIMR.A	S205	696.7799	1391.5453	1391.5462	-0.66	32	0.00094
K.TLSMNDAEIMR.A	T203, S205	696.7805	1391.5464	1391.5462	0.13	31	0.004
X9 mutant							
K.SWQCGEGGDSGIGGGGSR.G	S412	902.3414	1802.6682	1802.668	0.12	47	8.50E-05
R.KTLSMNDAEIMR.A	S205	744.833	1487.6515	1487.6513	0.11	62	3.70E-06
K.SWQCGEGGDSGIGGGGSR.G	S405	902.3408	1802.6671	1802.668	-0.49	41	0.00014
R.RKSAVQETPLQWMLK.R	S41	632.3252	1893.9538	1893.9536	0.11	27	0.0032
R.KTLSMNDAEIMR.A	T203, S205	752.8309	1503.6473	1503.6462	0.72	33	0.00078
K.TKSWQCGEGGDSGIGGGGSR.G	T394, S396	1016.9127	2031.8109	2031.8106	0.14	29	0.0073
HIPASTTVLSPITELSQNMNGAR	S59, T60, T61, S64, T67		2532.2043	2532.2043	0.42		

Results from Mascot data analysis of mass spectrometry (ms/ms) spectra. Peptide sequences are depicted of the Cdc25-like protein Twine as predict from fragmentation spectra. Predicted phosphorylation sites are marked in red (bold colors for unambiguous annotations). Although peptides were identified independently in many cases, only highest scoring peptides are included. Observed mass/charge (M/Z) values indicate the result of the measurement and the calculated relative molecular weight (Mr) from the M/Z is indicated as experimental (expt) Mr in Dalton (Da). Mr calc depicts the calculated relative molecular weight in Dalton (Da) as calculated from the expected Mr from the database. Ppm indicates the error value between Mr expt and Mr calc and the ion score indicates the number of spectral ions matching the annotated fragments in the database. The expectation value is a statistical representation of the ion score expressed as p-value. Mass spectrometry of the phosphopeptide analysis was carried out by Prof. Dr. H.-A. Müller and the staff in Proteomics Facility, University of Dundee, UK.

Supplemental Table 7: Code of fluctuation analysis in MATLAB programming (Dr. I. Gregor)

Data extraction

```matlab
names = dir('e*.fcs');

for n = 1:numel(names)
    fname = names(n).name;
    p = strfind(fname,'-');
    if ~isempty(p)

        fid = fopen(fname,'r');
        s = 0;
        tmp = deblank(fgetl(fid));
        while ~feof(fid)
            while
~feof(fid)&&((numel(tmp)<21)||(~strcmp(tmp(4:21),'CountRateArraySize')))
                tmp = deblank(fgetl(fid));
            end
            if ~feof(fid)
                tmp = fgetl(fid);
                A = sscanf(tmp,'%*s = %d %d');
                if A(1)>0
                    s = s +1;
                    data_cnt = fscanf(fid,'%f %f',[A(2) A(1)]);
                    C{n,s}   = data_cnt;
                end
            end


            while
~feof(fid)&&((numel(tmp)<23)||(~strcmp(tmp(4:23),'CorrelationArraySize')))
                tmp = deblank(fgetl(fid));
            end
            if ~feof(fid)
                tmp = fgetl(fid);
                A = sscanf(tmp,'%*s = %d %d');
                if A(1)>0
                    data_fcs = fscanf(fid,'%f %f',[A(2) A(1)]);
                    D{n,s}   = data_fcs;
                end
            end
            em(n,s)  = sscanf(fname((p(1)-1)),'%d');
            ti(n,s)  = sscanf(fname((p(1)+1):(end-4)),'%d');
        end
        fclose(fid);
    end
end
```

Analysis

```
read_data;

t  = D{1,1}(1,:);
em = em(:,1);
ti = ti(:,1);

n_em = unique(em);

for EM = 1:numel(n_em);

    e_ind = (em == n_em(EM));

    ei = find(e_ind,1,'first');

    t_str = names(ei).name(1:9);

    e_ti = ti(e_ind);
    [e_ti, ord] = sort(e_ti);

    e_D  = D(e_ind,:);
    e_D  = e_D(ord,:);
    e_C  = C(e_ind,:);
    e_C  = e_C(ord,:);

    rep = size(e_D,2);

    for j = 1:size(e_D,1)
        for k = 1:rep
            if size(e_D{j,k},2)==numel(t)
                y(k+ (j-1)*rep,:) = e_D{j,k}(2,:)-1;
            else
                y(k+ (j-1)*rep,:) = zeros(1,size(y,2));
            end
            if ~isempty(e_C{j,k})
                r(k+ (j-1)*rep) = mean(e_C{j,k}(2,:),2);
                p(k+ (j-1)*rep) = var(e_C{j,k}(2,:),1,2);
            else
                r(k+ (j-1)*rep) = NaN;
                p(k+ (j-1)*rep) = NaN;
            end
            tt(k+ (j-1)*rep) = e_ti(j);
        end
    end

    ind = (t>2e-1);

    m = mean(y(:,ind),2);
    s = std(y(:,ind),[],2);
    v = (m<2e-2)&(s<2e-2);
%    v = true(1,numel(r));

    I{EM} = r(v);
    N{EM} = r(v).^2./(p(v)-r(v));
    B{EM} = (p(v)-r(v))./r(v);
    T{EM} = tt(v);
```

Appendix

```matlab
end

e_color = [[1 0 0];[0 1 0];[0 0 1];[0 0 0];[0 1 1];[1 0 1];[1 1 0];[0.2 0.2
0.2];[0.5 0 0];[0 0.5 0]];

for EM = 1:numel(n_em);
    l{EM} = sprintf('embryo %d',n_em(EM));
end

figure

plot(T{1},I{1},'x','Color',e_color(1,:),'MarkerSize',10);
hold on
for EM = 2:numel(n_em);
    plot(T{EM},I{EM},'x','Color',e_color(EM,:),'MarkerSize',10);
end
xlabel('time / s');
ylabel('avg. count rate / cps');
axis tight
ax = axis;
axis([-0.05.*ax(2) 1.05.*ax(2) 0 1.05*ax(4)])
legend(l)
legend('location','SouthEast')
legend('boxoff')
ExportFigure('CountRate','png')

figure

plot(T{1},N{1},'x','Color',e_color(1,:),'MarkerSize',10);
hold on
for EM = 2:numel(n_em);
    plot(T{EM},N{EM},'x','Color',e_color(EM,:),'MarkerSize',10);
end
xlabel('time / s');
ylabel('avg. particle number');
axis tight
ax = axis;
axis([-0.05.*ax(2) 1.05.*ax(2) 0 1.05*ax(4)])
legend(l)
legend('location','SouthEast')
legend('boxoff')

ExportFigure('Numbers','png')

figure

plot(T{1},B{1},'x','Color',e_color(1,:),'MarkerSize',10);
hold on
for EM = 2:numel(n_em);
    plot(T{EM},B{EM},'x','Color',e_color(EM,:),'MarkerSize',10);
end
xlabel('time / s');
ylabel('avg. particle brightness / cps');
axis tight
ax = axis;
axis([-0.05.*ax(2) 1.05.*ax(2) 0 1.05*ax(4)])
legend(l)
legend('location','SouthEast')
legend('boxoff')
```

```matlab
ExportFigure('Brightness','png')

mtmp = 0;
for k = 1:size(C,1)
    for l = 1:size(C,2)
        tmp = max(max(C{k,l}));
        if tmp > mtmp
            mtmp = tmp;
        end
    end
end

for EM = 1:numel(n_em)

    e_ind = (em == n_em(EM));
    e_ti  = ti(e_ind);

    Ct = C(e_ind==1,:);

    anz = numel(T{EM});
    z   = sum(e_ind);
    tt  = repmat(11.*(0:size(C,2)-1),[numel(e_ti) 1])+repmat(e_ti,[1
size(C,2)]);

    figure
    axis([0 max(tt(:))+11 0 ceil(mtmp./10^(floor(log10(mtmp))-
1)).*10^(floor(log10(mtmp))-1)])
    hold on

    for k = 1:size(Ct,1)
        for l = 1:size(Ct,2)
            tmp = Ct{k,l};
            if ~isempty(tmp)
                plot(tt(k,l)+tmp(1,:),tmp(2,:));
            end
        end
    end
    xlabel('time / s');
    ylabel('count rate / cps');
    fname = ['Rate_Embryo_' int2str(n_em(EM))];
    ExportFigure(fname,'png')
end

for EM = 1:numel(n_em)
    Te = T{EM};
    Ie = I{EM};
    Be = B{EM};
    Ne = N{EM};

    Tu = unique(Te)';

    Iu = zeros(numel(Tu),numel(Ie));
    Bu = zeros(numel(Tu),numel(Ie));
    Nu = zeros(numel(Tu),numel(Ie));

    for Ti = 1:numel(Tu)
        ind = (Te == Tu(Ti));
        Iu(Ti,1:sum(ind)) = Ie(ind);
        Bu(Ti,1:sum(ind)) = Be(ind);
```

Appendix

```matlab
        Nu(Ti,1:sum(ind)) = Ne(ind);
    end

    ind = sum(Iu) > 0;
    Iu = Iu(:,ind);
    Bu = Bu(:,ind);
    Nu = Nu(:,ind);

    tmp = [[Tu Nu]; [Tu Iu]; [Tu Bu]];
    fname = ['Results_Embryo_' int2str(n_em(EM)) '.dat'];
    save(fname,'tmp','-ASCII');
end
```

Supplemental Figure 1: Exponential fitting of fluctuation analysis measurements.

(A) Twine-GFP/+
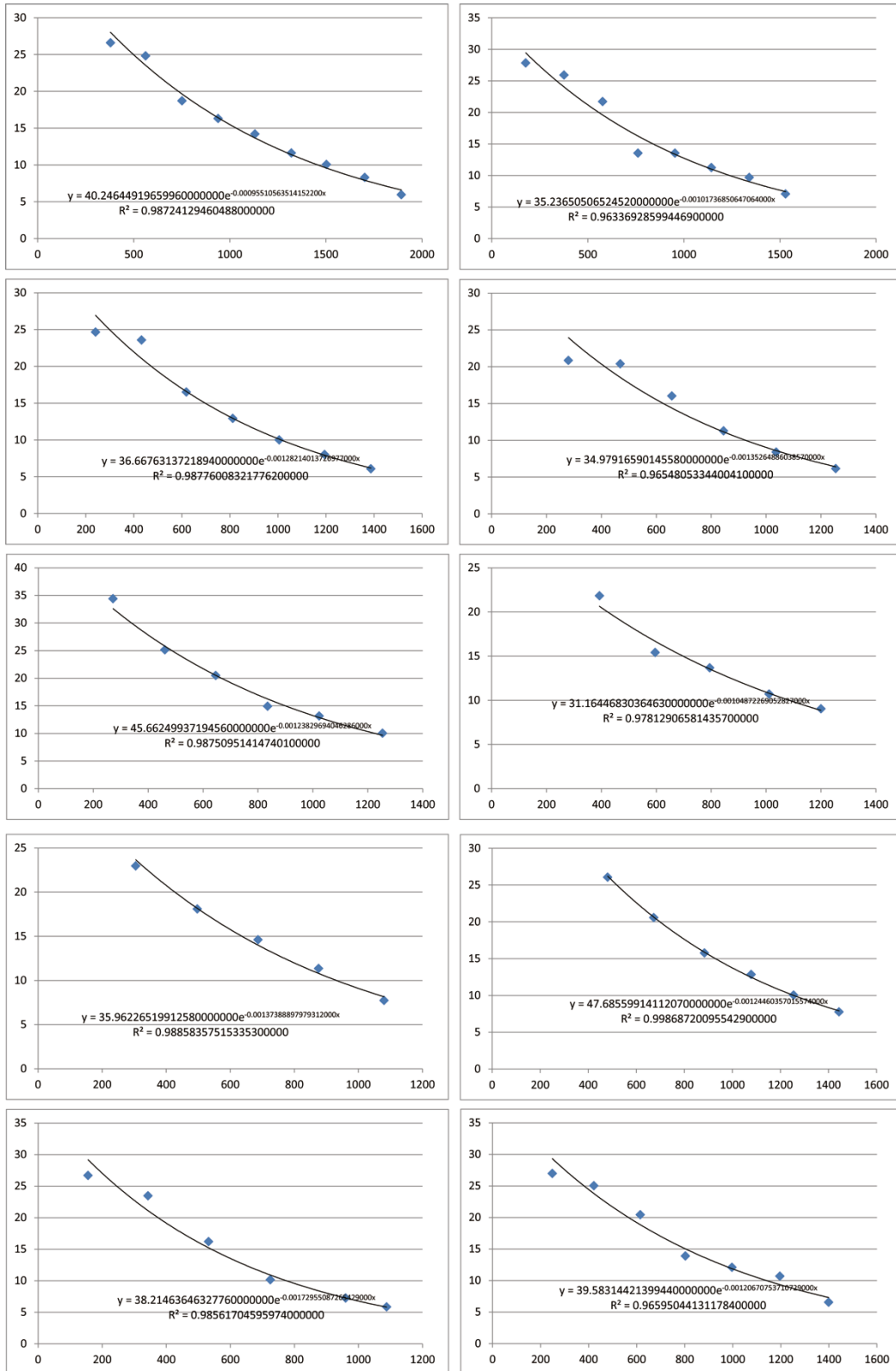
Appendix

Supplemental Figure 1-continuation

(B) Twine-GFP
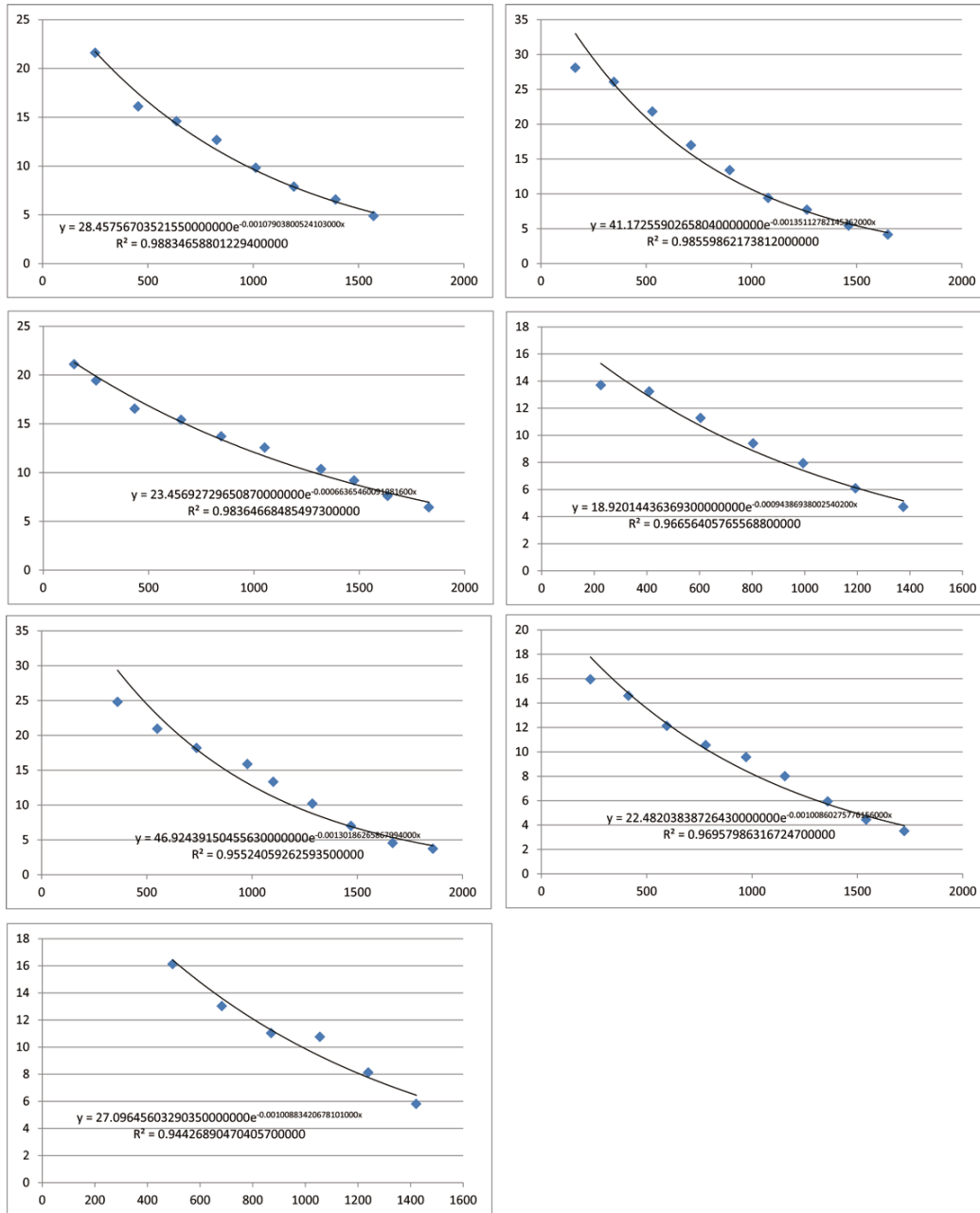
Supplemental Figure 1-continuation

(C) X9; Twine-GFP/+
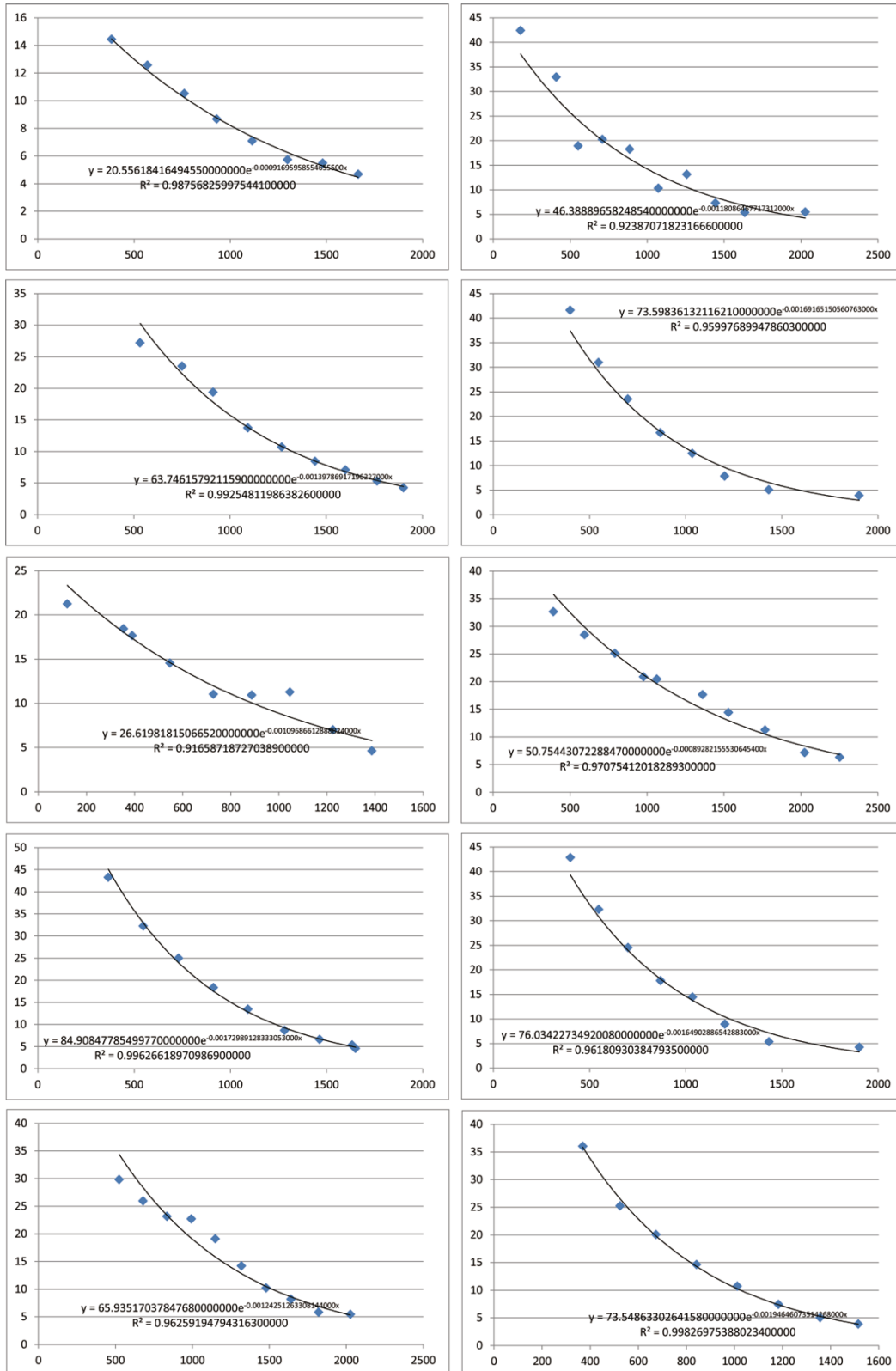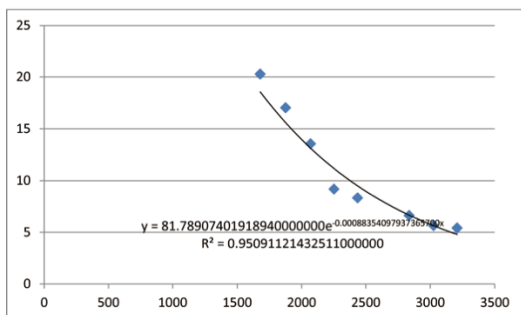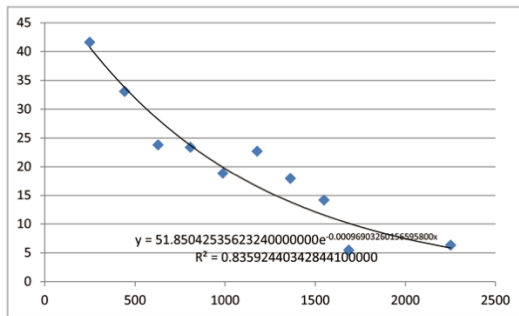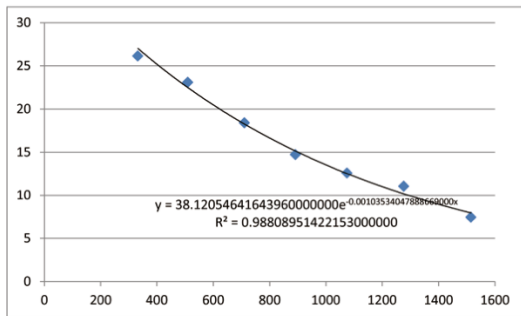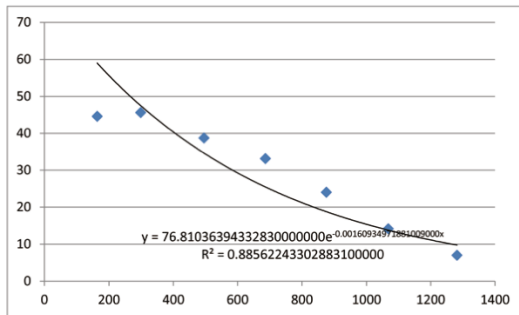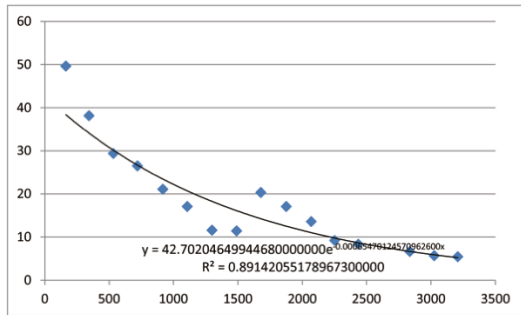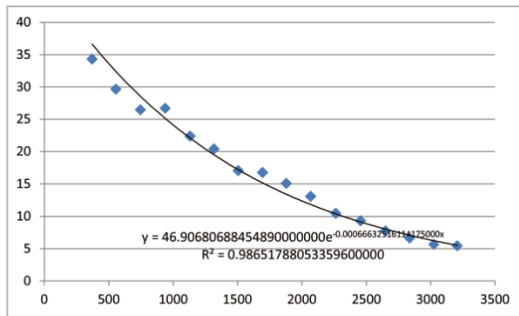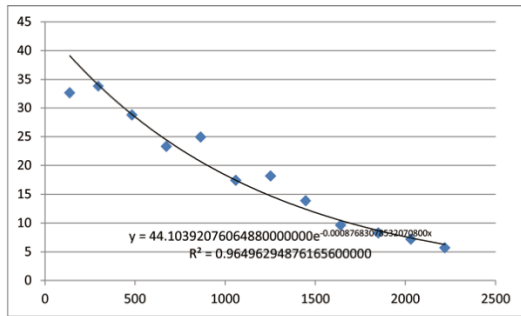
Supplemental Figure 1-continuation

(D) *tribbles*, Twine-GFP/*tribbles*

Appendix
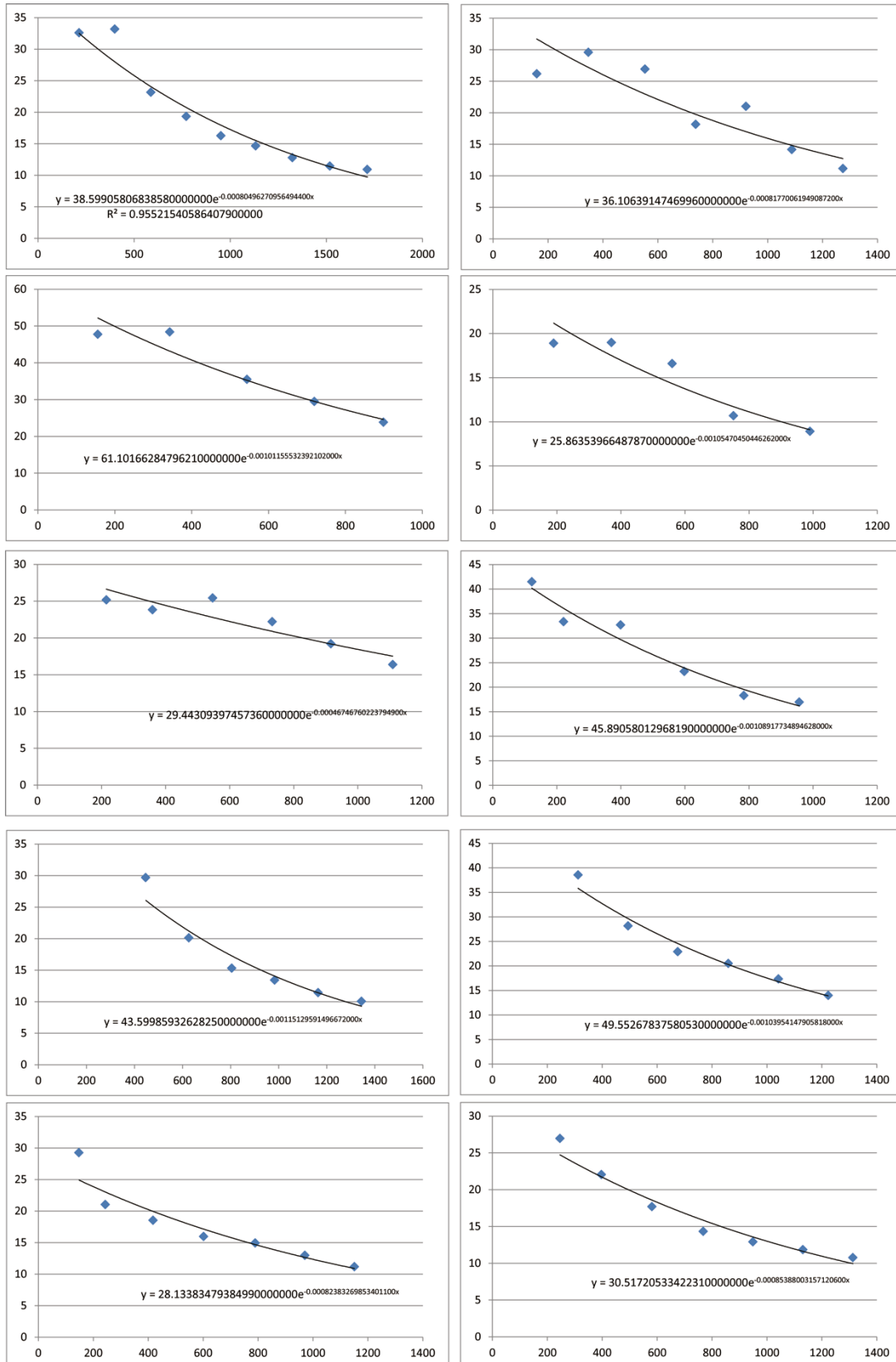
Supplemental Figure 1-continuation

(E) Twine-GFP-Ala/TM3
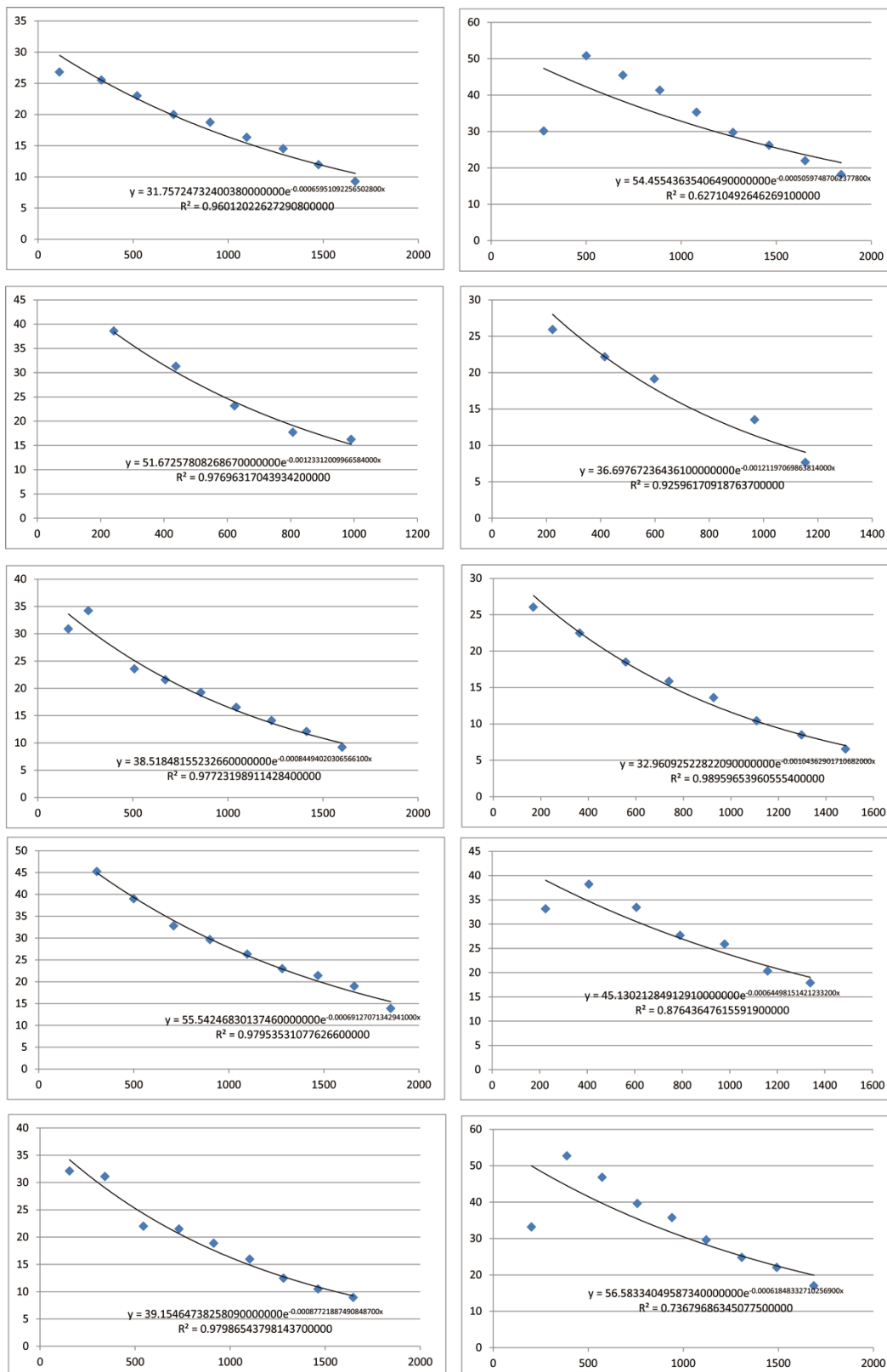
Supplemental Figure 1-continuation

(F) Twine-GFP-Asp/TM3
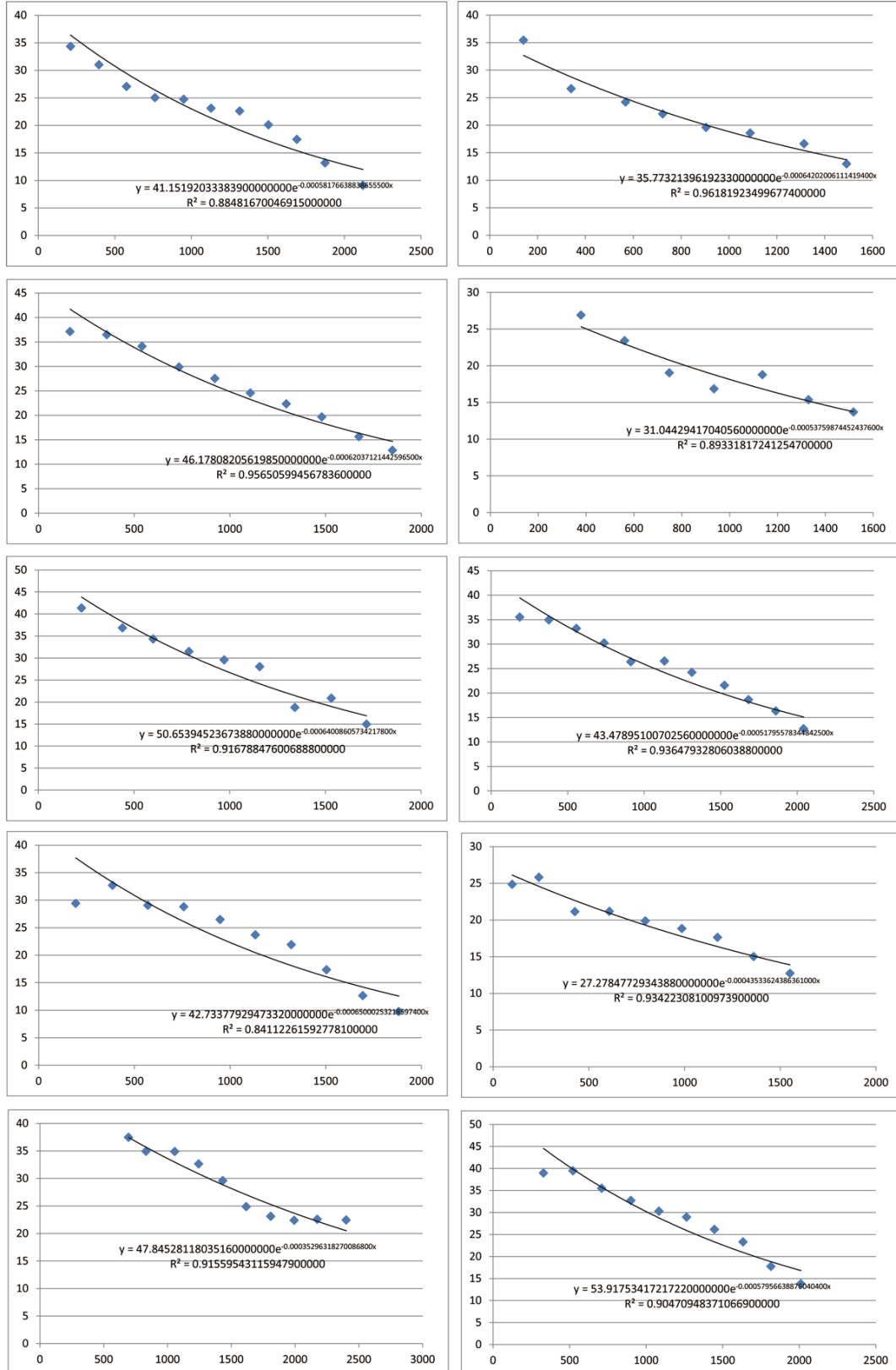
Supplemental Figure 2: Exponential fitting of fluctuation analysis measurements.

(A) *twine*; Twine-GFP-WT/TM3
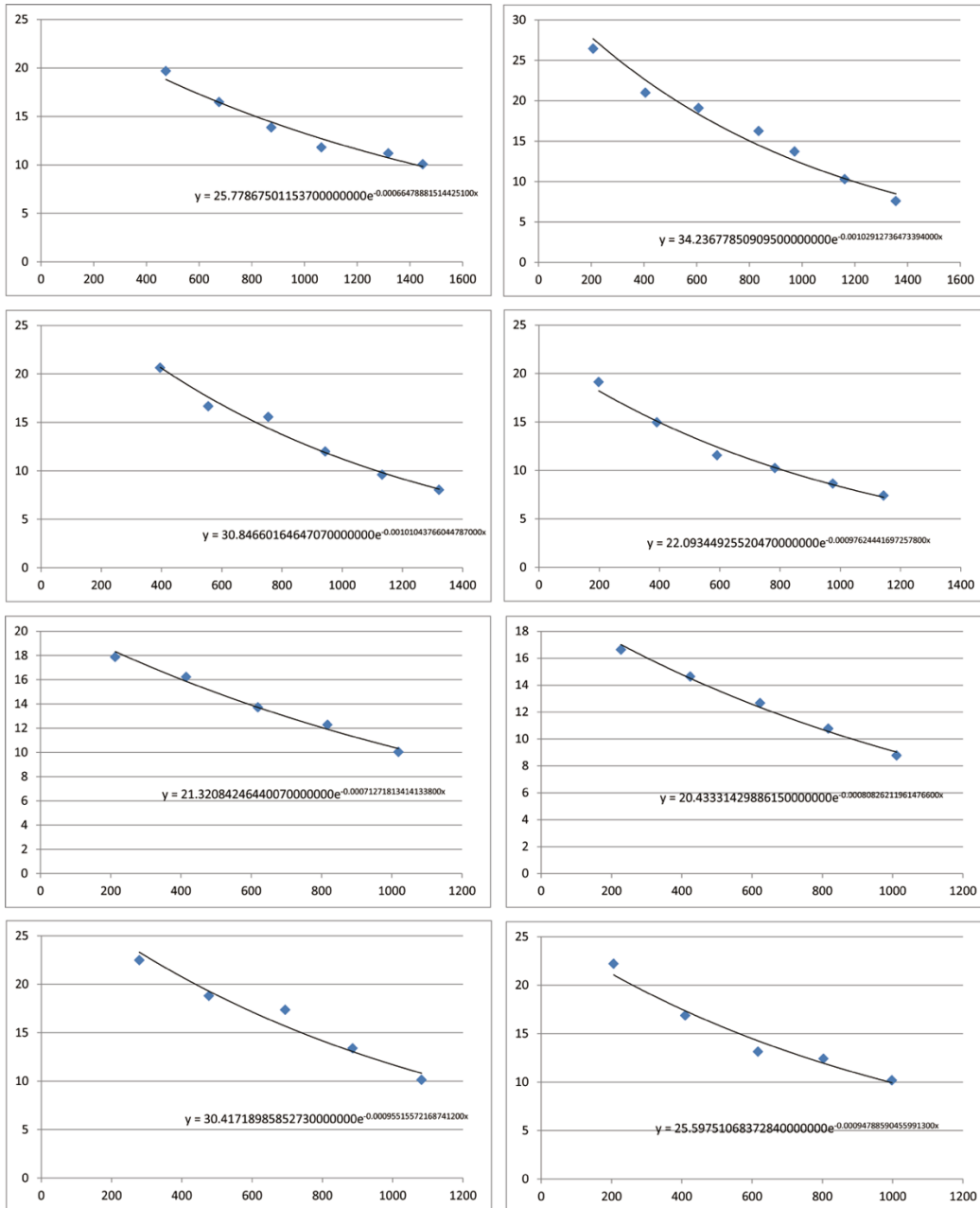
Supplemental Figure 2-continuation

(B) *twine*; Twine-GFP-WT
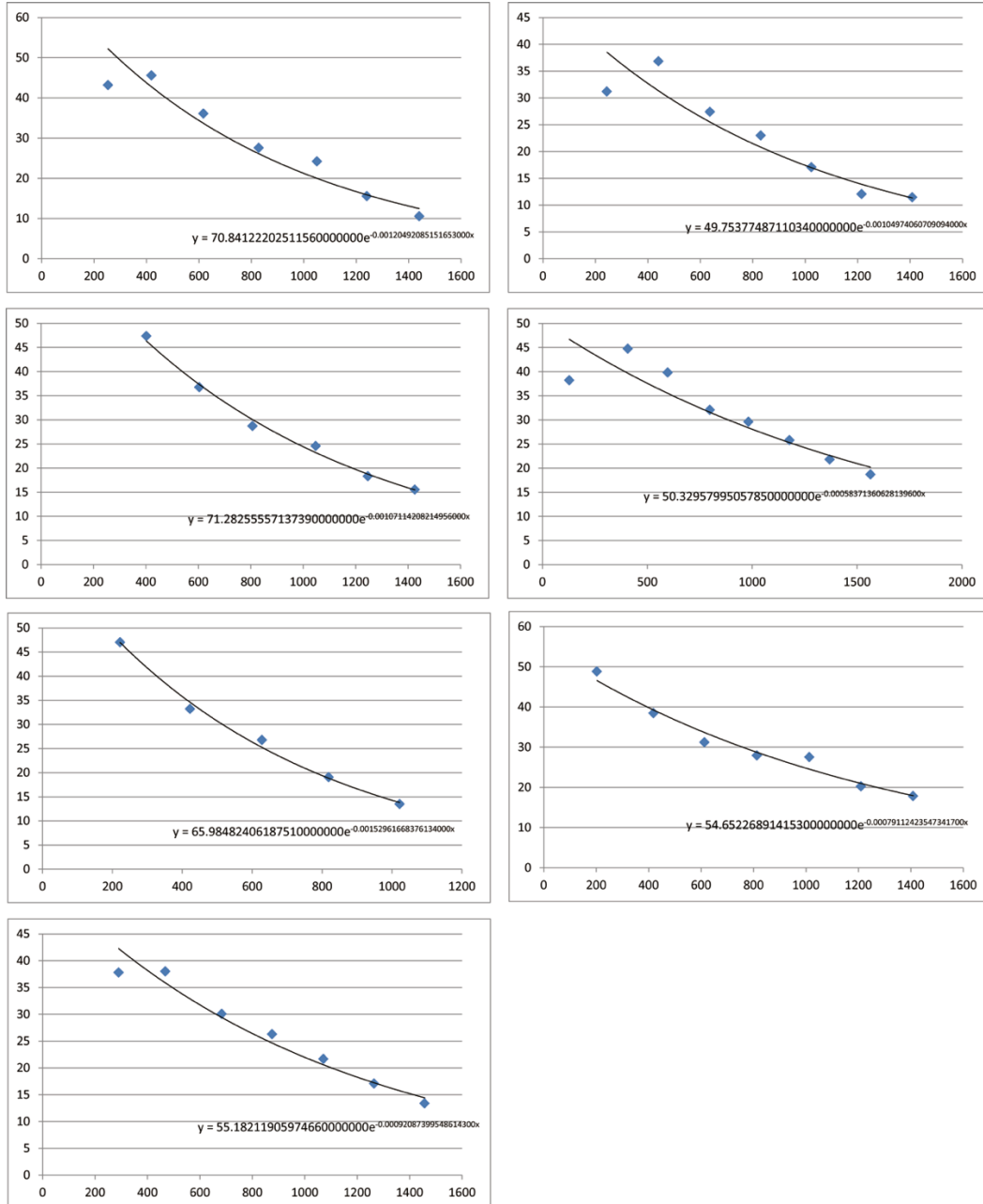
Supplemental Figure 2-continuation

(C) *twine*; Twine-GFP-Ala/TM3
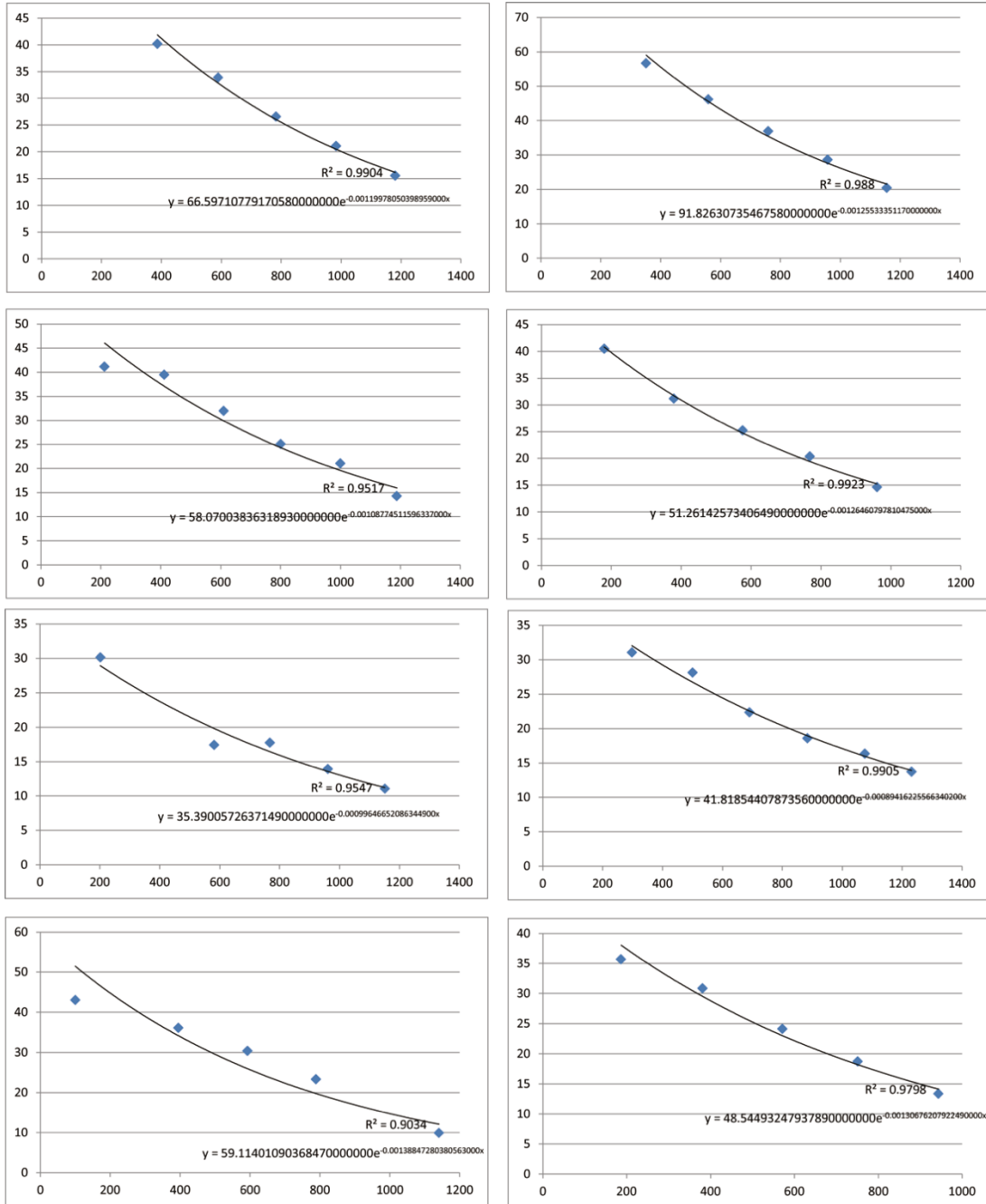
Supplemental Figure 2-continuation

(D) *twine*; Twine-GFP-Ala

Appendix
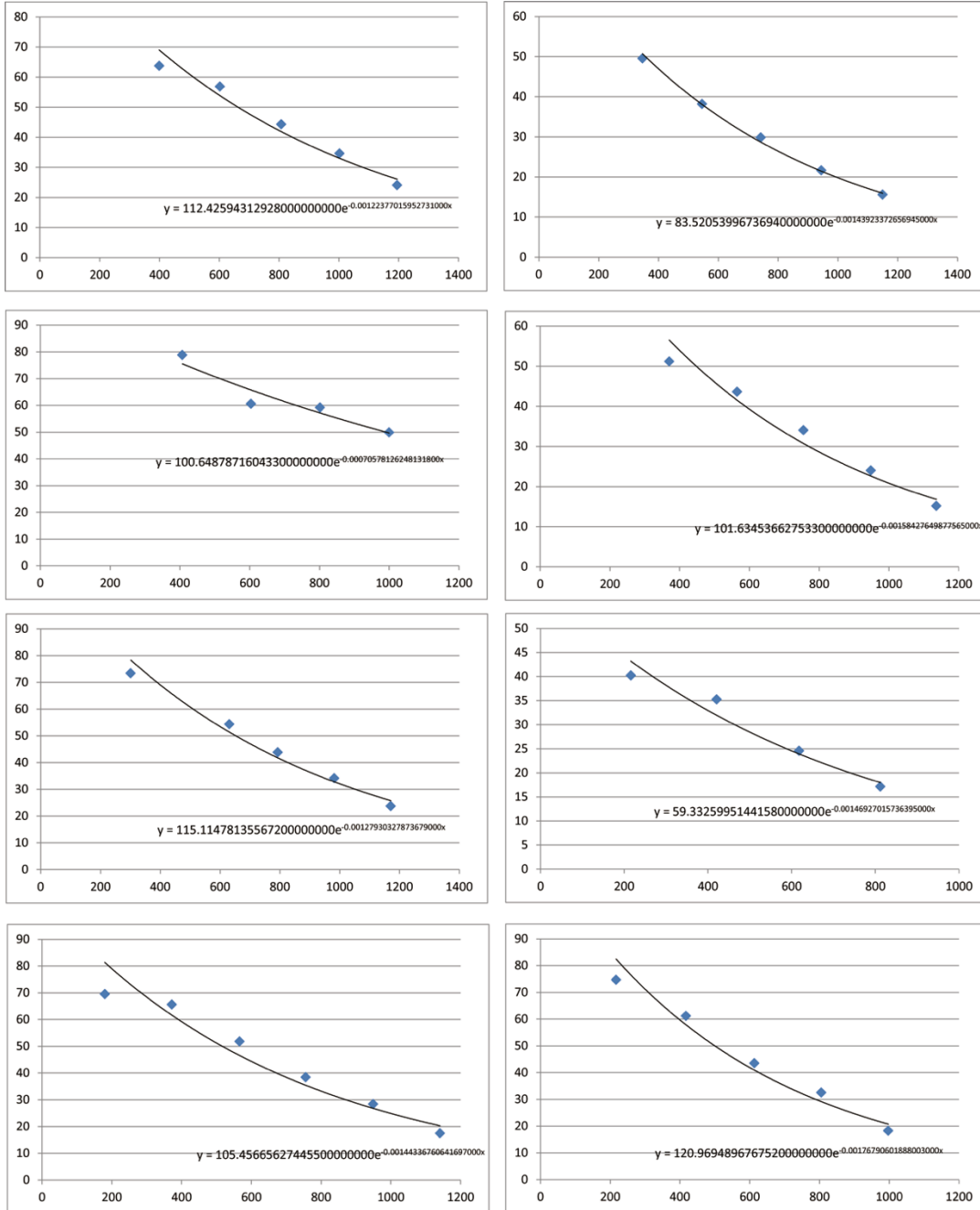
Supplemental Figure 2-continuation

(E) *twine*; Twine-GFP-Asp/TM3
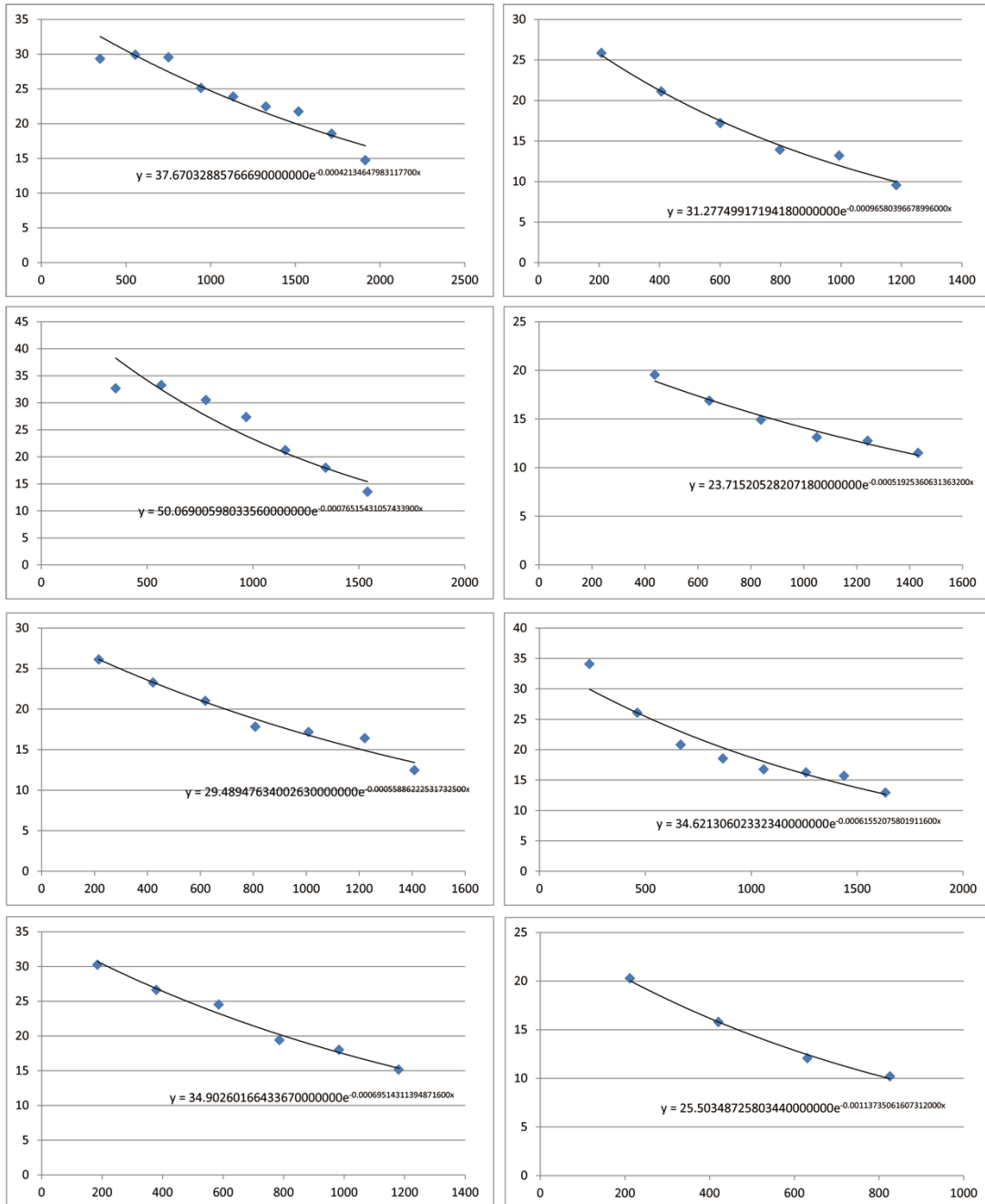
$y = 37.67032885766690000000e^{-0.00042134647983117700x}$

$y = 31.27749917194180000000e^{-0.00096580396678996000x}$

$y = 50.06900598033560000000e^{-0.00076515431057433900x}$

$y = 23.71520528207180000000e^{-0.00051925360631363200x}$

$y = 29.48947634002630000000e^{-0.00055886222531732500x}$

$y = 34.62130602332340000000e^{-0.00061552075801911600x}$

$y = 34.90260166433670000000e^{-0.00069514311394871600x}$

$y = 25.50348725803440000000e^{-0.00113735061607312000x}$

Bibliography

Acharya S, Laupsien P, Wenzl C, Yan S, Grosshans J. 2014. Function and dynamics of slam in furrow formation in early Drosophila embryo. *Dev Biol* **386**: 371-384.

Afshar K, Werner ME, Tse YC, Glotzer M, Gonczy P. 2010. Regulation of cortical contractility and spindle positioning by the protein phosphatase 6 PPH-6 in one-cell stage C. elegans embryos. *Development* **137**: 237-247.

Ali-Murthy Z, Lott SE, Eisen MB, Kornberg TB. 2013. An essential role for zygotic expression in the pre-cellular Drosophila embryo. *PLoS Genet* **9**: e1003428.

Alphey L, Jimenez J, White-Cooper H, Dawson I, Nurse P, Glover DM. 1992. twine, a cdc25 homolog that functions in the male and female germline of Drosophila. *Cell* **69**: 977-988.

Amodeo AA, Jukam D, Straight AF, Skotheim JM. 2015. Histone titration against the genome sets the DNA-to-cytoplasm threshold for the Xenopus midblastula transition. *Proc Natl Acad Sci U S A* **112**: E1086-1095.

Ashburner M. 1989. *Drosophila: A Laboratory Mannual*. Cold Spring Harbor Laboratory Press, Cold spring Harbor, NY.

Axton JM, Shamanski FL, Young LM, Henderson DS, Boyd JB, Orr-Weaver TL. 1994. The inhibitor of DNA replication encoded by the Drosophila gene plutonium is a small, ankyrin repeat protein. *EMBO J* **13**: 462-470.

Ayeni JO, Varadarajan R, Mukherjee O, Stuart DT, Sprenger F, Srayko M, Campbell SD. 2014. Dual phosphorylation of cdk1 coordinates cell proliferation with key developmental processes in Drosophila. *Genetics* **196**: 197-210.

Bashirullah A, Halsell SR, Cooperstock RL, Kloc M, Karaiskakis A, Fisher WW, Fu W, Hamilton JK, Etkin LD, Lipshitz HD. 1999. Joint action of two RNA degradation pathways controls the timing of maternal transcript elimination at the midblastula transition in Drosophila melanogaster. *EMBO J* **18**: 2610-2620.

Bastians H, Ponstingl H. 1996. The novel human protein serine/threonine phosphatase 6 is a functional homologue of budding yeast Sit4p and fission yeast ppe1, which are involved in cell cycle regulation. *J Cell Sci* **109 (Pt 12)**: 2865-2874.

Benoit B, He CH, Zhang F, Votruba SM, Tadros W, Westwood JT, Smibert CA, Lipshitz HD, Theurkauf WE. 2009. An essential role for the RNA-binding protein Smaug during the Drosophila maternal-to-zygotic transition. *Development* **136**: 923-932.

Bettencourt-Dias M, Giet R, Sinka R, Mazumdar A, Lock WG, Balloux F, Zafiropoulos PJ, Yamaguchi S, Winter S, Carthew RW et al. 2004. Genome-wide survey of protein kinases required for cell cycle progression. *Nature* **432**: 980-987.

Bischof J, Maeda RK, Hediger M, Karch F, Basler K. 2007. An optimized transgenesis system for Drosophila using germ-line-specific phiC31 integrases. *Proc Natl Acad Sci U S A* **104**: 3312-3317.

Bischoff JR, Anderson L, Zhu Y, Mossie K, Ng L, Souza B, Schryver B, Flanagan P, Clairvoyant F, Ginther C et al. 1998. A homologue of Drosophila aurora kinase is oncogenic and amplified in human colorectal cancers. *EMBO J* **17**: 3052-3065.

Blumenthal AB, Kriegstein HJ, Hogness DS. 1974. The units of DNA replication in Drosophila melanogaster chromosomes. *Cold Spring Harb Symp Quant Biol* **38**: 205-223.

Blythe SA, Wieschaus EF. 2015a. Coordinating Cell Cycle Remodeling with Transcriptional Activation at the Drosophila MBT. *Curr Top Dev Biol* **113**: 113-148.

Blythe SA, Wieschaus EF. 2015b. Zygotic genome activation triggers the DNA replication checkpoint at the midblastula transition. *Cell* **160**: 1169-1181.

Bodenmiller B, Wanka S, Kraft C, Urban J, Campbell D, Pedrioli PG, Gerrits B, Picotti P, Lam H, Vitek O et al. 2010. Phosphoproteomic analysis reveals interconnected system-wide responses to perturbations of kinases and phosphatases in yeast. *Sci Signal* **3**: rs4.

Boettiger AN, Bintu B, Moffitt JR, Wang S, Beliveau BJ, Fudenberg G, Imakaev M, Mirny LA, Wu CT, Zhuang X. 2016. Super-resolution imaging reveals distinct chromatin folding for different epigenetic states. *Nature* **529**: 418-422.

Boettiger AN, Levine M. 2009. Synchronous and stochastic patterns of gene activation in the Drosophila embryo. *Science* **325**: 471-473.

Bouldin CM, Kimelman D. 2014. Cdc25 and the importance of G2 control: insights from developmental biology. *Cell Cycle* **13:** 2165-2171.

Boveri T. 1893. An Organism Produced Sexually without Characteristics of the Mother. *American Society of Naturalists* **27**: 222-232.

Bushati N, Stark A, Brennecke J, Cohen SM. 2008. Temporal reciprocity of miRNAs and their targets during the maternal-to-zygotic transition in Drosophila. *Curr Biol* **18**: 501-506.

Campbell SD, Sprenger F, Edgar BA, O'Farrell PH. 1995. Drosophila Wee1 kinase rescues fission yeast from mitotic catastrophe and phosphorylates Drosophila Cdc2 in vitro. *Mol Biol Cell* **6**: 1333-1347.

Chen F, Archambault V, Kar A, Lio P, D'Avino PP, Sinka R, Lilley K, Laue ED, Deak P, Capalbo L et al. 2007. Multiple protein phosphatases are required for mitosis in Drosophila. *Curr Biol* **17**: 293-303.

Chen J, Peterson RT, Schreiber SL. 1998. Alpha 4 associates with protein phosphatases 2A, 4, and 6. *Biochem Biophys Res Commun* **247**: 827-832.

Chen K, Johnston J, Shao W, Meier S, Staber C, Zeitlinger J. 2013. A global change in RNA polymerase II pausing during the Drosophila midblastula transition. *Elife* **2**: e00861.

Chen L, Dumelie JG, Li X, Cheng MH, Yang Z, Laver JD, Siddiqui NU, Westwood JT, Morris Q, Lipshitz HD et al. 2014. Global regulation of mRNA translation and stability in the early Drosophila embryo by the Smaug RNA-binding protein. *Genome Biol* **15**: R4.

Chen Y, Muller JD, Ruan Q, Gratton E. 2002. Molecular brightness characterization of EGFP in vivo by fluorescence fluctuation spectroscopy. *Biophys J* **82**: 133-144.

Chou TB, Perrimon N. 1996. The autosomal FLP-DFS technique for generating germline mosaics in Drosophila melanogaster. *Genetics* **144**: 1673-1679.

Collart C, Allen GE, Bradshaw CR, Smith JC, Zegerman P. 2013. Titration of four replication factors is essential for the Xenopus laevis midblastula transition. *Science* **341**: 893-896.

Collart C, Owens ND, Bhaw-Rosun L, Cooper B, De Domenico E, Patrushev I, Sesay AK, Smith JN, Smith JC, Gilchrist MJ. 2014. High-resolution analysis of gene activity during the Xenopus mid-blastula transition. *Development* **141**: 1927-1939.

Cygnar KD, Gao X, Pan D, Neufeld TP. 2005. The phosphatase subunit tap42 functions independently of target of rapamycin to regulate cell division and survival in Drosophila. *Genetics* **170**: 733-740.

De Renzis S, Elemento O, Tavazoie S, Wieschaus EF. 2007. Unmasking activation of the zygotic genome using chromosomal deletions in the Drosophila embryo. *PLoS Biol* **5**: e117.

Di Talia S, She R, Blythe SA, Lu X, Zhang QF, Wieschaus EF. 2013. Posttranslational control of Cdc25 degradation terminates Drosophila's early cell-cycle program. *Curr Biol* **23**: 127-132.

Digman MA, Dalal R, Horwitz AF, Gratton E. 2008. Mapping the number of molecules and brightness in the laser scanning microscope. *Biophys J* **94**: 2320-2332.

Douglas P, Zhong J, Ye R, Moorhead GB, Xu X, Lees-Miller SP. 2010. Protein phosphatase 6 interacts with the DNA-dependent protein kinase catalytic subunit and dephosphorylates gamma-H2AX. *Mol Cell Biol* **30**: 1368-1381.

Duffy JB. 2002. GAL4 system in Drosophila: a fly geneticist's Swiss army knife. *Genesis* **34**: 1-15.

Dutertre S, Cazales M, Quaranta M, Froment C, Trabut V, Dozier C, Mirey G, Bouche JP, Theis-Febvre N, Schmitt E et al. 2004. Phosphorylation of CDC25B by Aurora-A at the centrosome contributes to the G2-M transition. *J Cell Sci* **117**: 2523-2531.

Edgar BA, Datar SA. 1996. Zygotic degradation of two maternal Cdc25 mRNAs terminates Drosophila's early cell cycle program. *Genes Dev* **10**: 1966-1977.

Edgar BA, Kiehle CP, Schubiger G. 1986. Cell cycle control by the nucleo-cytoplasmic ratio in early Drosophila development. *Cell* **44**: 365-372.

Edgar BA, Lehner CF. 1996. Developmental control of cell cycle regulators: a fly's perspective. *Science* **274**: 1646-1652.

Edgar BA, O'Farrell PH. 1989. Genetic control of cell division patterns in the Drosophila embryo. *Cell* **57**: 177-187.

Edgar BA, O'Farrell PH. 1990. The three postblastoderm cell cycles of Drosophila embryogenesis are regulated in G2 by string. *Cell* **62**: 469-480.

Edgar BA, Schubiger G. 1986. Parameters controlling transcriptional activation during early Drosophila development. *Cell* **44**: 871-877.

Edgar BA, Sprenger F, Duronio RJ, Leopold P, O'Farrell PH. 1994. Distinct molecular mechanism regulate cell cycle timing at successive stages of Drosophila embryogenesis. *Genes Dev* **8**: 440-452.

Edgar BA, Zielke N, Gutierrez C. 2014. Endocycles: a recurrent evolutionary innovation for post-mitotic cell growth (vol 15, pg 197, 2014). *Nat Rev Mol Cell Bio* **15**.

Ertych N, Stolz A, Valerius O, Braus GH, Bastians H. 2016. CHK2-BRCA1 tumor-suppressor axis restrains oncogenic Aurora-A kinase to ensure proper mitotic microtubule assembly. *Proc Natl Acad Sci U S A* **113**: 1817-1822.

Farrell JA, O'Farrell PH. 2013. Mechanism and regulation of Cdc25/Twine protein destruction in embryonic cell-cycle remodeling. *Curr Biol* **23**: 118-126.

Farrell JA, O'Farrell PH. 2014. From egg to gastrula: how the cell cycle is remodeled during the Drosophila mid-blastula transition. *Annu Rev Genet* **48**: 269-294.

Farrell JA, Shermoen AW, Yuan K, O'Farrell PH. 2012. Embryonic onset of late replication requires Cdc25 down-regulation. *Genes Dev* **26**: 714-725.

Fasulo B, Koyama C, Yu KR, Homola EM, Hsieh TS, Campbell SD, Sullivan W. 2012. Chk1 and Wee1 kinases coordinate DNA replication, chromosome condensation, and anaphase entry. *Mol Biol Cell* **23**: 1047-1057.

Fauman EB, Cogswell JP, Lovejoy B, Rocque WJ, Holmes W, Montana VG, Piwnica-Worms H, Rink MJ, Saper MA. 1998. Crystal structure of the catalytic domain of the human cell cycle control phosphatase, Cdc25A. *Cell* **93:** 617-625.

Fenger DD, Carminati JL, Burney-Sigman DL, Kashevsky H, Dines JL, Elfring LK, Orr-Weaver TL. 2000. PAN GU: a protein kinase that inhibits S phase and promotes mitosis in early Drosophila development. *Development* **127**: 4763-4774.

Ferrari S, Marin O, Pagano MA, Meggio F, Hess D, El-Shemerly M, Krystyniak A, Pinna LA. 2005. Aurora-A site specificity: a study with synthetic peptide substrates. *Biochem J* **390**: 293-302.

Ferraro T, Lucas T, Clemot M, De Las Heras Chanes J, Desponds J, Coppey M, Walczak AM, Dostatni N. 2016. New methods to image transcription in living fly embryos: the insights so far, and the prospects. *Wiley Interdiscip Rev Dev Biol* doi:10.1002/wdev.221.

Foe VE, Alberts BM. 1983. Studies of nuclear and cytoplasmic behaviour during the five mitotic cycles that precede gastrulation in Drosophila embryogenesis. *J Cell Sci* **61**: 31-70.

Fogarty P, Campbell SD, Abu-Shumays R, Phalle BS, Yu KR, Uy GL, Goldberg ML, Sullivan W. 1997. The Drosophila grapes gene is related to checkpoint gene chk1/rad27 and is required for late syncytial division fidelity. *Curr Biol* **7**: 418-426.

Foo SM, Sun Y, Lim B, Ziukaite R, O'Brien K, Nien CY, Kirov N, Shvartsman SY, Rushlow CA. 2014. Zelda potentiates morphogen activity by increasing chromatin accessibility. *Curr Biol* **24**: 1341-1346.

Frasch M, Levine M. 1987. Complementary patterns of even-skipped and fushi tarazu expression involve their differential regulation by a common set of segmentation genes in Drosophila. *Genes Dev* **1**: 981-995.

Frazer C, Young PG. 2012. Phosphorylation Mediated Regulation of Cdc25 Activity, Localization and Stability In *Protein Phosphorylation in Human Health*, doi:10.5772/48315 (ed. C Huang), pp. 395-436. InTech, Rijeka, Croatia

Fu S, Nien CY, Liang HL, Rushlow C. 2014. Co-activation of microRNAs by Zelda is essential for early Drosophila development. *Development* **141**: 2108-2118.

Gawlinski P, Nikolay R, Goursot C, Lawo S, Chaurasia B, Herz HM, Kussler-Schneider Y, Ruppert T, Mayer M, Grosshans J. 2007. The Drosophila mitotic inhibitor Fruhstart specifically binds to the hydrophobic patch of cyclins. *EMBO Rep* **8**: 490-496.

Gerhart JC. 1980. Mechanisms Regulating Pattern Formation in the Amphibian Egg and Early Embryo. In *Biological Regulation and Development*, (ed. R Goldberger), pp. 133-316. Springer US, Boston, MA.

Giet R, McLean D, Descamps S, Lee MJ, Raff JW, Prigent C, Glover DM. 2002. Drosophila Aurora A kinase is required to localize D-TACC to centrosomes and to regulate astral microtubules. *J Cell Biol* **156**: 437-451.

Glotzer M, Murray AW, Kirschner MW. 1991. Cyclin is degraded by the ubiquitin pathway. *Nature* **349**: 132-138.

Glover DM, Leibowitz MH, McLean DA, Parry H. 1995. Mutations in aurora prevent centrosome separation leading to the formation of monopolar spindles. *Cell* **81**: 95-105.

Gottardo M, Callaini G, Riparbelli MG. 2015. Aurora A inhibition by MNL8054 promotes centriole elongation during Drosophila male meiosis. *Cell Cycle* **14:** 2844-2852.

Graveley BR, Brooks AN, Carlson JW, Duff MO, Landolin JM, Yang L, Artieri CG, van Baren MJ, Boley N, Booth BW et al. 2011. The developmental transcriptome of Drosophila melanogaster. *Nature* **471**: 473-479.

Grosshans J, Muller HA, Wieschaus E. 2003. Control of cleavage cycles in Drosophila embryos by fruhstart. *Dev Cell* **5**: 285-294.

Grosshans J, Wenzl C, Herz HM, Bartoszewski S, Schnorrer F, Vogt N, Schwarz H, Muller HA. 2005. RhoGEF2 and the formin Dia control the formation of the furrow canal by directed actin assembly during Drosophila cellularisation. *Development* **132**: 1009-1020.

Grosshans J, Wieschaus E. 2000. A genetic link between morphogenesis and cell division during formation of the ventral furrow in Drosophila. *Cell* **101**: 523-531.

Guven-Ozkan T, Nishi Y, Robertson SM, Lin R. 2008. Global transcriptional repression in C. elegans germline precursors by regulated sequestration of TAF-4. *Cell* **135**: 149-160.

Haelterman NA, Jiang L, Li Y, Bayat V, Sandoval H, Ugur B, Tan KL, Zhang K, Bei D, Xiong B et al. 2014. Large-scale identification of chemically induced mutations in Drosophila melanogaster. *Genome Res* **24**: 1707-1718.

Hamm DC, Bondra ER, Harrison MM. 2015. Transcriptional activation is a conserved feature of the early embryonic factor Zelda that requires a cluster of four zinc fingers for DNA binding and a low-complexity activation domain. *J Biol Chem* **290**: 3508-3518.

Hammond D, Zeng K, Espert A, Bastos RN, Baron RD, Gruneberg U, Barr FA. 2013. Melanoma-associated mutations in protein phosphatase 6 cause chromosome instability and DNA damage owing to dysregulated Aurora-A. *J Cell Sci* **126**: 3429-3440.

Harrison MM, Eisen MB. 2015. Transcriptional Activation of the Zygotic Genome in Drosophila. *Curr Top Dev Biol* **113**: 85-112.

Harrison MM, Li XY, Kaplan T, Botchan MR, Eisen MB. 2011. Zelda binding in the early Drosophila melanogaster embryo marks regions subsequently activated at the maternal-to-zygotic transition. *PLoS Genet* **7**: e1002266.

Heyn P, Kircher M, Dahl A, Kelso J, Tomancak P, Kalinka AT, Neugebauer KM. 2014. The earliest transcribed zygotic genes are short, newly evolved, and different across species. *Cell Rep* **6**: 285-292.

Hiiragi T, Solter D. 2004. First cleavage plane of the mouse egg is not predetermined but defined by the topology of the two apposing pronuclei. *Nature* **430**: 360-364.

Hodis E, Watson IR, Kryukov GV, Arold ST, Imielinski M, Theurillat JP, Nickerson E, Auclair D, Li L, Place C et al. 2012. A landscape of driver mutations in melanoma. *Cell* **150**: 251-263.

Hofmann K, Bucher P, Kajava AV. 1998. A model of Cdc25 phosphatase catalytic domain and Cdk-interaction surface based on the presence of a rhodanese homology domain. *J Mol Biol* **282:** 195-208.

Hontelez S, van Kruijsbergen I, Georgiou G, van Heeringen SJ, Bogdanovic O, Lister R, Veenstra GJ. 2015. Embryonic transcription is controlled by maternally defined chromatin state. *Nat Commun* **6**: 10148.

Hu MW, Wang ZB, Teng Y, Jiang ZZ, Ma XS, Hou N, Cheng X, Schatten H, Xu X, Yang X et al. 2015. Loss of protein phosphatase 6 in oocytes causes failure of meiosis II exit and impaired female fertility. *J Cell Sci* **128**: 3769-3780.

Huntzinger E, Izaurralde E. 2011. Gene silencing by microRNAs: contributions of translational repression and mRNA decay. *Nat Rev Genet* **12**: 99-110.

Jevtic P, Levy DL. 2015. Nuclear size scaling during Xenopus early development contributes to midblastula transition timing. *Curr Biol* **25**: 45-52.

Ji JY, Squirrell JM, Schubiger G. 2004. Both cyclin B levels and DNA-replication checkpoint control the early embryonic mitoses in Drosophila. *Development* **131**: 401-411.

Jin Z, Homola EM, Goldbach P, Choi Y, Brill JA, Campbell SD. 2005. Drosophila Myt1 is a Cdk1 inhibitory kinase that regulates multiple aspects of cell cycle behavior during gametogenesis. *Development* **132**: 4075-4085.

Juven-Gershon T, Kadonaga JT. 2010. Regulation of gene expression via the core promoter and the basal transcriptional machinery. *Dev Biol* **339**: 225-229.

Kane DA, Kimmel CB. 1993. The zebrafish midblastula transition. *Development* **119**: 447-456.

Kang Q, Srividhya J, Ipe J, Pomerening JR. 2014. Evidence toward a dual phosphatase mechanism that restricts Aurora A (Thr-295) phosphorylation during the early embryonic cell cycle. *J Biol Chem* **289**: 17480-17496.

Krauthammer M, Kong Y, Ha BH, Evans P, Bacchiocchi A, McCusker JP, Cheng E, Davis MJ, Goh G, Choi M et al. 2012. Exome sequencing identifies recurrent somatic RAC1 mutations in melanoma. *Nat Genet* **44**: 1006-1014.

Laver JD, Li X, Ray D, Cook KB, Hahn NA, Nabeel-Shah S, Kekis M, Luo H, Marsolais AJ, Fung KY et al. 2015a. Brain tumor is a sequence-specific RNA-binding protein that directs maternal mRNA clearance during the Drosophila maternal-to-zygotic transition. *Genome Biol* **16**: 94.

Laver JD, Marsolais AJ, Smibert CA, Lipshitz HD. 2015b. Regulation and Function of Maternal Gene Products During the Maternal-to-Zygotic Transition in Drosophila. *Curr Top Dev Biol* **113**: 43-84.

Lecuyer E, Yoshida H, Parthasarathy N, Alm C, Babak T, Cerovina T, Hughes TR, Tomancak P, Krause HM. 2007. Global analysis of mRNA localization reveals a prominent role in organizing cellular architecture and function. *Cell* **131**: 174-187.

Lee LA, Orr-Weaver TL. 2003. Regulation of cell cycles in Drosophila development: intrinsic and extrinsic cues. *Annu Rev Genet* **37:** 545-578.

Lee LA, Van Hoewyk D, Orr-Weaver TL. 2003. The Drosophila cell cycle kinase PAN GU forms an active complex with PLUTONIUM and GNU to regulate embryonic divisions. *Genes Dev* **17**: 2979-2991.

Lee MT, Bonneau AR, Giraldez AJ. 2014. Zygotic genome activation during the maternal-to-zygotic transition. *Annu Rev Cell Dev Biol* **30**: 581-613.

Lee MT, Bonneau AR, Takacs CM, Bazzini AA, DiVito KR, Fleming ES, Giraldez AJ. 2013. Nanog, Pou5f1 and SoxB1 activate zygotic gene expression during the maternal-to-zygotic transition. *Nature* **503**: 360-364.

Lehner CF, O'Farrell PH. 1990. Drosophila cdc2 homologs: a functional homolog is coexpressed with a cognate variant. *EMBO J* **9**: 3573-3581.

Li XY, Harrison MM, Villalta JE, Kaplan T, Eisen MB. 2014. Establishment of regions of genomic activity during the Drosophila maternal to zygotic transition. *Elife* **3**.

Li XY, MacArthur S, Bourgon R, Nix D, Pollard DA, Iyer VN, Hechmer A, Simirenko L, Stapleton M, Luengo Hendriks CL et al. 2008. Transcription factors bind thousands of active and inactive regions in the Drosophila blastoderm. *PLoS Biol* **6**: e27.

Li XY, Thomas S, Sabo PJ, Eisen MB, Stamatoyannopoulos JA, Biggin MD. 2011. The role of chromatin accessibility in directing the widespread, overlapping patterns of Drosophila transcription factor binding. *Genome Biol* **12**: R34.

Liang HL, Nien CY, Liu HY, Metzstein MM, Kirov N, Rushlow C. 2008. The zinc-finger protein Zelda is a key activator of the early zygotic genome in Drosophila. *Nature* **456**: 400-403.

Liang KL, Paredes R, Carmody R, Eyers PA, Meyer S, McCarthy TV, Keeshan K. 2016. Human TRIB2 Oscillates during the Cell Cycle and Promotes Ubiquitination and Degradation of CDC25C. *Int J Mol Sci* **17**.

Lindeman LC, Andersen IS, Reiner AH, Li N, Aanes H, Ostrup O, Winata C, Mathavan S, Muller F, Alestrom P et al. 2011. Prepatterning of developmental gene expression by modified histones before zygotic genome activation. *Dev Cell* **21**: 993-1004.

Lott SE, Villalta JE, Schroth GP, Luo S, Tonkin LA, Eisen MB. 2011. Noncanonical compensation of zygotic X transcription in early Drosophila melanogaster development revealed through single-embryo RNA-seq. *PLoS Biol* **9**: e1000590.

Lu X, Li JM, Elemento O, Tavazoie S, Wieschaus EF. 2009. Coupling of zygotic transcription to mitotic control at the Drosophila mid-blastula transition. *Development* **136**: 2101-2110.

Luschnig S. 2000. Genetische Suche nach neuen Komponenten der achsenbildenden Systeme im Embryo von Drosophila melanogaster. In *VVB Laufersweiler Verlag*, PhD Dissertation, p. 77. Eberhard-Karls-Universität Tübingen.

Luschnig S, Moussian B, Krauss J, Desjeux I, Perkovic J, Nusslein-Volhard C. 2004. An F1 genetic screen for maternal-effect mutations affecting embryonic pattern formation in Drosophila melanogaster. *Genetics* **167**: 325-342.

Manfredi MG, Ecsedy JA, Meetze KA, Balani SK, Burenkova O, Chen W, Galvin KM, Hoar KM, Huck JJ, LeRoy PJ et al. 2007. Antitumor activity of MLN8054, an orally active small-molecule inhibitor of Aurora A kinase. *Proc Natl Acad Sci U S A* **104**: 4106-4111.

Mann DJ, Dombradi V, Cohen PT. 1993. Drosophila protein phosphatase V functionally complements a SIT4 mutant in Saccharomyces cerevisiae and its amino-terminal region can confer this complementation to a heterologous phosphatase catalytic domain. *EMBO J* **12**: 4833-4842.

Mata J, Curado S, Ephrussi A, Rorth P. 2000. Tribbles coordinates mitosis and morphogenesis in Drosophila by regulating string/CDC25 proteolysis. *Cell* **101**: 511-522.

Mazzolini L, Broban A, Froment C, Burlet-Schiltz O, Besson A, Manenti S, Dozier C. 2016. Phosphorylation of CDC25A on SER283 in late S/G2 by CDK/cyclin complexes accelerates mitotic entry. *Cell Cycle* **15:** 2742-2752.

McCleland ML, O'Farrell PH. 2008. RNAi of mitotic cyclins in Drosophila uncouples the nuclear and centrosome cycle. *Curr Biol* **18**: 245-254.

Merrill PT, Sweeton D, Wieschaus E. 1988. Requirements for autosomal gene activity during precellular stages of Drosophila melanogaster. *Development* **104**: 495-509.

Miskei M, Adam C, Kovacs L, Karanyi Z, Dombradi V. 2011. Molecular evolution of phosphoprotein phosphatases in Drosophila. *PLoS One* **6**: e22218.

Monzo K, Papoulas O, Cantin GT, Wang Y, Yates JR, 3rd, Sisson JC. 2006. Fragile X mental retardation protein controls trailer hitch expression and cleavage furrow formation in Drosophila embryos. *Proc Natl Acad Sci U S A* **103**: 18160-18165.

Morrison DK, Murakami MS, Cleghon V. 2000. Protein kinases and phosphatases in the Drosophila genome. *J Cell Biol* **150**: F57-62.

Murphy JM, Nakatani Y, Jamieson SA, Dai W, Lucet IS, Mace PD. 2015. Molecular Mechanism of CCAAT-Enhancer Binding Protein Recruitment by the TRIB1 Pseudokinase. *Structure* **23**: 2111-2121.

Nanahoshi M, Nishiuma T, Tsujishita Y, Hara K, Inui S, Sakaguchi N, Yonezawa K. 1998. Regulation of protein phosphatase 2A catalytic activity by alpha4 protein and its yeast homolog Tap42. *Biochem Biophys Res Commun* **251**: 520-526.

Newport J, Kirschner M. 1982a. A major developmental transition in early Xenopus embryos: I. characterization and timing of cellular changes at the midblastula stage. *Cell* **30**: 675-686.

Newport J, Kirschner M. 1982b. A major developmental transition in early Xenopus embryos: II. Control of the onset of transcription. *Cell* **30**: 687-696.

Newport JW, Kirschner MW. 1984. Regulation of the cell cycle during early Xenopus development. *Cell* **37**: 731-742.

Nien CY, Liang HL, Butcher S, Sun Y, Fu S, Gocha T, Kirov N, Manak JR, Rushlow C. 2011. Temporal coordination of gene networks by Zelda in the early Drosophila embryo. *PLoS Genet* **7**: e1002339.

O'Farrell PH. 2015. Growing an Embryo from a Single Cell: A Hurdle in Animal Life. *Cold Spring Harb Perspect Biol* **7**.

O'Farrell PH, Stumpff J, Su TT. 2004. Embryonic cleavage cycles: how is a mouse like a fly? *Curr Biol* **14**: R35-45.

Ogoh H, Tanuma N, Matsui Y, Hayakawa N, Inagaki A, Sumiyoshi M, Momoi Y, Kishimoto A, Suzuki M, Sasaki N et al. 2016. The protein phosphatase 6 catalytic subunit (Ppp6c) is indispensable for proper post-implantation embryogenesis. *Mech Dev* **139**: 1-9.

Papoulas O, Monzo KF, Cantin GT, Ruse C, Yates JR, 3rd, Ryu YH, Sisson JC. 2010. dFMRP and Caprin, translational regulators of synaptic plasticity, control the cell cycle at the Drosophila mid-blastula transition. *Development* **137**: 4201-4209.

Perez-Montero S, Carbonell A, Moran T, Vaquero A, Azorin F. 2013. The embryonic linker histone H1 variant of Drosophila, dBigH1, regulates zygotic genome activation. *Dev Cell* **26**: 578-590.

Price D, Rabinovitch S, O'Farrell PH, Campbell SD. 2000. Drosophila wee1 has an essential role in the nuclear divisions of early embryogenesis. *Genetics* **155**: 159-166.

Pritchard DK, Schubiger G. 1996. Activation of transcription in Drosophila embryos is a gradual process mediated by the nucleocytoplasmic ratio. *Genes Dev* **10**: 1131-1142.

Rabinowitz M. 1941. Studies on the cytology and early embryology of the egg of Drosophila melanogaster. *Journal of Morphology* **69**: 1-49.

Risau W, Saumweber H, Symmons P. 1981. Monoclonal antibodies against a nuclear membrane protein of Drosophila. Localization by indirect immunofluorescence and detection of antigen using a new protein blotting procedure. *Exp Cell Res* **133**: 47-54.

Robertson S, Lin R. 2015. The Maternal-to-Zygotic Transition in C. elegans. *Curr Top Dev Biol* **113**: 1-42.

Rorth P, Szabo K, Texido G. 2000. The level of C/EBP protein is critical for cell migration during Drosophila oogenesis and is tightly controlled by regulated degradation. *Mol Cell* **6**: 23-30.

Rose L, Gonczy P. 2014. Polarity establishment, asymmetric division and segregation of fate determinants in early C. elegans embryos. *WormBook* doi:10.1895/wormbook.1.30.2: 1-43.

Royou A, McCusker D, Kellogg DR, Sullivan W. 2008. Grapes(Chk1) prevents nuclear CDK1 activation by delaying cyclin B nuclear accumulation. *J Cell Biol* **183**: 63-75.

Rudolph T, Yonezawa M, Lein S, Heidrich K, Kubicek S, Schafer C, Phalke S, Walther M, Schmidt A, Jenuwein T et al. 2007. Heterochromatin formation in Drosophila is initiated through active removal of H3K4 methylation by the LSD1 homolog SU(VAR)3-3. *Mol Cell* **26**: 103-115.

Rusin SF, Schlosser KA, Adamo ME, Kettenbach AN. 2015. Quantitative phosphoproteomics reveals new roles for the protein phosphatase PP6 in mitotic cells. *Sci Signal* **8**: rs12.

Sambrook J, Russell DW. 2001. *Molecular Cloning: A Laboratory Manual, Third Edition* Cold Spring Harbor Laboratory Press, New York.

Sandler JE, Stathopoulos A. 2016. Quantitative Single-Embryo Profile of Drosophila Genome Activation and the Dorsal-Ventral Patterning Network. *Genetics* **202**: 1575-1584.

Sardon T, Pache RA, Stein A, Molina H, Vernos I, Aloy P. 2010. Uncovering new substrates for Aurora A kinase. *EMBO Rep* **11**: 977-984.

Saunders A, Core LJ, Sutcliffe C, Lis JT, Ashe HL. 2013. Extensive polymerase pausing during Drosophila axis patterning enables high-level and pliable transcription. *Genes Dev* **27**: 1146-1158.

Schubeler D, Scalzo D, Kooperberg C, van Steensel B, Delrow J, Groudine M. 2002. Genome-wide DNA replication profile for Drosophila melanogaster: a link between transcription and replication timing. *Nat Genet* **32**: 438-442.

Schulz KN, Bondra ER, Moshe A, Villalta JE, Lieb JD, Kaplan T, McKay DJ, Harrison MM. 2015. Zelda is differentially required for chromatin accessibility, transcription factor binding, and gene expression in the early Drosophila embryo. *Genome Res* **25**: 1715-1726.

Schwille P. 2001. Fluorescence correlation spectroscopy and its potential for intracellular applications. *Cell Biochem Biophys* **34**: 383-408.

Seher TC, Leptin M. 2000. Tribbles, a cell-cycle brake that coordinates proliferation and morphogenesis during Drosophila gastrulation. *Curr Biol* **10**: 623-629.

Semotok JL, Cooperstock RL, Pinder BD, Vari HK, Lipshitz HD, Smibert CA. 2005. Smaug recruits the CCR4/POP2/NOT deadenylase complex to trigger maternal transcript localization in the early Drosophila embryo. *Curr Biol* **15**: 284-294.

Shermoen AW, McCleland ML, O'Farrell PH. 2010. Developmental control of late replication and S phase length. *Curr Biol* **20**: 2067-2077.

Shimuta K, Nakajo N, Uto K, Hayano Y, Okazaki K, Sagata N. 2002. Chk1 is activated transiently and targets Cdc25A for degradation at the Xenopus midblastula transition. *EMBO J* **21**: 3694-3703.

Sibon OC, Laurencon A, Hawley R, Theurkauf WE. 1999. The Drosophila ATM homologue Mei-41 has an essential checkpoint function at the midblastula transition. *Curr Biol* **9**: 302-312.

Sibon OC, Stevenson VA, Theurkauf WE. 1997. DNA-replication checkpoint control at the Drosophila midblastula transition. *Nature* **388**: 93-97.

Sigrist S, Ried G, Lehner CF. 1995. Dmcdc2 kinase is required for both meiotic divisions during Drosophila spermatogenesis and is activated by the Twine/cdc25 phosphatase. *Mech Dev* **53**: 247-260.

Sopko R, Foos M, Vinayagam A, Zhai B, Binari R, Hu Y, Randklev S, Perkins LA, Gygi SP, Perrimon N. 2014. Combining genetic perturbations and proteomics to examine kinase-phosphatase networks in Drosophila embryos. *Dev Cell* **31**: 114-127.

Staudt N, Fellert S, Chung HR, Jackle H, Vorbruggen G. 2006. Mutations of the Drosophila zinc finger-encoding gene vielfaltig impair mitotic cell divisions and cause improper chromosome segregation. *Mol Biol Cell* **17**: 2356-2365.

Stefansson B, Brautigan DL. 2007. Protein phosphatase PP6 N terminal domain restricts G1 to S phase progression in human cancer cells. *Cell Cycle* **6**: 1386-1392.

Stumpff J, Duncan T, Homola E, Campbell SD, Su TT. 2004. Drosophila Wee1 kinase regulates Cdk1 and mitotic entry during embryogenesis. *Curr Biol* **14**: 2143-2148.

Sulston JE, Schierenberg E, White JG, Thomson JN. 1983. The embryonic cell lineage of the nematode Caenorhabditis elegans. *Dev Biol* **100**: 64-119.

Sung HW, Spangenberg S, Vogt N, Grosshans J. 2013. Number of nuclear divisions in the Drosophila blastoderm controlled by onset of zygotic transcription. *Curr Biol* **23**: 133-138.

Tadros W, Goldman AL, Babak T, Menzies F, Vardy L, Orr-Weaver T, Hughes TR, Westwood JT, Smibert CA, Lipshitz HD. 2007. SMAUG is a major regulator of maternal mRNA destabilization in Drosophila and its translation is activated by the PAN GU kinase. *Dev Cell* **12**: 143-155.

Tadros W, Houston SA, Bashirullah A, Cooperstock RL, Semotok JL, Reed BH, Lipshitz HD. 2003. Regulation of maternal transcript destabilization during egg activation in Drosophila. *Genetics* **164**: 989-1001.

Tadros W, Lipshitz HD. 2009. The maternal-to-zygotic transition: a play in two acts. *Development* **136**: 3033-3042.

ten Bosch JR, Benavides JA, Cline TW. 2006. The TAGteam DNA motif controls the timing of Drosophila pre-blastoderm transcription. *Development* **133**: 1967-1977.

Thomas S, Li XY, Sabo PJ, Sandstrom R, Thurman RE, Canfield TK, Giste E, Fisher W, Hammonds A, Celniker SE et al. 2011. Dynamic reprogramming of chromatin accessibility during Drosophila embryo development. *Genome Biol* **12**: R43.

Thorpe HM, Wilson SE, Smith MC. 2000. Control of directionality in the site-specific recombination system of the Streptomyces phage phiC31. *Mol Microbiol* **38**: 232-241.

Vastag L, Jorgensen P, Peshkin L, Wei R, Rabinowitz JD, Kirschner MW. 2011. Remodeling of the metabolome during early frog development. *PLoS One* **6**: e16881.

Vastenhouw NL, Zhang Y, Woods IG, Imam F, Regev A, Liu XS, Rinn J, Schier AF. 2010. Chromatin signature of embryonic pluripotency is established during genome activation. *Nature* **464**: 922-926.

Verni F, Somma MP, Gunsalus KC, Bonaccorsi S, Belloni G, Goldberg ML, Gatti M. 2004. Feo, the Drosophila homolog of PRC1, is required for central-spindle formation and cytokinesis. *Curr Biol* **14**: 1569-1575.

Vogt N, Koch I, Schwarz H, Schnorrer F, Nusslein-Volhard C. 2006. The gammaTuRC components Grip75 and Grip128 have an essential microtubule-anchoring function in the Drosophila germline. *Development* **133**: 3963-3972.

Walser CB, Lipshitz HD. 2011. Transcript clearance during the maternal-to-zygotic transition. *Curr Opin Genet Dev* **21**: 431-443.

Wang N, Leung HT, Mazalouskas MD, Watkins GR, Gomez RJ, Wadzinski BE. 2012. Essential roles of the Tap42-regulated protein phosphatase 2A (PP2A) family in wing imaginal disc development of Drosophila melanogaster. *PLoS One* **7**: e38569.

Wang R, Jung SY, Wu CF, Qin J, Kobayashi R, Gallick GE, Kuang J. 2010. Direct roles of the signaling kinase RSK2 in Cdc25C activation during Xenopus oocyte maturation. *Proc Natl Acad Sci U S A* **107:** 19885-19890.

Wenzl C, Yan S, Laupsien P, Grosshans J. 2010. Localization of RhoGEF2 during Drosophila cellularization is developmentally controlled by Slam. *Mech Dev* **127:** 371-384.

Wera S, Hemmings BA. 1995. Serine/threonine protein phosphatases. *Biochem J* **311 (Pt 1)**: 17-29.

Yan S, Xu Z, Lou F, Zhang L, Ke F, Bai J, Liu Z, Liu J, Wang H, Zhu H et al. 2015. NF-kappaB-induced microRNA-31 promotes epidermal hyperplasia by repressing protein phosphatase 6 in psoriasis. *Nat Commun* **6**: 7652.

Yu J, Fleming SL, Williams B, Williams EV, Li Z, Somma P, Rieder CL, Goldberg ML. 2004. Greatwall kinase: a nuclear protein required for proper chromosome condensation and mitotic progression in Drosophila. *J Cell Biol* **164**: 487-492.

Yuan K, Farrell JA, O'Farrell PH. 2012. Different cyclin types collaborate to reverse the S-phase checkpoint and permit prompt mitosis. *J Cell Biol* **198**: 973-980.

Yuan K, O'Farrell PH. 2015. Cyclin B3 is a mitotic cyclin that promotes the metaphase-anaphase transition. *Curr Biol* **25**: 811-816.

Yuan K, O'Farrell PH. 2016. TALE-light imaging reveals maternally guided, H3K9me2/3-independent emergence of functional heterochromatin in Drosophila embryos. *Genes Dev* doi:10.1101/gad.272237.115.

Zabidi MA, Arnold CD, Schernhuber K, Pagani M, Rath M, Frank O, Stark A. 2015. Enhancer-core-promoter specificity separates developmental and housekeeping gene regulation. *Nature* **518**: 556-559.

Zamir E, Kam Z, Yarden A. 1997. Transcription-dependent induction of G1 phase during the zebra fish midblastula transition. *Mol Cell Biol* **17**: 529-536.

Zeitlinger J, Stark A, Kellis M, Hong JW, Nechaev S, Adelman K, Levine M, Young RA. 2007. RNA polymerase stalling at developmental control genes in the Drosophila melanogaster embryo. *Nat Genet* **39**: 1512-1516.

Zeng K, Bastos RN, Barr FA, Gruneberg U. 2010. Protein phosphatase 6 regulates mitotic spindle formation by controlling the T-loop phosphorylation state of Aurora A bound to its activator TPX2. *J Cell Biol* **191**: 1315-1332.

Zhang M, Kothari P, Mullins M, Lampson MA. 2014a. Regulation of zygotic genome activation and DNA damage checkpoint acquisition at the mid-blastula transition. *Cell Cycle* **13**: 3828-3838.

Zhang Y, Vastenhouw NL, Feng J, Fu K, Wang C, Ge Y, Pauli A, van Hummelen P, Schier AF, Liu XS. 2014b. Canonical nucleosome organization at promoters forms during genome activation. *Genome Res* **24**: 260-266.

Zhao R, Nakamura T, Fu Y, Lazar Z, Spector DL. 2011. Gene bookmarking accelerates the kinetics of post-mitotic transcriptional re-activation. *Nat Cell Biol* **13**: 1295-1304.

Zhong J, Liao J, Liu X, Wang P, Liu J, Hou W, Zhu B, Yao L, Wang J, Li J et al. 2011. Protein phosphatase PP6 is required for homology-directed repair of DNA double-strand breaks. *Cell Cycle* **10**: 1411-1419.

Zingsheim HP, Neher E. 1974. The equivalence of fluctuation analysis and chemical relaxation measurements: a kinetic study of ion pore formation in thin lipid membranes. *Biophys Chem* **2**: 197-207.

Zou L, Elledge SJ. 2003. Sensing DNA damage through ATRIP recognition of RPA-ssDNA complexes. *Science* **300**: 1542-1548.

List of Figures

List of Tables

Acknowledgements

First of all, I would like to thank my "Doktorvater" Prof. Dr. Jörg Großhans for offering me this precious opportunity to join his laboratory. I really appreciate his continuous support, constant guidance and weekly discussions. His patience, optimism and passion for science inspired me a lot.

I am greatly indebted to my thesis committee members. I thank Prof. Dr. Gregor Bucher for his illuminating discussions, helpful suggestions and kind review of my thesis. I thank Prof. Dr. Stefan Luschnig and his lab members in University of Zurich for giving me many supervisions and helps, and for sharing excellent research environment during my staying in Zurich.

I am very grateful to my collaborators Dr. Ingo Gregor, as well as Prof. Dr. Arno Müller and Proteomics Facility in University of Dundee.

I owe many thanks to all of my colleagues, present and past. They are Dr. Shuling Yan, Dr. Hung-wei Sung, Dr. Michaela Clever, Dr. Maheshwar Gummalla, Dr. Zhiyi Lv, Dr. Laszlo Henn, Dr. Sreemukta Acharya, Dr. Franziska Winkler, Dr. Roman Petrovsky, Saskia Spangenberg, Deqing Kong, Anja Schmidt, Stephanie Gröning, Maria Kriebel, Johannes Sattmann, Lenin Chandran, Prachi Richa and Long Li. Their helps, encouragements and friendships will always keep in my memory.

I am thankful to Prof. Dr. Tomas Pieler and all the members of Institute for Developmental Biochemistry for fabulous scientific atmosphere and fruitful discussions in the weekly seminar.

I would like to express my gratitude to China Scholarship Council (CSC) for the financial support during my PhD study in the last four years.

My sincere thanks go to all of my friends in Göttingen. Without them, my life would not be so colourful and gratified.

I acknowledge also the University of Göttingen. It is my great honour to be a member of her. I will always regard her motto as mine: "*In publica commoda*"- For the good of all.

Most importantly, I would like to give my deepest thanks to my family. Thanks to my parents for their untiring support, consideration and understanding. Thanks to my wife Qian and our daughter Jasmin, for their unconditional and endless love.

Curriculum vitae

Mr. Boyang Liu

Institute for Developmental Biochemistry

Universitätsmedizin Göttingen

Justus-von-Liebig-Weg 11

37077 Göttingen, Germany

Phone: +49-(0)551-39-14610

E-mail: boyang.liu@med.uni-goettingen.de

Education

Oct 2012 – Sept 2016	Doctoral studies of Developmental Biology
	University of Göttingen, Göttingen, Germany
Jun 2013 – Sept 2013	Visiting PhD student
	University of Zurich, Zurich, Switzerland
Jul 2012 – Aug 2012	German training
	Beijing Language and Culture University, Beijing, China
Sept 2009 – Jun 2012	Graduate studies of Animal Molecular Genetics
	Jilin University, Changchun, China
Sept 2005 – Jul 2009	Undergraduate studies of Animal Science
	Southwest University, Chongqing, China
Sept 2002 – Jul 2005	Affiliated Middle School to Inner Mongolia Normal University
	Hohhot, China

Awards and Scholarships

Göttingen International Conference Grants, University of Göttingen, 2016

PhD scholarship, China Scholarship Council (CSC), 2012–2016

Academic Conferences

May 2016	13th Cold Spring Harbor Laboratory Meeting -The Cell Cycle
	Cold Spring Harbor, NY, USA (Poster presentation)
Mar 2015	Joint Meeting of the German and French Societies of Developmental Biologists
	Nürnberg, Germany (Poster presentation)